U.PORTO
FEUP FACULDADE DE ENGENHARIA
UNIVERSIDADE DO PORTO

Eduardo Pereira Coelho Fernandes de Carvalho

Computational tools to analyse electrophysiological data in Deep Brain Stimulation

Thesis submitted to the Faculty of Engineering, University of Porto, for the Master's Program of Bioengineering

FINAL VERSION

Supervisor: Paulo Aguiar

Co-supervisor: Miguel Aroso

July 2022

Resumo

A estimulação cerebral profunda é uma terapia comprovada para doenças neurodegenerativas que afetam o movimento, como a doença de Parkinson. Esta envolve a colocação de um dispositivo capaz de estimular regiões cerebrais ao enviar impulsos elétricos para elétrodos implantados nessas regiões. Apesar do seu conceito-base permanecer praticamente inalterado desde as primeiras aplicações, avanços tecnológicos recentes abriram a possibilidade de ajustar a terapia às necessidades do paciente, em tempo-real. Este paradigma, cunhado de adaptativo, contrapõe-se ao convencional, em que os parâmetros de estimulação são selecionados por clínicos especializados e ajustados periodicamente. Pelo contrário, os sistemas adaptativos utilizam mecanismos retroativos, onde um algoritmo recebe como input biomarcadores que refletem os estados momentâneos do paciente e gera um output de parâmetros de estimulação.

Atualmente, a maioria da investigação debruça-se sobre a procura de biomarcadores ideais – i.e., aqueles que refletem inequivocamente estados patológicos – quer na clínica quer fora dela. Pensa-se que o campo elétrico cerebral e a motricidade dos pacientes possam conter estes biomarcadores. Contudo, existe uma carência de ferramentas dedicadas para levar a bom porto o empreendimento. Assim, esta dissertação distribui-se em três vertentes: primeiro, o desenvolvimento de um sistema wearable capaz de registar e analisar sinais motores; segundo, a criação de um conjunto de ferramentas computacionais para a análise de dados crónicos (captados fora da clínica); e, por último, a aplicação dessas ferramentas em dados clínicos de uma forma orientada para a investigação. A execução de todas estas vertentes exigiu uma revisão literária abrangente e interdisciplinar, uma vez que os métodos utilizados incluem domínios que vão desde a eletrónica e processamento de sinal até à estatística e aprendizagem automática.

No final, todas os objetivos foram alcançados. Foi desenvolvido um wearable em forma de luva capaz de registar dados motores e de quantificar a intensidade de sintomas parkinsonianos. Desenvolveu-se um vasto leque de ferramentas computacionais para a análise de dados crónicos, com posterior integração numa

toolbox. E, finalmente, a aplicação destas ferramentas gerou resultados preliminares, que aguardam futura validação e promovem novas linhas de investigação.

Abstract

Deep brain stimulation is a well-established therapy for movement disorders, such as Parkinson's disease, that involves the placement of a neurostimulation device, which sends electrical impulses through electrodes implanted in the brain. Although the DBS concept remains mostly unchanged since its first applications, recent technological advances have unravelled the possibility of tailoring the therapy to the patient's needs in real-time. This paradigm, called adaptive deep brain stimulation, contrasts with the conventional approach where the stimulation parameters are set by highly trained clinicians and must be periodically adjusted. Instead, adaptive systems rely on a feedback mechanism, where biomarkers that reflect the patient's ongoing states serve as the input of an algorithm that changes the stimulation parameters.

Current research still revolves around finding the ideal biomarkers – i.e., those that unequivocally reflect pathological states – both in clinical and non-clinical settings. The brain's electrical field and the patient's motor signals are thought to harbour such biomarkers. However, there is still a lack of dedicated tools for the enterprise. Therefore, the aim of this thesis was threefold: first, the development of a wearable system capable of recording and analysing motor signals; second, the creation of a set of computational tools for the analysis of chronic (outside the clinic) data; and third, the application of some of the developed tools in clinical data to provide a framework for further research. All these required a comprehensive and interdisciplinary literature review, for the used methods encompass domains that range from electronics and signal processing to statistics and machine-learning.

In the end, the three goals were successfully achieved. A wearable glove system made of off-the-shelf components could record, store, and quantify the symptomatic intensity of motor activity. A wide array of visuo-analytical tools was devised for chronic data analysis and integrated in an extensive toolbox. And, finally, the application of these tools yielded some preliminary results that wait for further validation and set future lines of research.

Agradecimentos

Em primeiro lugar, gostaria de agradecer aos meus orientadores, o Dr. Paulo Aguiar e o Dr. Miguel Aroso, por todo o apoio e por me terem mostrado o que é a ciência na verdadeira acepção da palavra. Neste sentido, deixo também um agradecimento especial à incansável Andreia, que, para além de trazer alguma ordem às minhas tendências mais caóticas, ainda teve que aturar os meus devaneios. A toda a equipa do NCN[1], que desde o início me recebeu de braços abertos, fico reconhecido por todas as sugestões e por todos os momentos lúdicos que me proporcionaram ao longo desta jornada. Não posso deixar de agradecer ao Dr. Rui Vaz e ao Dr. Manuel Pinto, do CHUSJ[2], pelo interesse mostrado no projeto e pela sua crucial contribuição para o mesmo.

Num tom mais pessoal, gostaria de agradecer à minha família e, em particular, aos meus pais por terem acompanhado a minha jornada académica de perto e pelos interrogatórios ocasionais, cuja utilidade espero ficar patente durante a defesa desta tese. Aos amigos, que não enumerarei por receio de incorrer em omissões imperdoáveis ou em ordenações inadvertidas, pelos momentos de descontração e quebra de monotonia. À FEUP, por ter sido o palco de inúmeras aventuras e desventuras (*não mencionarei a primeira frequência de Análise Matemática I*), sendo as segundas tão importantes quanto as primeiras.

Por último, resta-me louvar a simples existência (*perdoem-me se esta adjetivação for paradoxal*) de Borges, de Brahms, das panquecas de alfarroba, do número 42 e de enumerações compostas por um número primo de elementos.

E.F.C.

---

[1] NCN – Neuroengineering and Computational Neuroscience, Instituto de Investigação e Inovação em Saúde (i3S)

[2] CHUSJ – Centro Hospitalar Universitário de São João

"To be sure, a part of the impulse to science is simply curiosity,
to hold the unheld and watch the unwatched.
We are all children in the unknown."

– The Origins of Consciousness in the Breakdown of the Bicameral Mind, Julian Jaynes.

Contents

List of Figures

List of Tables

List of Abbreviations

aDBS – Adaptive Deep Brain Stimulation

AM – Amplitude Modulation

cDBS – Continuous Deep Brain Stimulation

DBS – Deep Brain Stimulation

DT – Decision Tree

EMG - Electromyography

FFT – Fast Fourier Transform

GUI – Graphical User Interface

IMU – Inertial Measurement Unit

KNN – K-Nearest Neighbours

LFP – Local Field Potential

ML – Machine-Learning

NCN – Neuroengineering and Computational Neuroscience

PCA – Principal Component Analysis

PD – Parkinson's Disease

QoL – Quality of Life

sEMG – Surface Electromyography

SVM – Support Vector Machine

UPDRS – Unified Parkinson's Disease Rating Scale

VTA – Volume of Tissue Activated

Part I

Introduction and State of the Art

Chapter 1
Introduction

1.1 Context and Motivation

Parkinson's disease (PD) is a neurodegenerative disease that is becoming increasingly prevalent worldwide [1]. Although its cardinal symptoms are movement-related, the lives of the patients are also affected in non-motor ways. While medication is still the standard therapeutic approach for minimising its impact, electrical stimulation-based therapies have gained considerable attention in the past decades [17]. Deep brain stimulation (DBS) is a well-established surgical treatment that involves the insertion of an electrode in the subthalamic nucleus, and the ensuing electrical stimulation of the region. DBS has shown tremendous potential in the alleviation of the intensity and frequency of the PD symptomatology [18]. Notwithstanding, the underlying technology is far from perfect, and has seen considerable improvements in the last couple of years.

The DBS conventional approach consists in the manual feeding of continuous stimulation parameters (e.g., current amplitude, frequency, and pulse-width) into the implanted pulse generator, and subsequent evaluation of their efficacy in reducing the symptoms. This evaluation is frequently based on subjective metrics, such as the Unified Parkinson Disease Rating Scale (UPDRS). Despite providing some relief to the patients, this approach is clearly limited, insofar as it lacks out-clinical coverage (for the evaluation is done in clinically controlled environments) and the adequate sensitivity to situational changes (i.e., significant changes within a patient's life or in the disease's progression), which demand additional parameter-tuning sessions. Hence arises the need for new DBS paradigms.

Adaptive closed-loop DBS (aDBS) is a field as active as it is recent in the DBS research landscape. Its main goal is to provide optimal therapeutic results by adjusting the stimulation parameters in real-time, according to the patient's own physiology [36]. An aDBS system relies on three pillars: the patient's biomarkers (input), a set of stimulation parameters (output), and an algorithm that transforms the given biomarkers in the adequate stimulation parameters.

A useful biomarker must be quantifiable and reflect ongoing changes within the patient's state. To comply with the first requisite, it is crucial to implement objective quantitative metrics in the evaluation of Parkinsonian symptoms, wherever subjective judgement still prevails. Wearable technologies emerge as a suitable solution for this task [102]. In fact, the past few years have shown the feasibility of such technologies, namely on tremor analysis. Conversely, the second requisite is somewhat harder to fulfil, for the research is still at an early stage. This is particularly true with respect to the exploration of chronic biomarkers – i.e., those that work both in the clinic and in the real-world. Indeed, chronic long-term aDBS has still a long way to go.

Recent technological advances in the DBS devices made the concurrent recording of the brain's electrical field possible [120]. Since then, several studies have unveiled the potential of using brain signals as biomarkers for aDBS systems, even though most were exclusively applied in clinical settings. After going through a conventional DBS clinical session – which culminates with the selection of the adequate stimulation settings – the patient returns to his daily routine. Given that Parkinsonian symptomatology evolves over time, these session intermissions present a major opportunity to assess not only potential chronic biomarkers, but also the effect of daily activities or states (events) on these signals.

1.2 Objectives

The central goal of this thesis is to create computational tools for the analysis of electrophysiological data in DBS. In particular, for the analysis of outside the clinic, or chronic, data. Given that this data is dependent on a subjective choice of stimulation parameters, this thesis also sets up as a goal the development of a wearable system capable of recording the patient's motricity, and objectively assessing symptom intensity. Finally, the lack of research concerning chronic data fosters the intent of applying some of the developed tools in a research-oriented manner.

To fulfil the first two goals, specific marks were established:

- Design visual and analytical tools, for further integration in a toolbox that is being developed by the NCN lab.
- Build a wearable device from scratch.
- Design a Graphical user Interface (GUI), for the recording and storing of motor data.

- Develop functions that quantitatively assess the tremor and rigidity intensities of the recorded data.

To meet the final goal, four research questions were formulated and tackled separately. The questions and their underlying logic are explained later in the document.

1.3 Contributions

The proposed work had the following main contributions:

- The enrichment of the toolbox that is being developed by the NCN lab for the analysis of data obtained from the Medtronic's Percept™ + BrainSense™ system.
- The creation of a wearable system and a GUI that can be used during clinical sessions to record motor signals.
- The development of functions for tremor and rigidity quantification – the second of which is novel, to the best of our knowledge.
- The establishment of preliminary results and guidelines in the study of chronic DBS data.

1.4 Document Structure

This document is structured in two parts. The first part is comprised by Chapters 1 and 2, which contain, respectively, the introduction and a state-of-the-art overview on the topics that this thesis elaborates upon: a) the impact of Parkinson's disease and its pathophysiology; b) the deep brain stimulation therapy and its current paradigms; c) hardware and software technologies involved in adaptive deep brain stimulation therapies.

The second part contains the bulk of the practical work, encompassing Chapters 3, 4 and 5. In Chapter 3, one finds the methodology used to achieve a wearable glove system for tremor and rigidity quantification, as well as some preliminary results on its application. Chapter 4 explores novel ways to interpret the out-clinical data of PD patients with implanted DBS devices, and displays some potentially useful analytical tools. Finally, Chapter 5 concludes this liminal work and forecasts the next steps in the creation of robust adaptive deep brain stimulation systems.

Chapter 2

Literature Review

This chapter outlines important aspects of the three main areas addressed in this work: Parkinson's disease, deep brain stimulation, and wearables and computational tools for adaptive stimulation technologies.

2.1 Parkinson's Disease

Parkinson's disease (PD) is the fastest growing neurodegenerative disease in the world [1] and the second most prevalent, just behind Alzheimer's disease [2]. Nonetheless, the epidemiological literature concerning its incidence, prevalence and mortality is not unanimous. In 2016, the Global Burden of Disease Study (GBD) reported 6 million global cases [1], whereas in 2020, a different study estimated the worldwide prevalence as 9.4 million [3]. In any case, the general increase in life expectancy suggests that these figures will more than double by 2040 [4].

2.1.1 Pathophysiology

PD is mainly characterised by the loss of dopaminergic innervation that connects the substantia nigra in the midbrain to the striatum – putamen and caudate nucleus, structures that regulate movement (see Figure 1). The expansive nature of this neurodegeneration accounts for the heterogeneity of the disorder. In other words, even though the afflicted share a disruption in the dopamine levels, the symptomatology and rate of progression vary from patient to patient.

Although the exact cause of the neurodegeneration remains unknown, both genetic and environmental factors seem to play a role in the development of PD [5]. With respect to the latter, while the exposure to pesticides and heavy metals have been reported to increase the likelihood of the disease [6], smoking and caffeine consumption are associated with its decrease [7]. Additionally, ageing, medication side effects and traumatic brain injury are also linked with its appearance.

Most people with PD develop the disease after the age of 60, but about 5% to 10% experience an early onset, before the age of 50. Genetic factors are usually associated with the latter group.

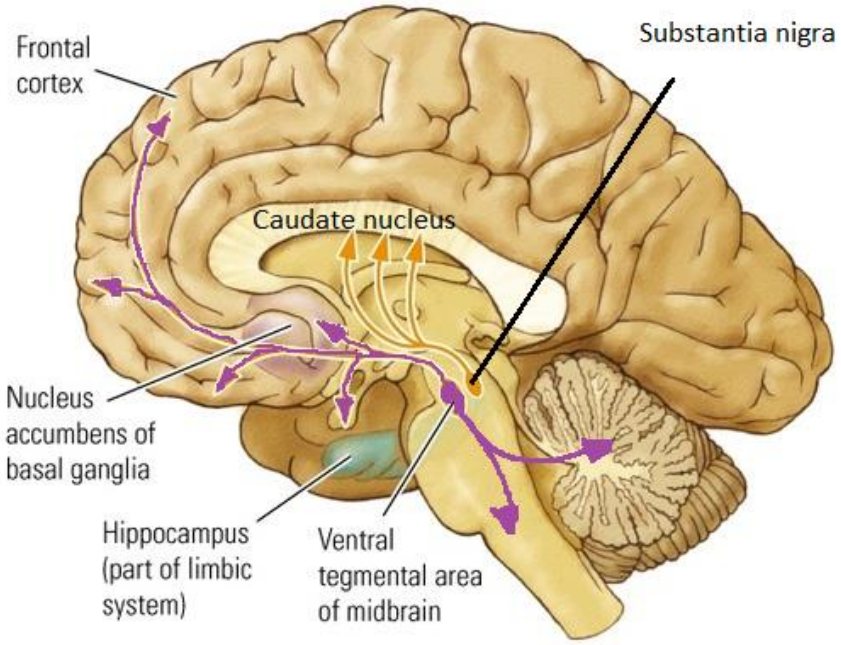

Figure 1 – Dopaminergic pathways. The nigrostriatal pathway is represented in yellow. Dopamine travels from the substantia nigra to brain regions – that include the caudate nucleus, the globus pallidus, and the thalamus – responsible for balance and movement control. From [8].

2.1.2 Symptoms and Quality of Life

PD is known to cause a substantial reduction in the quality of life (QoL) of the patients in three main domains: motor symptoms, non-motor symptoms and treatment side effects. The early stages of PD are usually characterised by a significant decrease in QoL due

Table 1 – Parkinsonian symptomatology. Adapted from [11].

CARDINAL MOTOR FEATURES	OTHER MOTOR FEATURES	NONMOTOR FEATURES
Bradykinesia Rest tremor Rigidity Postural instability	Micrographia Masked facies (hypomimia) Reduced eye blinking Drooling Soft voice (hypophonia) Dysphagia Freezing	Anosmia Sensory disturbances (e.g., pain) Mood disorders (e.g., depression) Sleep disturbances (e.g., RBD) Autonomic disturbances Orthostatic hypotension Gastrointestinal disturbances Genitourinal disturbances Sexual dysfunction Cognitive impairment/Dementia

Abbreviation: RBD, rapid eye movement behavior disorder.

to non-motor symptoms, such as depression, anxiety, pain, olfactory dysfunction, memory loss and sleep problems. The appearance of motor symptoms tends to succeed these early stages, and it is at this point that most of the clinical diagnoses are made – and, consequently, the antiparkinsonian therapies start. Both the cardinal and the less common features of the disease are summarised in Table 1.

When treatment is initiated, the QoL of the patient often stabilises for the first 18 months. Nevertheless, the deterioration of QoL follows a slow but steady rhythm thereafter [9]. At advanced disease stages, more than 40% of the afflicted develop dementia [10].

2.1.3 Current Treatments

Since a cure for PD is yet to be found, current treatments focus on alleviating symptoms, so that the patients can maintain an active lifestyle and a normal life expectancy. These treatments include medication, diet, exercise, and, as a last resort, deep brain stimulation.

The main therapy for PD consists in the taking of levodopa, a dopaminergic drug. This drug stimulates the dopamine production, replenishing the receding supply of this neurotransmitter. Yet, it also causes some adverse side effects, such as nausea, confusion, and sleepiness [12]. For this reason, patients tend to complement the therapy with medications that minimise those side effects (e.g., carbidopa), reduce the amount of levodopa needed, and minimize other specific symptoms. It is worth noting that once this type of therapy starts, a patient should never stop taking levodopa without medical consent, for its abstinence may result in serious side effects, including breathing difficulties and inability to move [13].

Concurrently, people with PD can undergo physical, occupational, and speech therapies, which may help with the motor symptoms and the decline in mental functions. A healthy diet, frequent massages and yoga are also common strategies at their disposal.

Unfortunately, notwithstanding the toil of daily ingestion, most of the drugs lose efficacy in the long-term [14]. In fact, the majority of patients starts to have complications after 5 years of therapy, including the emergence of levodopa-induced dyskinesias [15] – which are involuntary, erratic, writhing movements of the face, arms, legs or trunk –, and the so-called “on-off fluctuations”, in which periods of effective symptom reduction alternate with periods of its exacerbation [16]. This is particularly problematic for early-onset patients, that are still expected to live for decades. For these, deep brain

stimulation poses an unvaluable alternative. This therapy involves a surgical procedure, where electrodes are inserted into part of the brain, and connected to a small electrical device implanted in the chest. In a nutshell, the device generates electrical pulses and stimulates the specific areas in the brain that are mainly associated with the manifestation of the cardinal symptoms. The next section explores this therapy in detail.

2.2 Deep Brain Stimulation

Deep brain stimulation (DBS) is regarded as an effective, long-term treatment for PD [17][18], as well as for other movement disorders like essential tremor [19] or dystonia [20].

Despite having its electrical, chemical, and other neural-network influences thoroughly studied over the last decades, it remains unclear exactly how DBS leads to changes in the Parkinsonian symptomatology. Most studies highlight the role of DBS in the inhibition and excitation of the cells and fibres located closest to the electrodes [21][22]. As illustrated in Figure 2, this can happen either by directly interfering with the

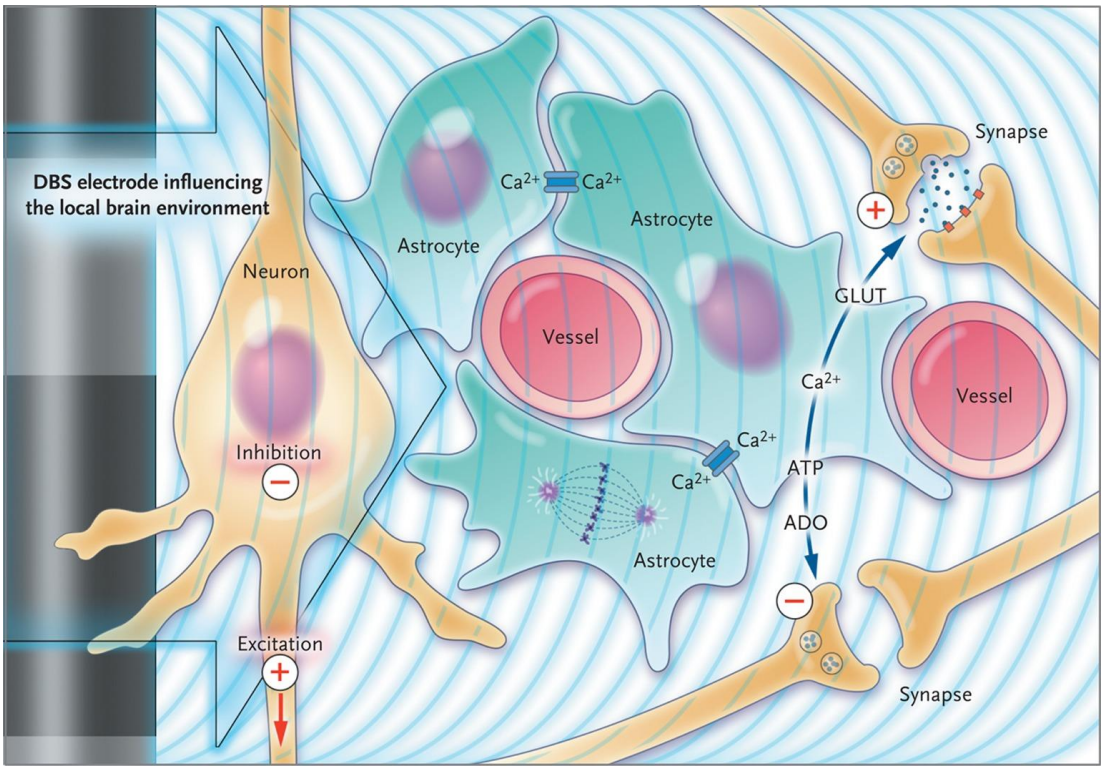

Figure 2 – Local effects of DBS. Inhibition of neuronal-cell bodies (−) and the excitation (+) of neighbouring axons. Stimulated astrocytes release calcium, which may lead to a release of glutamate (GLUT) and adenosine (ADO), as well as local increase in cerebral blood flow. Adapted from [16].

firing patterns of individual neurons [23] or by triggering the release of calcium ions of astrocytes [24] – which in turn, promote the local release of neurotransmitters - in the basal ganglia. Subsequently, these changes can affect other brain regions, via the thalamocortical circuits and other pathways shown in Figure 3.

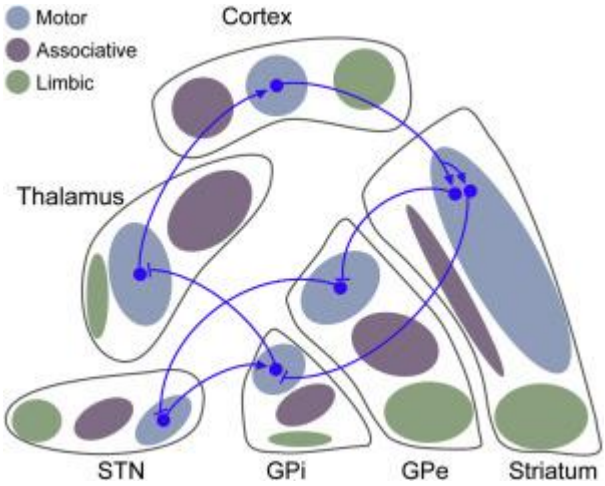

Figure 3 – Parallel Circuit Model of the Basal Ganglia. The activated motor circuit is exemplified. Normal arrows represent excitatory projections and flat arrows inhibitory projections. Adapted from [25].

The increasing incidence of neurological disorders and the growing awareness of DBS as an effective therapy – which is clear by recent supportive government policies and laws – have propelled the DBS global market in the last couple of years. Presently, the DBS global market for PD surpasses the $800 million mark and is expected to reach $1.9 billion ($10^9$) by 2028 [26]. Notwithstanding, the DBS journey was neither short nor obstacle-free, as one will see in the next section.

2.2.1 History of DBS

Although one can make the case that the roots of modern DBS stretch back to experiences of the late 19th and early 20th centuries – where clinicians were using electrodes to explore the functions of various brain areas and identify the appropriate regions for ablative therapy [27] – the first reported use of a stereotactic device happened in the late-1940s (Figure 4). The next decades brought several technological enhancements to the device. However, it was only in the 1980s that the next big step was taken. The advent of lithium batteries allowed the production of neurostimulators that could last several years after implantation, while providing the necessary levels of stimulation.

While these technological increments were taking place, structural changes in the medical devices' regulation – which was now under the purview of the American Food and Drug Administration (FDA) agency and other international regulation bodies – put DBS therapies in a dicey position. Although the skills and expertise necessary to incorporate the technology into working therapies existed, the new regulatory system required robust clinical assessments of efficacy and safety, due to its invasiveness. This was a problem, since neurostimulation treatments still lacked assessment tools to quantify the improvement on the conditions being treated. It was only in 1987 that this problem was cracked, when a consortium of movement specialists established the Movement Disorder Society and created the Unified Parkinson's Disease Rating Scale (UPDRS) – a five-part scale system that determines the severity of all the different aspects of the Parkinsonian symptomatology [28].

Having a standardised tool that enabled patients to be compared before and during treatment and across the globe, DBS was now amenable to undergo clinical trials. In 1997, FDA approved unilateral DBS for extreme cases of essential tremor and PD, but there were still some concerns about long-term adverse effects regarding subtle neurological changes. It would take a couple more years of sponsored trials to broaden the therapy to more general PD cases in the United States of America, a landmark finally achieved in 2002.

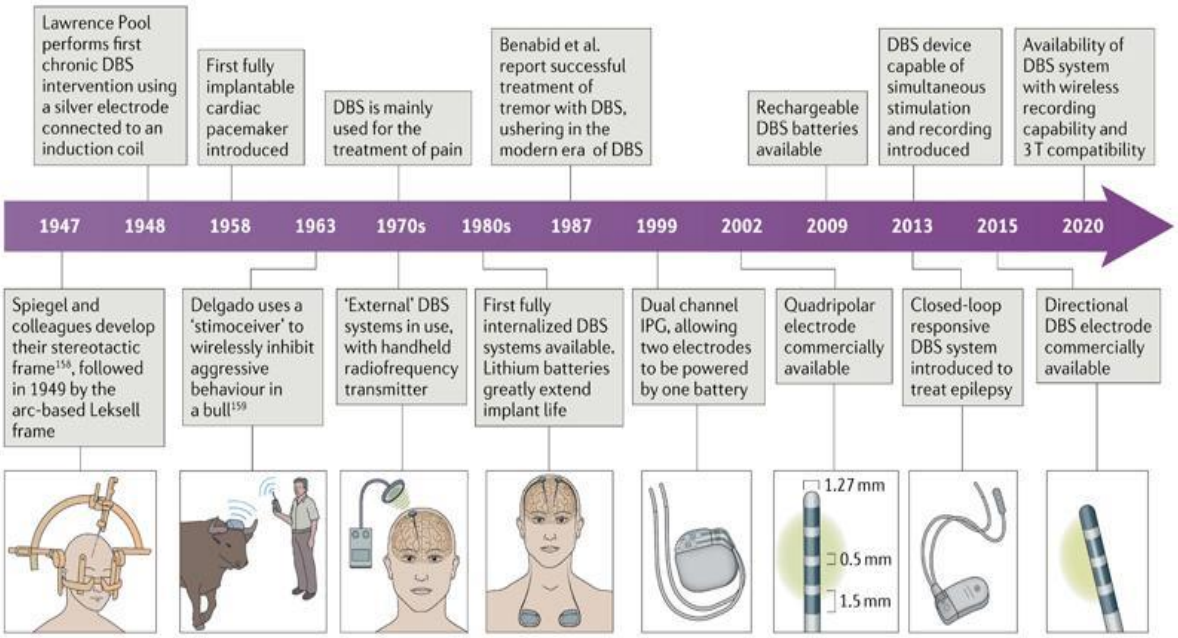

Figure 4 – Timeline of the DBS technology development. From [29].

Since then, the appearance of multiple manufacturers of DBS technology generated a new wave of technological improvements, namely the introduction of electrode designs that can shape the stimulation field, and the ability to simultaneously stimulate and record the brain – which plays a central role in the creation of closed-loop DBS systems.

2.2.2 The DBS Device

Nowadays, a DBS implant is composed of two parts: a thin wire lead (<1.5mm in diameter) with multiple electrodes at the tip, and a pulse generator. These parts are connected by a wire that traverses the neck subcutaneously. While the first is responsible for registering and delivering the electrical signals to the brain, the latter stores the information, communicates with external devices, and generates the electrical pulses for

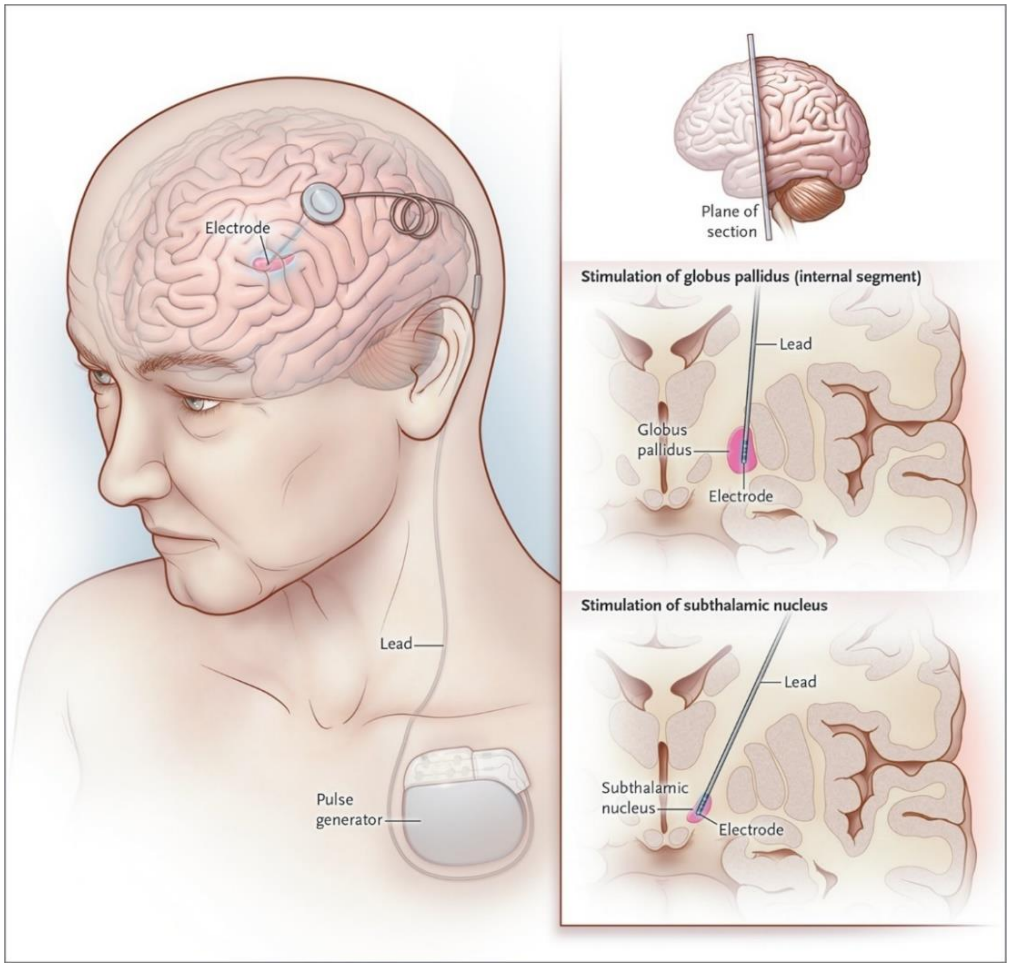

Figure 5 – Electrode and IPG implantation in DBS. The lead is implanted in either the subthalamic nucleus or the internal segment of the globus pallidus. The lead passes through a burr hole in the skull and is connected, under the skin of the scalp and neck, to an impulse generator that is placed at the interior chest wall. From [16].

the stimulation. Since these parts have different target sites, the DBS surgery is divided into two portions.

The two most common DBS target sites for the lead in PD are the subthalamic nucleus (STN) and the globus pallidum internus (GPi) [30], both regions of the basal ganglia-thalamic circuit (see Figure 3). Conversely, the pulse generator is implanted under the skin near the collarbone area, as seen in Figure 5.

Current electrode configurations use segmented rings with 4 or 8 contacts, varying in terms of contact length and inter-contact spacing. This type of configuration (see Figure 6) allows the customization of the stimulation field, which proves to be an effective way of reducing the current threshold for beneficial and adverse effects of DBS, as well as a strategy for compensating small inaccuracies in lead placement [31].

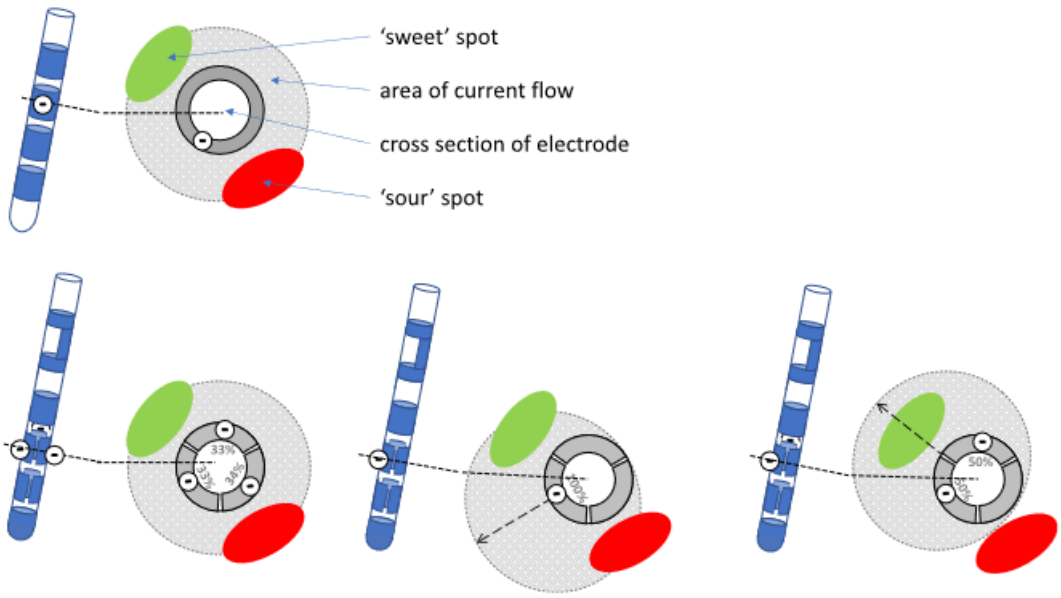

Figure 6 – Concept of directional DBS. Instead of using all 3 segmented contacts of a directional electrode in the same location, one can steer the current flow away from the 'sour' spot by activating only 1 or 2 of the segmented contacts which are oriented towards the 'sweet' spot. From [31].

2.2.3 Existing DBS Technologies

Currently, there are three main manufacturers of implantable DBS devices: Boston Scientific, Medtronic, and Abbott. All three have already introduced to the market electrodes capable of both stimulating the surrounding tissue and recording its electric field, as well as directional leads. Moreover, a new generation of devices with rechargeable batteries has entered the market recently, which claim to prolong the

battery longevity by 3-fold (up to 15 years). Medtronic's Percept™ device is one of the most recent and complex [32]. A significant feature is its ability to record the patient's data outside the clinical environment.

All these companies have also created their own software platforms. These platforms are mainly Patient-Specific Visualization Tools – they allow the change of the stimulation parameters and can display the lead orientation or the stimulating field in 3D representations. Indeed, these platforms are optimised to facilitate DBS in general. However, and even though some include an option of programming stimulation routines, they still lack the necessary tools for closing the therapeutic loop (see section 2.2.4).

Finally, Medtronic has a simple mobile app (Figure 7) that allows the registering of events (e.g., taking medication, feeling well or off, falling, etc.) by the patients with the Percept™ device, outside the clinic. This app is connected to the implant, via Bluetooth, and can command the device to take a snapshot of the brain signal.

Figure 7 – Medtronic's software platform and mobile app for Percept™. The software devices can communicate with the implantable pulse generator, via Bluetooth. From [32].

2.2.4 Conventional DBS and Closed-Loop Adaptive DBS

Though the DBS concept remains almost unchanged since its first application, recent advances in neurophysiology, neuroimaging and neural engineering have uncovered a new paradigm: tailoring DBS to a patient's real-time needs.

The conventional approach to DBS, where the stimulation settings are manually fed into the controller device and then evaluated by the clinician during outpatient visits,

are quite limited. First, it relies on continuous stimulation (cDBS), which has been associated with adverse side effects (such as dysarthria and postural instability) and habituation – i.e., the narrowing of the therapeutic window [33]. Second, cDBS is incapable of differentiating symptom intensity and/or daily activities. This results in periods of stimulation in the absence of symptoms and in situations (that were not anticipated in the clinic) where it may cause discomfort or pain. Additionally, it also causes a significant drainage of the neurostimulator batteries, prompting avoidable replacement surgeries [34].

For those reasons, conventional DBS is being replaced by strategies that automatically optimise these parameters, while considering other important factors such as power consumption and disease severity progression. Closed loop adaptive DBS (aDBS) systems have been hypothesised for decades but only now are some of them being brought to fruition. The aim of these systems is quite straightforward: provide optimal therapeutic results by adjusting the stimulation parameters in real-time, using the patient's own physiological signals [30][35] - [37].

The development of a valid aDBS system relies on three pillars: the choosing of the biomarkers (input variables), the selection of the output parameters, and the development of an algorithm that translates the first into the second. Each will be explored in the next section.

2.3 The aDBS System

2.3.1 Biomarkers

The aDBS system must receive one or more biomarkers as control variables. These biomarkers should reflect ongoing changes in the patient's clinical state. Since there is a high symptom variability across the afflicted, this is a challenging step, for distinct combinations of biomarkers may work better for different patients.

2.3.1.1 Local Field Potentials

Local field potentials (LFP) represent the collective activity of a neuronal population and carry information about their state of synchrony (see Figure 8A). The synchronous activity of the neural tissue is commonly described according to the frequency of oscillation. These frequencies are grouped into different bands, which are described in Table 2.

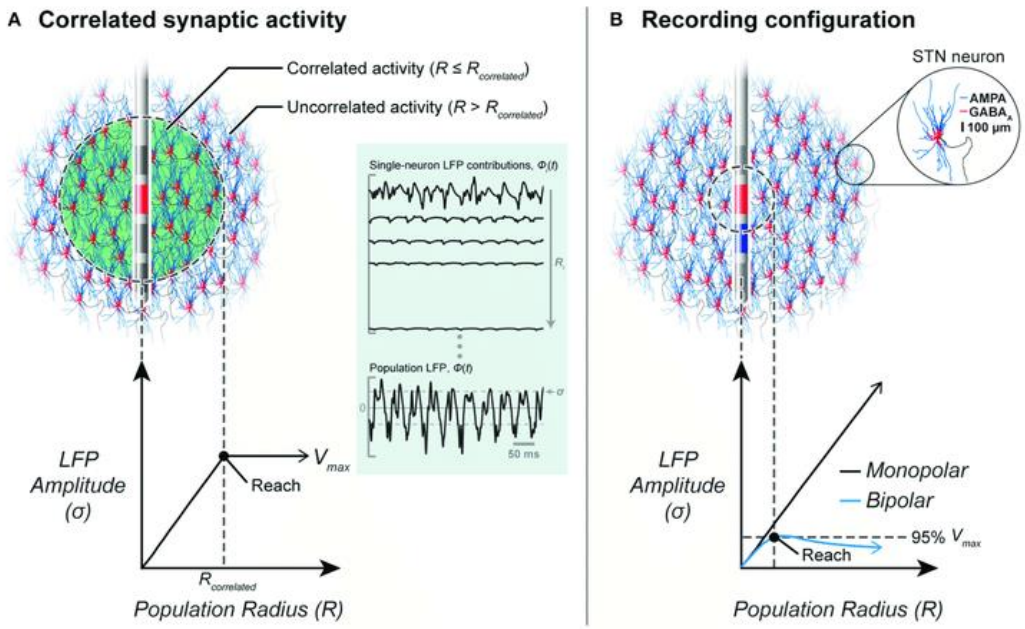

Figure 8 – LFP Recordings from DBS electrodes. (A) Correlated synaptic activity results in the LFP signal. Within correlated regions, an increase in the population radius produces a linear increase in the amplitude of the LFP. Outside of the correlated volume, there is no significant increase in the LFP amplitude. **(B)** For a monopolar recording (red electrode only), the LFP amplitude increases linearly with an increase in the population radius and does not converge to a maximum value. However, a bipolar recording (red electrode-blue electrode) limits the amplitude and spatial reach of the LFP recording. Adapted from [47].

Table 2 – LFP frequency bands described in PD literature.

Designation	Frequency (Hz)	Description
Delta	0-3	Deep, dreamless sleep; no physical awareness
Theta	4-8	Mediation, REM sleep, reduced consciousness; non-motor domains
Alpha	8-12	Relaxed state, awake but drowsy; non-motor domains
Beta	13-35	Mental activity; conscious perception, attention; prokinetic
Gamma	31-200	Heightened perception; extreme attention; processing large amounts of information; prokinetic
High frequency oscillations	>200	Associated with prokinetic activity in the STN

An exaggerated synchronisation of neuronal activity has been observed in the beta band, around both the pallidal and subthalamic regions, in PD patients [38] - [40]. Furthermore, it has been shown that these hypersynchronous activities are correlated with motor sign severity [135], usually assessed with the Unified Parkinson's Disease

Rating Scale part III (UPDRS-III) – a rating tool used to gauge the course of PD in patients, where segment III evaluates the motor abilities [28]. These findings are also corroborated by the fact that using dopaminergic medication decreases beta band activity and improves akinesia, bradykinesia, and rigidity [41]. Interestingly, it has been reported that the presence of dyskinesias is inversely correlated with beta band activity [42].

Other bands of neuronal activity are also thought to be potential biomarkers, such as the theta band and the so-called high-frequency oscillations (HFO) at ~250 Hz, for tremor detection [43][44]; and the gamma band, for hyperkinetic symptoms [45]. It is also worth noting that these bands are affected by daily-life activities, which makes the isolation of disease-related signals even more difficult [46].

The use of LFPs as input for aDBS is advantageous, since there is no need for additional hardware – the signal acquisition can be done by non-stimulating contacts of the implant. However, LFPs are affected by the stimulation pulses – and the literature has yet to converge on what constitutes a stimulation artefact and what derives from effective neurological changes.

2.3.1.2 Motor Biomarkers

Electromyography (EMG) or surface electromyography (sEMG) devices and inertial measurement units (IMU) are used not only in the detection and quantification of tremor, but also in its prediction [34][48].

Tremor is present in most PD cases, mainly occurring in stable positions as rest tremor or in postural positions as postural tremor (see Figure 9). These two types of tremors have different, albeit overlapping, characteristic frequency ranges. A third type of tremor, but less common, is kinetic or action tremor, which happens during voluntary limb movement and has higher frequency ranges. The tremor frequency ranges described in the literature are summarised in Table 3.

Frequency analysis seems inseparable from tremor assessment or quantification. In fact, the most common metrics used to quantify tremor are the RMS value and the power of the signal in or around the dominant frequency. On another note, different machine learning approaches have successfully been used to estimate the severity of tremor.

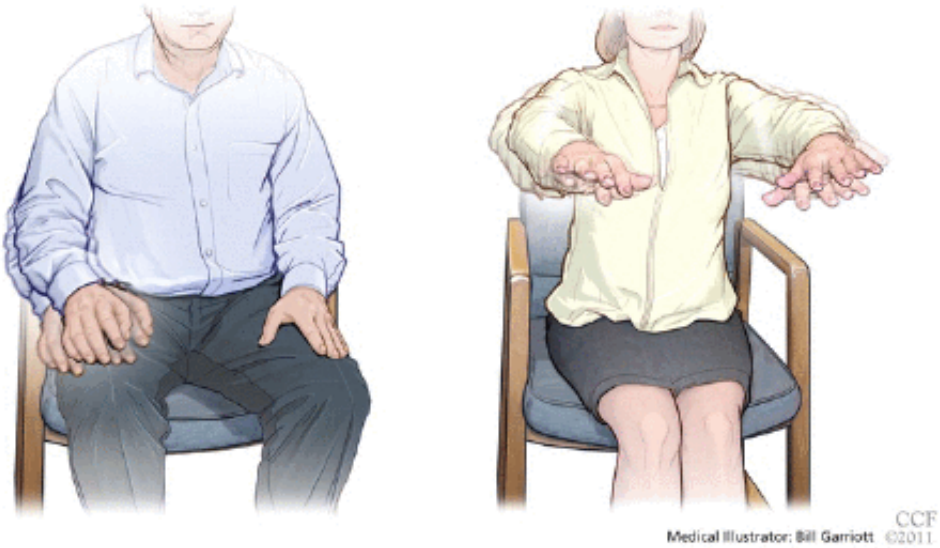

Figure 9 – Representation of rest tremor (left) and postural tremor (right). From [49].

Concurrently, sEMG and IMU sensors can also be used in the quantification of rigidity [50]. Approximately 9 in 10 PD patients frequently experience rigidity episodes [51]. Rigidity in PD (see Figure 10) is commonly described as an opposition to the movement of the arms or legs beyond what would result from normal ageing or arthritis. When compared to the other Parkinsonian cardinal symptoms, rigidity is deemed as the hardest to objectively evaluate. While sEMG can directly measure the muscular activity – reason why it is deemed as the most reliable measurement technique –, accelerometry

Table 3 – Frequency of rest, postural and action tremors in PD.

Tremor / Author	Rest	Postural	Action
Massano & Bhatia [53]	3-6 Hz	6-8 Hz	
Vaillacourt & Newell [54]	4-6 Hz	5-12 Hz	
Heida, Wentink & Marani [55]		4-9 Hz	8-12 Hz
Basu et al. [48]		7-11 Hz	
Baumann [56]	4-7 Hz		
Ferrigno et al. [57]		5-8 Hz	9-13Hz
Buijink et al. [58]	4-9 Hz		

and gyroscopy rely on indirect metrics to quantify the patients' rigidity. Among these are the angular velocity, range of motion, and torque [50].

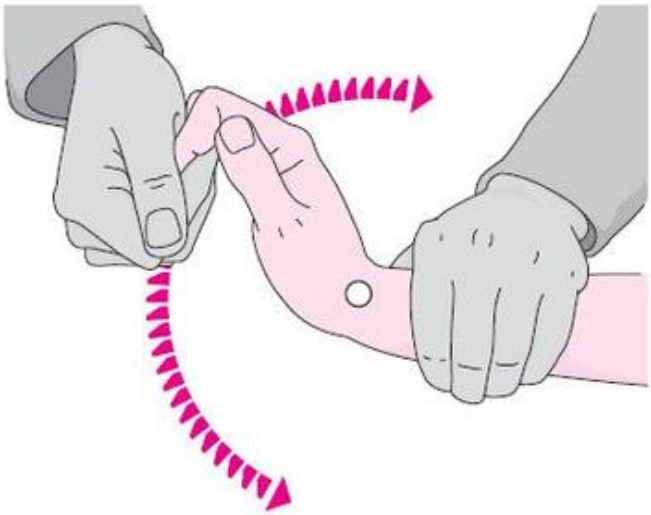

Figure 10 – Representation of a rigidity test in the radiocarpal joint (cogwheel phenomenon). Adapted from [59].

Although both tremor and rigidity are good indicators of the severity of the symptoms, there is still a lack of chronic aDBS systems that incorporate them in real-world settings. The necessary additional equipment as well as the continuous device communication can make their use in such settings impractical, uncomfortable, and battery unfriendly. Moreover, studies suggest that, to integrate a reliable aDBS system, they must be paired with brain signals [52].

2.3.1.3 Other Potential Biomarkers

Cortical signals such as electrocorticography (ECoG) are widely studied for epilepsy seizure detection. In fact, closed-loop systems for epilepsy patients are already commercially available for chronic implants [60]. One hallmark of PD is the hyperactivity of the cortico-basal pathways, where exaggerated beta-gamma phase-amplitude coupling (PAC) is observed [61][62]. An advantage of recording the cortical signals lies on the fact that there is a low sensitivity for stimulation artifacts – the recording area is far from the stimulation site.

Besides electrophysiological signals, stimulation-evoked dopamine responses have been proposed as a control variable for aDBS. Experiments in rodents, showed that DBS caused measurable fluctuations in dopamine levels [63]. However, the

relationship between neurotransmitter levels and symptomatology are still dim and need further studying.

2.3.2 Stimulation Parameters

The parametrization of the output stimulation signal is the probably the main challenge for the development of aDBS systems. While the existence of several different options to modulate the stimulation provides a landscape of opportunities, it also makes research more difficult. In fact, the literature can seem conflicting at times, when concurring studies alternate multiple parameters and end up with different conclusions. The next sections contain an overview of these parameters.

2.3.2.1 Current vs. Voltage

There are two ways of stimulating the nervous system: constant current and constant voltage. While the first maintains the current intensity between the electrode and the surrounding tissue by varying the voltage (according to the interface's impedance), the latter fixes the voltage levels and generates a dynamic current, which is linearly dependent on the electrode-brain impedance. Although both alternatives have shown therapeutic effect on PD patients, the capacitive components in the electrode-brain interface provoke differences in the volume of tissue activated (VTA), and possibly in their effects.

While the first DBS applications relied on the constant voltage mode – mainly because the device was developed from a cardiac pacemaker – constant-current stimulation has been the preferred mode in the past decades. A possible reason for preferring this type of stimulation is that the electrode-brain impedance changes over time, especially in the first months after surgery [64].

2.3.2.2 Monopolar vs. Bipolar

The stimulation can also be monopolar or bipolar. In the first, the stimulating contact in the brain acts as the cathode and the pulse generator's contact with the chest wall as the anode, whereas, in the latter, both poles are in the brain. More specifically, there are different types of bipolar pulses, as shown in Figure 11. Despite sharing many similarities, the monopolar and bipolar modes differ in some fundamental ways. It has been reported that impedances are generally greater during bipolar stimulation. This results in a smaller VTA (see Figure 8B), which in turn leads to higher thresholds for both symptomatic efficacy and potential side effects [66]. Interestingly, although bipolar stimulation needs higher current amplitudes to achieve the same VTA of monopolar

stimulation, it seems to be more energetically efficient than monopolar in long-term implanted patients [66].

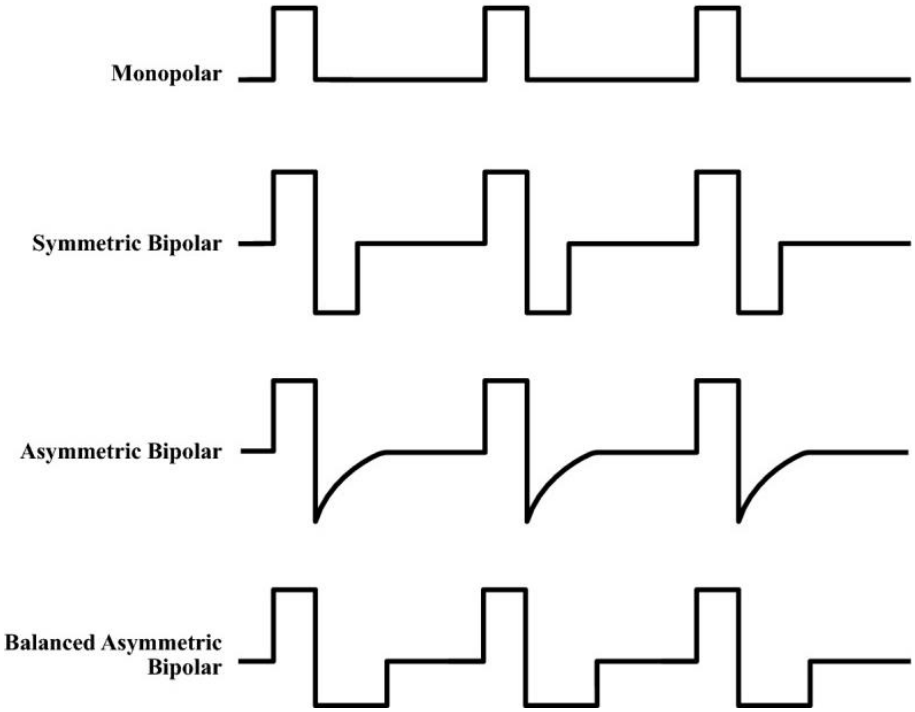

Figure 11 – Examples of pulses used for functional electrical stimulation. Adapted from [65].

2.3.2.3 Pulse Modulation

Regardless of the mode of stimulation chosen, the electrical pulse has three changeable parameters: amplitude, frequency, and pulse-width (see Figure 12). Most aDBS systems in PD until now are based on automatic amplitude modulation (AM) [36]. A possible reason may be the fact that current amplitude directly influences the VTA in the brain. By increasing the amplitude, we are also increasing the chance of activating a region that will alleviate the symptoms. However, this can also be said for regions that provoke adverse side-effects. Thankfully, this problem can be overcome by combining AM with directional DBS.

Besides amplitude modulation, aDBS systems can explore frequency or pulse-width variations. While low-frequency stimulation tends to worsen the cardinal symptoms of PD, high frequencies have shown promising therapeutic benefits [67][68]. However, some studies have shown suboptimal results in some patients at certain high frequencies [69], which suggests that frequency modulation may prove itself useful in the tailoring of this therapy. It is also hypothesised that pulse-width modulation provides clinical benefits

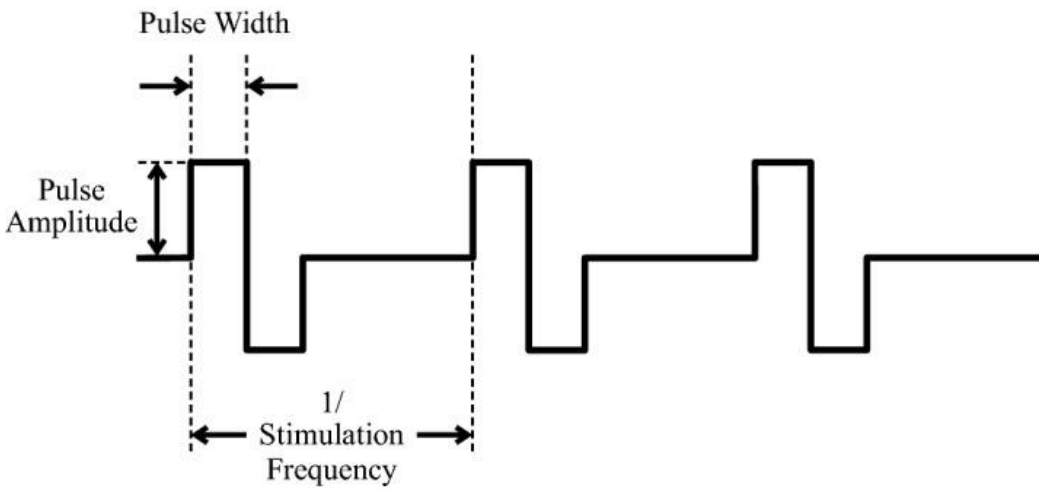

Figure 12 – Functional electrical stimulation parameters. Adapted from [65].

by exciting brain sites more selectively, while still increasing therapeutic windows (the difference in amplitude between the first meaningful improvement and the first intolerable or persistent side effect) and using less energy [70][71].

2.3.2.4 Directional Steering & Bilateral Stimulation

Another major stimulation paradigm is current steering, which consists in the delivery of different current pulses through different contacts on the same electrode, allowing the

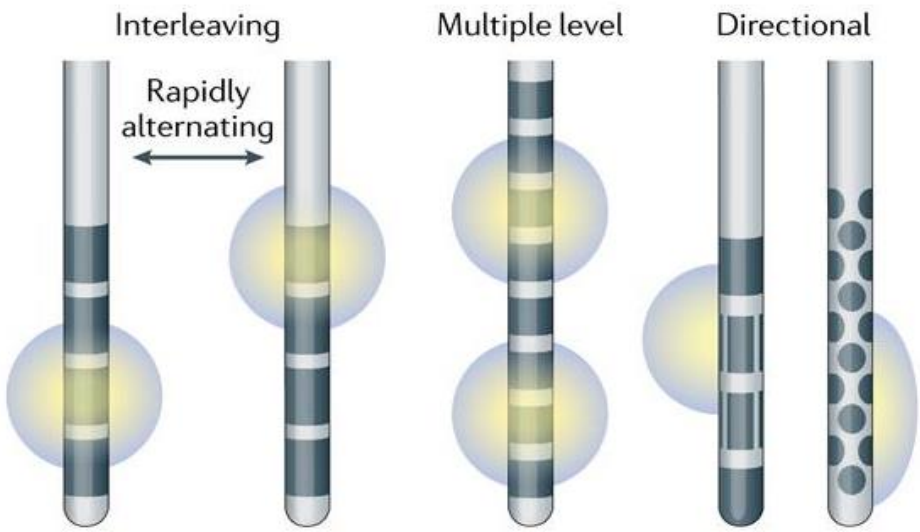

Figure 13 – Current steering in DBS electrodes. Interleaving stimulation refers to the alternation of different stimulation settings. Multiple level stimulation enables multiple neural targets to be stimulated, along the electrode trajectory. With directional stimulation, current can be directed or 'shaped' according to local anatomy or clinical symptoms**.** Adapted from [29].

shaping of the electric field, as in directional DBS or multilevel DBS (see Figure 13). The new electrode designs permit the electric field to steer both along its axis and orthogonally. A special type of current steering is interleaving stimulation, which consists in the alternation of two “programs” through the different contacts. It has been suggested that this method of stimulation reduces side effects in some cases [72].

It is known that every person has a unique brain anatomy. In fact, even within a person, one finds such differences between hemispheres: numerous studies have shown that hemispheric asymmetries are ubiquitous [73]. In other words, they occur in almost all neurological functions. Thus, in the same way that current steering explores the use of different stimulation parameters within the same electrode, aDBS systems can evaluate and adjust the stimulation per hemisphere, as in bilateral stimulation [75].

2.3.3 Algorithms

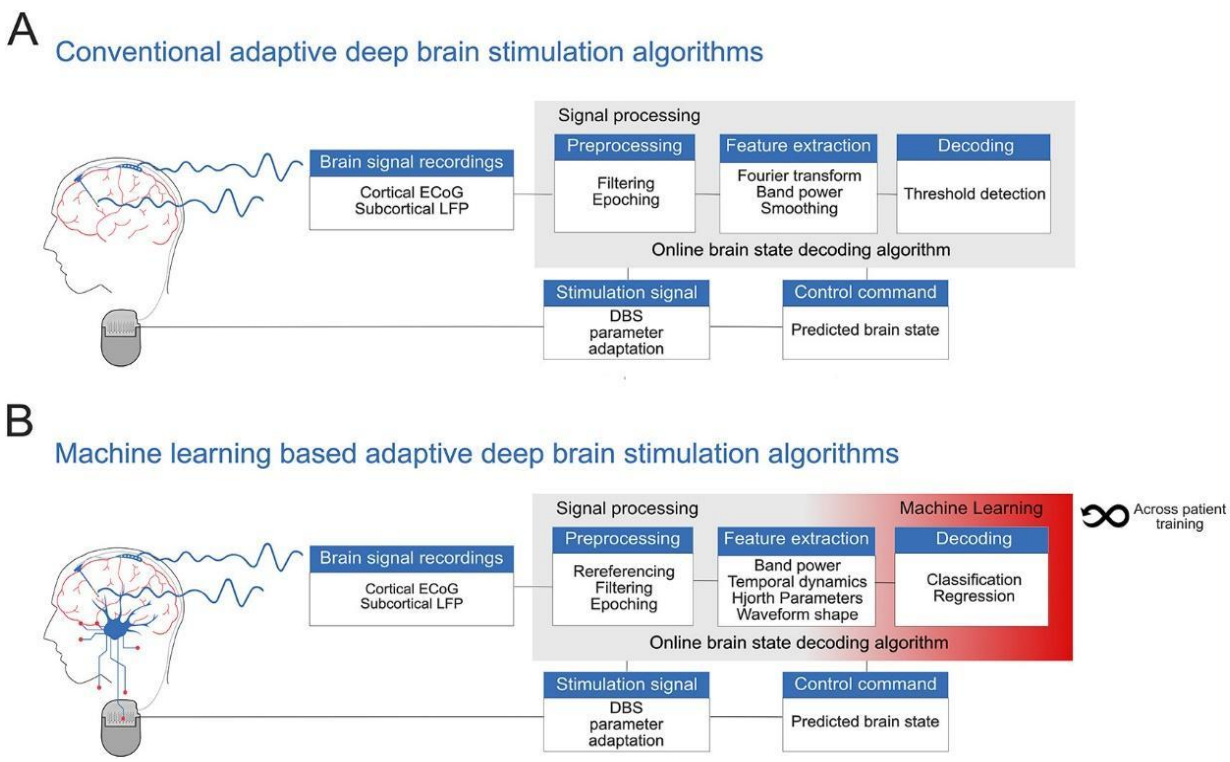

Figure 14 – Schematic representation of a conventional adaptive deep brain stimulation algorithm compared to a machine learning-based adaptive deep brain stimulation system. (A) The control algorithm is a simple threshold detection of a predefined feature: the brain state (e.g., pathological or non-pathological state) is predicted, and translated into a control command, such that the DBS stimulation parameters are adapted. **(B)** Machine learning-based adaptive deep brain stimulation can use multimodal features to decode a variety of brain states (e.g., classification for decoding of tremor or regression for indication of severity of bradykinesia in PD) and translate them into adequate stimulation parameters. Adapted from [75].

There are two major groups of algorithms in aDBS: the conventional and the machine-learning based. And, even though the overall aDBS loop remains the same, as illustrated in Figure 14, the overall implications of their use are significantly different.

2.3.3.1 Conventional Algorithms

As previously mentioned, the most common approach in aDBS involves automatic amplitude modulation (AM). There are three main paradigms in AM: ON/OFF, gradual, and continuous (see Figure 15).

In ON/OFF systems the amplitude alternates between a predefined amplitude (and fixed frequency and pulse width) and zero. In conventional algorithms, the transition between these two states is triggered when the recorded signals exceed or go below a certain threshold [76]. Furthermore, ON/OFF systems can implement other stimulation

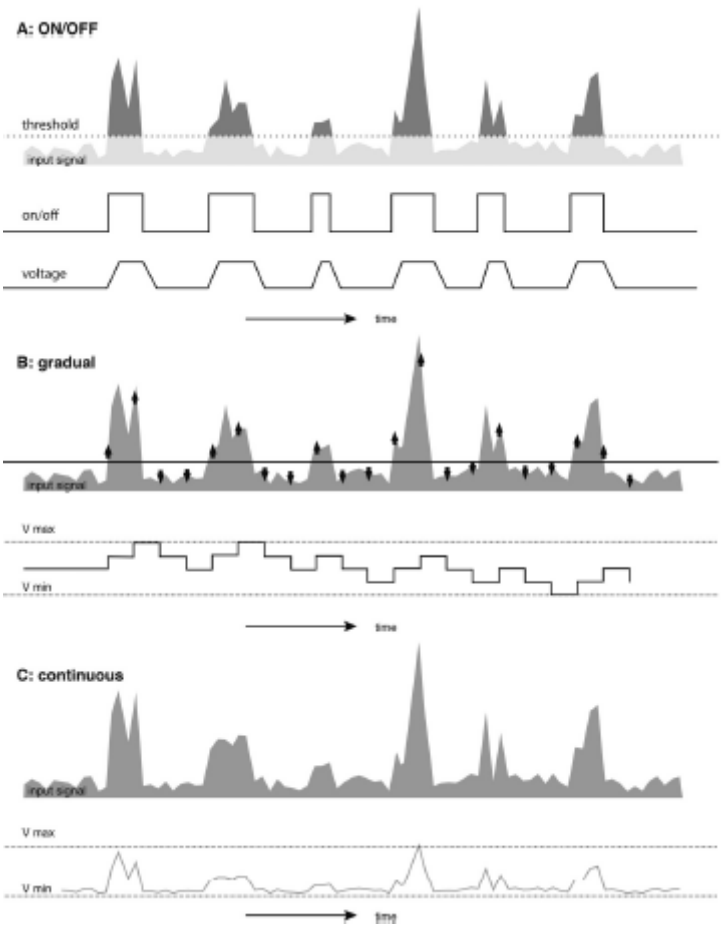

Figure 15 – The different types of amplitude modulation. (A) In the ON/OFF paradigm, the stimulation occurs when the input signals exceed a certain threshold. **(B)** In the gradual paradigm, it increases or decreases stepwise when input signal exceeds or does not exceed a certain threshold respectively. **(C)** In the continuous paradigm, the stimulation amplitude is modulated according to the strength of the input signal. From [36].

features such as ramping onsets [77] (to avoid abrupt changes in voltage) or phase-dependent stimulation [78] (in which a stimulus is applied with a fixed latency to an input signal). Gradual AM systems have multiple amplitude steps – with minimal, maximal and step amplitudes predefined – that can increase or decrease also via thresholds. Finally, continuous AM uses the input signal as the output, after rescaling it to a predefined range [79].

A major limitation of the conventional algorithms is that they lack the required symptom- and situational-specificity. In other words, different symptoms or activities (e.g., sitting, walking, and sleeping) may demand different thresholds – and these algorithms are scarcely able to make such distinctions.

2.3.3.2 Machine-learning based Algorithms

The advent of machine-learning revolutionised the scientific landscape, pervading nowadays every field of research. However, due to the recentness of the aDBS field, its application is still relatively unexplored.

When compared to conventional algorithms, machine-learning techniques show the highest potential in achieving highly personalised treatments [95], for they allow the recognition of different and more complex patterns of neuronal and motor activity. Yet, they do not come without disadvantages. While thresholding can be promptly applied without requiring much data, ML models must be curated in an offline state (during which the training and validation stages occur) and tend to require larger amounts of data – resulting in time-consuming individual training sessions [75].

During model training, features are extracted from the training data. These features can be manually selected – a recurrent situation when a field's literature converges towards an agreement. Otherwise, unsupervised learning allows the most relevant features to be selected. The predictive model, either for classification or regression, is obtained by optimising the parameters that transform input features into known outputs. Once the model yields satisfactory performance metrics on the training data, the learned parameters can be directly applied to the features of new data. A model in which training and testing performances remain similar is considered good.

Some studies have developed ML models that use LFPs in aDBS systems, both in animals [92] and humans [91]. Moreover, ML is also being employed in the recognition of behavioural activities [86][87] – a limitation of conventional aDBS algorithms. The used ML models vary from simple Support Vector Machines (SVM) or Linear Regressions (LR) to more complex hierarchical Multi-kernel Learning (MKL) and Convolutional Neural

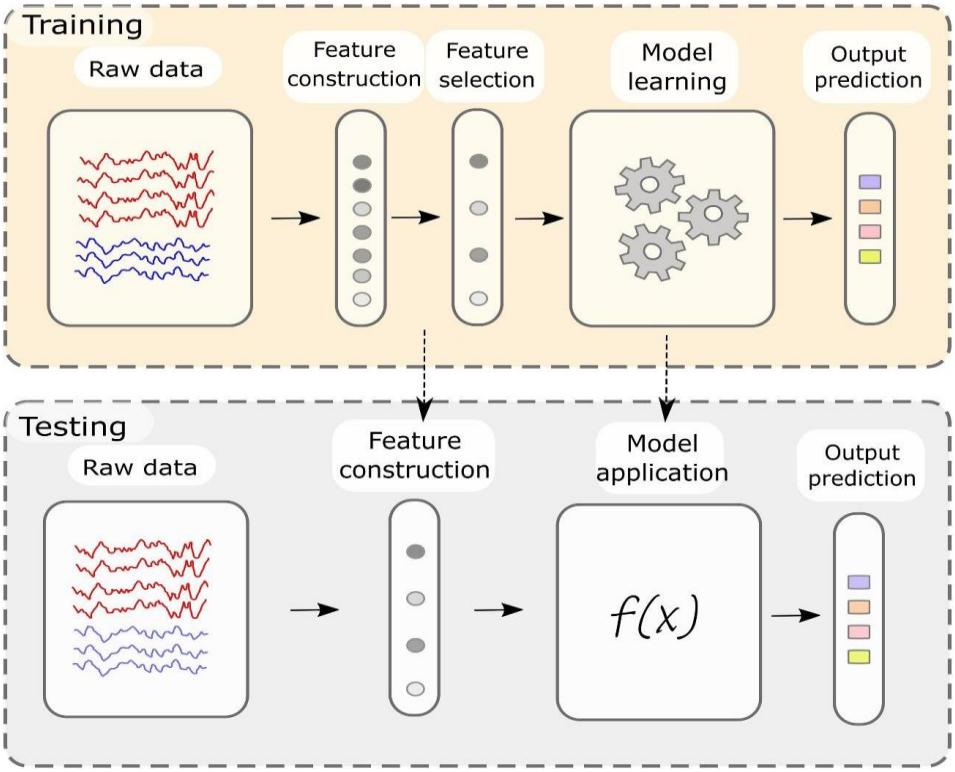

Figure 16 – Representation of a machine-learning pipeline. During model training, features are extracted from the training data. The prediction model, either for classification or regression, is based on optimized parameters that transform input features into predicted model output. During training, parameters are optimized. Once the model yields satisfactory performance metrics on training data, the learned parameters can be directly applied to new input features for test set model predictions. A good decoding model is a model in which training and testing performances remain similar. From [75].

Networks (CNN). Some of the developed ML-based algorithms for aDBS are shown in Table 4.

Table 4 – Examples of machine-learning based algorithms in the aDBS literature.

Method	References
Support Vector Machine (SVM)	[84] [85] [86] [87] [89] [91] [92]
Random Forest (RF)	[80]
Logistic Regression (LR)	[82] [90]
Decision Tree (DT)	[81]
K-Nearest Neighbours (KNN)	[93]
Hidden Markov Model (HMM)	[89]
Gaussian Mixture Model (GMM)	[84]
Neural Networks (NN)	[81] [83] [94]
Convolutional Neural Networks (CNN)	[88]
Multiple Kernel Learning (MKL)	[86] [87]

Finally, it is also worth mentioning that ML algorithms can be used beyond the loop of aDBS systems. In fact, they prove to be useful for DBS in general, namely in the prediction of the optimal treatment regimens for PD patients. In one study, a ML model estimated the optimal stimulation and medication dosage based on patient-specific details, such as the preoperative response to levodopa [96], while in another it used preoperative patient and disease characteristics to predict the best stimulation frequency out of two alternatives [97].

2.4 Wearables in aDBS

Since the cardinal symptoms of PD are motor, wearables that can successfully detect and quantify them go hand-in-hand with aDBS [98][99]. Wearables are considered minimally or non-invasive electronic devices that detect, analyse, and transmit information concerning either body signals or ambient data [100]. Most of the wearable-based aDBS systems rely heavily on machine-learning approaches for distinguishing symptoms from voluntary movements [36][101]. In order to understand how these technologies can integrate the feedback mechanism of the aDBS framework, first we must comprehend how they reflect the ongoing changes within the patient. In other words, how effective and consistent is the characterization of the Parkinsonian symptoms.

2.4.1 Wearables for Tremor Analysis

Tremor is perhaps the most studied and well-documented symptom in PD. In fact, beyond tremor, no other PD symptom has yet been systematically used with success on wearable aDBS systems. As was previously shown in Table 3, there are three types of tremor: rest, postural and kinetic (action). The most common monitoring systems for tremor involve the use of inertial measurement unit (IMU) sensors – which include accelerometers, gyroscopes, and sometimes magnetometers. These sensors are usually placed in the upper limbs, more concretely in the wrists or fingers. An alternative to IMU-based wearable systems are the EMG-based systems, that rely on electrodes that can be placed in the posterior and anterior arm. Regardless of the type of sensor chosen, tremor assessment is usually based on rhythmicity and frequency analysis. Some of the existing wearable systems implemented for tremor analysis in the literature are summarised in Table 5.

On a sidenote, some wearables can also assume a therapeutic role in tremor suppression [107].

Table 5 – Examples of wearable systems used for tremor analysis. Based on [102].

Reference	Method	Placement on body	Parameters
[34]	Electromyography Accelerometer and gyroscope	Upper limbs	Frequency of the peak power
[103]	Accelerometer (in smartphone)	Unknown	Maximum amplitude acceleration Peak power, median power and power distribution of acceleration
[104]	Accelerometer and gyroscope	Index finger	Amplitude
[105]	Accelerometer	Upper and lower limbs	Root mean square of acceleration
[94]	Electromyography Accelerometer	Forearm Index finger	Frequency of the peak power, peak power Entropy, Recurrence Rate
[106]	Accelerometer, gyroscope, and magnetometer	All body	Root mean square of angular displacement

2.4.2 Wearables for Rigidity Analysis

Rigidity is, perchance, the hardest cardinal symptom to evaluate [108]. While EMG sensors are the most suitable for its detection and quantification – because they allow the direct monitoring of muscular tone –, other types of sensors, such as IMUs, potentiometers and torque motors, have been used with the same intent. Besides muscular tone, the most relevant parameters in the evaluation of rigidity are angular velocity (measured by the gyroscopes), range of motion (ROM) and torque (measured by potentiometers and torque motors).

Table 6 – Examples of wearable systems used for rigidity analysis.

Reference	Method	Placement on body	Parameters
[109]	Torque motor Electromyography	Wrist	Position, Torque Range of motion
[108]	Accelerometer, gyroscope, and magnetometer	Upper limb	Total power Smoothness Fatigability
[110]	Accelerometer and gyroscope	Hand	Average angular velocity Average angular velocity peak value

A tell-tale of the difficulty in the assessment of rigidity is the fact that the used protocols vary significantly between studies, as well as the sensor placements. Some of these attempts are summarized in Table 6.

2.4.3 Wearables for Other Symptoms

Bradykinesia, another cardinal symptom of PD, can be defined as “slowness in the initiation and execution of movement”. This slowness can be experienced at several levels, namely in fine motor coordination (e.g., handwriting [113]), changes in walking, episodes of freezing, and difficulty turning in bed or rising in a chair. While rigidity can also be a cause of slowness – for it generally affects the muscular engagement – bradykinesia deals with the motor velocity *per se*. Numerous studies have employed wearables, often IMUs, in the quantitative evaluation of this symptom [111][112].

The study of gait is also well-established in the PD literature, for it represents one of the highest vulnerabilities in a patient – i.e., the risk of falling, and, consequently, acquiring long-term disabilities. The two most common gait disorders are shuffling gait, where the patient exhibits a bent posture and tends to take very small steps, and freezing of gait, where he is frequently incapable of taking any. Nowadays, there are several mobile apps that use the smartphone’s accelerometer to monitor the changes of walking patterns (e.g., step length and step frequency) [114]. IMUs are also extensively used for this purpose [115]. Moreover, gait analysis can rely on motion sensing technology, such as camera-based optical motion-capture systems [116], or on piezoelectrical devices [117].

Finally, there are multi-modal wearable systems capable of assessing multiple symptoms, depending on the task [102][118].

2.5 Computational Tools for aDBS

Despite the significant technological advances in the DBS field, the clinicians still play a vital role in the interface between said technologies and human application. While they bear the moral responsibility of keeping up to date with their fields, it is not reasonable to expect them to know the intricacies of any given novel device or algorithm. Thus, it is crucial to provide them with clear instructions of use and with intuitive tools, in the form of software applications.

Before the integration of automatised aDBS systems in a clinical environment, one must develop first clinically validated systems. And, for that, signal analysis tools are

required. Medtronic has laid the foundations in the creation of valid aDBS systems with its investigational prototype research-only system (Activa™ PC+S-Nexus D3) [119].

More recently, in 2021, the company initiated a randomized study [120] using the state-of-the-art neurostimulator Percept™ PC, which extends the study and treatment to outside the clinic. This study involves several medical facilities, throughout the US and Europe. The recent nature of the Percept™ PC device + BrainSense™ Technology is reflected on the lack of dedicated, extensive, and fully functional computational tools for the analysis of the data it generates. In fact, up to the time of delivery of the present thesis, only two open-source toolboxes have been reported: Perceive Toolbox and Percept Toolbox. It is worth stressing that none of these are incorporated in a graphical user interface (GUI) – i.e., they come as a bundle of functions. Both are further explored in the next sections.

2.5.1 Perceive Toolbox

The Perceive Toolbox was developed for research purposes, using custom-written scripts in MATLAB, by W. J. Neumann's group (Interventional & Cognitive Neuromodulation, Charité Berlin, Germany). The toolbox (v.02, available on https://github.com/neuromodulation/perceive) has the following main functionalities:

- Opens the .json files generated by the BrainSense™ system and creates new folders to allocate the data, in data files corresponding to the specific aspects of the recording session (e.g., Calibration, Streaming, Survey, etc.).
- Converts the data files to other formats, so that they can be used in other programming languages.
- Removes ECG-related artifacts.
- Plots raw signals.
- Converts time domain signals to the frequency domain.

The toolbox has been used in a study that characterised diurnal fluctuations in beta amplitude in PD patients under cDBS [121].

2.5.2 Percept Toolbox

The Percept Toolbox (available on https://github.com/YohannThenaisie/PerceptToolbox) was designed by Y. Thenaisie et al. (Lausanne University Hospital Barth Keulen, Switzerland), also using MATLAB. Its features include:

- The extraction of the data contained in the .json files generated by the BrainSense™ system.
- Conversion from time domain to frequency domain.
- Several plotting options (raw signal, spectrogram, power spectrum, etc.).

A report that explored the potentialities and pitfalls of the Percept™ + BrainSense™ system used the toolbox for data analysis [122].

2.6 Perspectives on Current Work & Critical Appreciation

The galloping advances in the aDBS research field are not yet reflected on the clinical scene. There, conventional forms of DBS, alongside old methods of subjective symptom evaluation, still prevail. Thus, the gradual conversion of the first to aDBS systems must be accompanied by the transformation of the second into objective methods of quantification. The versatility and reported feasibility of wearables allows the second of these transformations to take place (especially in the case of Parkinsonian tremor), even in an open-loop framework. Indeed, the introduction of reliable wearable systems in the clinic would not only exempt the clinicians from the risk of misevaluating the intensity of a symptom (which, in an open-loop framework, could result in the selection of suboptimal stimulation parameters), but also encourage their trust in future automatised systems, where wearables play a complementary role. Expanding on this idea, wearables can pave the road to the normalisation of probabilistic maps of clinical response (i.e., basing the stimulation routines of a patient on previously catalogued responses of patients with similar physiological profiles), through ML-based algorithms.

Nonetheless, before the dissemination of aDBS therapeutic systems, several challenges must be overcome. A handful of them stand at the level of biomarker selection. So far, the top contender pertains to the LFPs – i.e., the beta band power [16][38]. However, recent studies deem other bands of activity as equally or more relevant for some symptoms. Moreover, the LFPs are affected by the stimulation pulses and the literature has yet to properly depict what constitutes an artefact and what stems from actual neurological changes. Finally, the scarcity of outside the clinic data entails the lack of robust chronic biomarkers – for aDBS systems must be capable of navigating through the patients' everyday actions while differentiating pathological from non-pathological activities. Further studying of physiological data in chronic environments must happen before some of these problems can be solved.

The choosing of the type of control algorithm also presents some challenges. While conventional algorithms (thresholding being by far the most popular) are relatively easier to implement, they are devoid of situation-specificity and incapable of detecting temporal-dynamics (e.g., patterns of LFP activity that have pathological manifestations in a delayed fashion). The use of ML-based algorithms seems to tackle these issues. Nevertheless, large datasets will, most likely, be needed. Computational tools that integrate comprehensive visual and analytical functionalities may facilitate the handling of large datasets and, consequently, the creation of ML models. Moreover, if on a graphical user interface (GUI), these tools could help non-data scientists (or clinicians) in their practice.

Finally, even the hardware will require improvements, namely on the re-chargeability and memory fronts. The latter is of the utmost importance, for large amounts of high-resolution data may be necessary to achieve optimal therapeutic performances. Some electronic alternatives, such as memristors and other neuromorphic devices, have been put forward recently [123]. These types of devices promise to reduce the computational and energetic costs, while maintaining the therapeutic efficacy. On this score, only the future will tell.

Part II
Methodologies and Results

Chapter 3

Wearable Glove System

One of the goals of this thesis was to provide the clinicians with a wearable system that could record and store the patient's motor activity, while also providing objective metrics for the quantification of Parkinsonian symptoms. Despite the advancements in DBS technology of the past few years, the clinicians still rely on the UPDRS-III scale to evaluate the symptoms intensity. It is true that this scale played a pivotal role in the implementation of DBS as a therapy, nonetheless it is a subjective tool, insofar as it strictly relies on human judgement. The automatization of this process would, thereby, reduce human errors and biases, while also constituting a first step in the creation of future autonomous aDBS systems.

Wearable systems that perform accelerometry and gyroscopy are already available in the market. However, most of them are expensive, not easily adaptable to clinical use, and/or limited to specific applications. Since we aspired to keep the costs low and the setup as versatile as possible, we created our own system using off-the-shelf components: a textile fishing glove, Velcro stripes, two MPU-6050 integrated sensors, and an Arduino Mega2560. As for software, the system relied on the Arduino IDE (with additional libraries) and MATLAB.

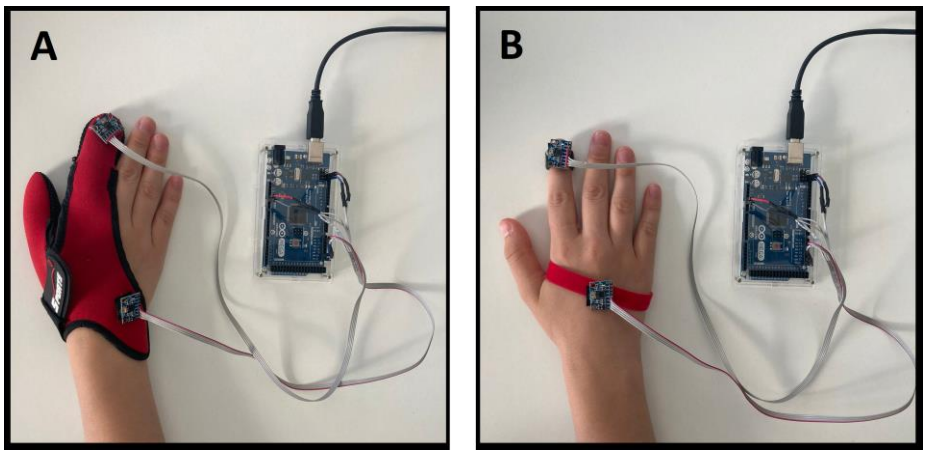

Figure 17 – Main and alternative setups of the wearable system. Light and long wires connect the sensors to the Arduino board. **(A)** In the main setup, the sensors are attached to a fishing textile glove by small Velcro squares. **(B)** In the alternative setup, the sensors are attached to Velcro stripes that go round the finger and hand.

3.1 Setup

The setup in Figure17A allows the attachment and detachment of the integrated sensors to the glove, enabling the assessment of tremor and rigidity either in the left or right hands. This represents an asset, for the symptom intensity may be unsymmetric (as the disease's progression in the brain) and easier to discern on one side. Special attention was given to the stability of the docking between sensor and glove. Several tests were made to ensure a tight mechanical coupling and, consequently, good quality recordings. An alternative setup was devised (see Figure 17B), for the cases where the glove does not fit the patient.

3.2 Hardware

3.2.1 Arduino Mega2560

There are many Arduino boards commercially available, which differ not only in features and design, but also in their footprint and processing capabilities. Most Arduino boards are based on the ATMEGA AVR microcontroller, which offers both digital and analog pins as well as pulse width modulated (PWM) outputs. Additionally, all boards can be programmed with an open-source software named "Arduino", a C-based programming language.

For the present work, the Arduino Mega2560 was chosen for a couple of reasons. First and foremost, it has two ports for I2C communication, with built-in pull-up resistors,

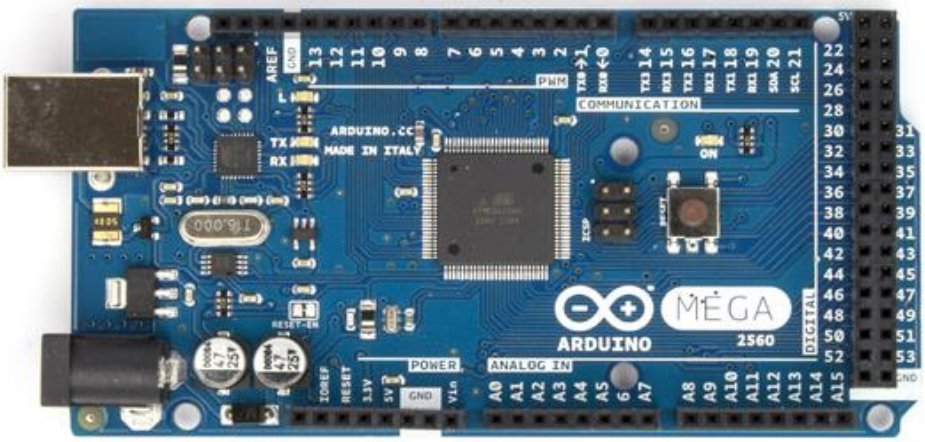

Figure 18 – An Arduino Mega2560 board.

allowing us to simply connect each sensor to a port. Second, it uses a more capable processor. Finally, it can run on 5V, the recommended voltage source for most of the sensors. To protect the board, we acquired an acrylic enclosure, specifically designed for Mega2560.

3.2.2 MPU-6050

MPU-6050 is a Micro Electro-Mechanical System (MEMS), consisting of a 16-bit analog to digital converter, that can also solve complex calculations. It contains a 3-axis accelerometer and a 3-axis gyroscope: the first measures the acceleration of the body

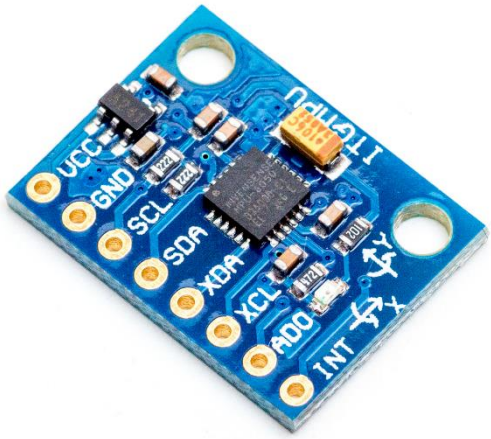

Figure 19 – A MPU6050 sensor. The orientation and polarity of rotation are written in the chip.

along each of the three axes; the latter assesses its angular velocity, also in the three axes.

While tremor is generally present at the hand level, it also occurs, at a finer level, in the thumb and index-fingers, causing the so-called “counting money” or “pill rolling” movement, shown in Figure 20. Most studies employ only one sensor, either in the index-

Figure 20 – Illustration of “pill-rolling” movement. From [124].

finger or in the back of the hand, depending on the task involved. Since we wanted our system to be versatile, we opted for a 2-sensor system that incorporates both the locations: thereby, reducing the chances of losing some valuable information and expanding the range of motor tasks at our disposal.

GY-25, a different type of integrated sensor, was also considered during the preliminary stages of the work. While it had its advantages over MPU-6050, such as:

- ↑ Smaller size (11.5mm × 15.5mm vs. 15.5mm × 20.2mm).
- ↑ Ability to communicate via I2C or Serial (instead of just I2C).
- ↑ Capability of calculating the orientation (Euler angles).

, it also had serious disadvantages:

- ↓ No address pin (that would allow an easy differentiation between two sensors).
- ↓ No personalised Arduino library (as in the case of MPU-6050).
- ↓ I2C and power supply pins on opposite sides of the chip (higher restriction of movement when connected to wires).

Given the relevance of the disadvantages of the GY-25, it was decided not to use this integrated sensor in the final version of the wearable glove system.

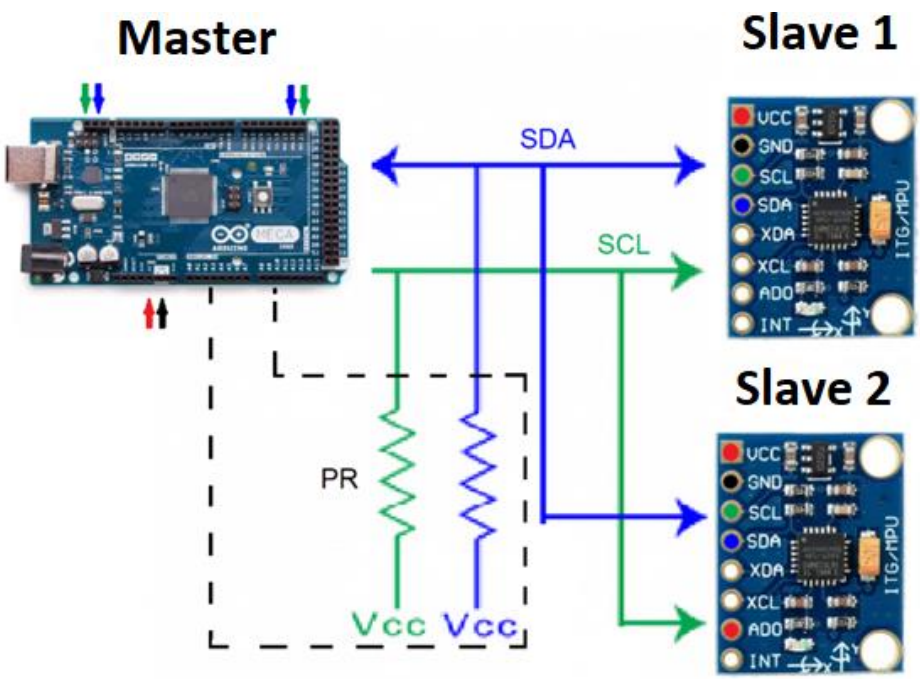

Figure 21 – I2C communication scheme. The MPU6050s are connected to the Arduino board at the pins indicated by the arrows. The pull-up resistors (PR) are intrinsic to the board. The MPU6050s' VCC and GND wires are wielded together and connected to the board's 5V and GND pins. One of the MPU6050 has the address pin connected to the VCC pin.

3.2.3 I2C Wiring Diagram

The I2C protocol can connect up to 127 devices via bus and it only requires two data wires: SDA and SCL. When the device configured as master wants to communicate with a slave it sends pulses through the SDA line, synchronized by the clock carried in the SCL line. The transmitted data includes the address of the slave (7 bits), and the remaining bits specify whether the master wants to read or write. In the present case, the Mega2560 board is the master and each MPU6050 is a slave.

By default, both MPU6050 sensors have the same address. To generate different addresses, we connected the ADD pin to the VCC pin in one of the sensors. The scheme shown in Figure 21 displays how the different hardware components communicate. It is worth noting that the pull-up resistors are intrinsic to the Mega2560 board.

3.3 Software

3.3.1 Arduino IDE

Arduino IDE is the official software to write and upload code to the Arduino boards. It is an open-source software that can be directly downloaded from the official Arduino website (https://www.arduino.cc/en/software). It is easy to use and contains numerous libraries and built-in examples. The version used in this thesis was 1.8.19.

Any Arduino code must have two main functions: setup() and loop(). The first runs only once, and is used to configure pins, initialise variables, set timers, and establish connection with other devices. The latter runs repeatedly and includes all the processes and conditions that we want to execute or evaluate.

In the present case, the setup function is used to:

- Initialise variables, including the sensors – making use of extra libraries (Wire and MPU6050).
- Establish the I2C communication between the MPU-6050 sensors and the Mega2560 board.
- Open the Serial communication between the Mega2560 and the desktop, sending metadata (sampling frequency and sensor ranges).
- Set a timer to guarantee a sampling frequency of 100 Hz.

Section 3.3.1.1. contains a more detailed explanation of the libraries used. Conversely, the loop function is used to:

- Fetch the data from the sensors.

- Send the data via Serial port, whenever a condition is met.

This condition is dependent on an interrupt routine, which is further explored in Section 3.3.1.2. Additionally, a function was created to keep the loop code as concise as possible. This function concatenates the values fetched from the sensors in a single string, so that it they can be sent via Serial port at one go.

3.3.1.1 Libraries

The Arduino IDE includes by default several useful functionalities, ranging from mathematical operations to analog and digital communication. These functionalities are all part of libraries. And just like most programming platforms, the Arduino environment can be extended through the use of additional libraries.

Besides the base-libraries, the present wearable glove system uses two extra ones: Wire and MPU6050. The first allows the device to communicate via I2C protocol; the second, designed by Electronic Cats [125], is specifically made to facilitate the use of MPU-6050 sensors (i.e., no need for “hard-coding”).

3.3.1.2 Timer & Interrupt Routine

Most Arduino models come with a 16 MHz clock, the Mega2560 included. Furthermore, they also come with timer functions, which are essentially counters. These timers are controllable, insofar as we can prescale them and change them in runtime.

Interrupts are one of the most useful features of Arduino programs, especially for solving timing problems [126]. An Interrupt Service Routine (ISR) is carried over, whenever a set timer reaches its limit or meets a certain condition, causing the main program to halt until the routine finishes.

In order to achieve a sampling rate of 100 Hz, we only need to guarantee that the Arduino sends the data in 10ms intervals. With that in mind, a timer was designed to interrupt every 10ms and change the state of a Boolean variable, used in a condition of the main loop. Whenever the condition is met, the fetched data is sent via Serial port and the Boolean variable changes to its original state, waiting for the next interrupt.

3.3.2 MATLAB

MATLAB is a high-level programming language and interactive environment with several built-in functions, ranging from basic arithmetic to interface development. Furthermore, it can be enhanced by extra libraries, that can be downloaded from the official website (https://www.mathworks.com/). Its versatility and its extensive graphical capabilities

make it widely used as a computational tool in scientific projects. The version used in the present thesis was R2022a.

3.3.2.1 Data acquisition

The MATLAB routine starts by establishing a connection with the Arduino board and receiving some metadata: the upcoming sampling frequency, the accelerometer range, and the gyroscope range were 100 Hz, $\pm$4g and $\pm$1000° s^{-1}, respectively.

Then, the routine executes a call-back function that opens a graphical user interface (GUI) and displays the data in real-time. This processing stage is described in section 3.3.2.2, and the GUI's functionalities in section 3.3.2.3.

3.3.2.2 Real-time Processing

The data acquired from the Arduino is first converted to acceleration and angular velocity based on the sensors' range settings:

$$a_i = \frac{i}{2^{15}} \cdot 4\, g\,, \qquad i = x, y, z \tag{1}$$

$$\omega_i = \frac{i}{2^{15}} \cdot 1000\ (^\circ\, s^{-1})\,, \qquad i = x, y, z \tag{2}$$

Afterwards, the total acceleration and total angular velocities are calculated, using Eq. 3 and 4.

$$a_t = \sqrt{a_x^2 + a_y^2 + a_z^2} \tag{3}$$

$$\omega_t = \sqrt{\omega_x^2 + \omega_y^2 + \omega_z^2} \tag{4}$$

One of the goals of the application was to give the user a visual cue that the sensors are working properly. To accomplish that we decided to introduce a 3D plot, where the orientation of a given sensor could be seen in real-time. The orientation of an object can be given by its angular position, or its Euler angles (see Figure 22). To obtain these angles, one could use data from either the accelerometer or the gyroscope. The accelerometer can do this by determining the position of the gravity vector (g-force), and the gyroscope by integrating the angular velocity over time. However, as it happens, the accelerometer measurements are very susceptible to disturbances by small forces, being only reliable on the long-term. Conversely, the gyroscope is very reliable on the short-term, but tends to drift, because of the integration over time.

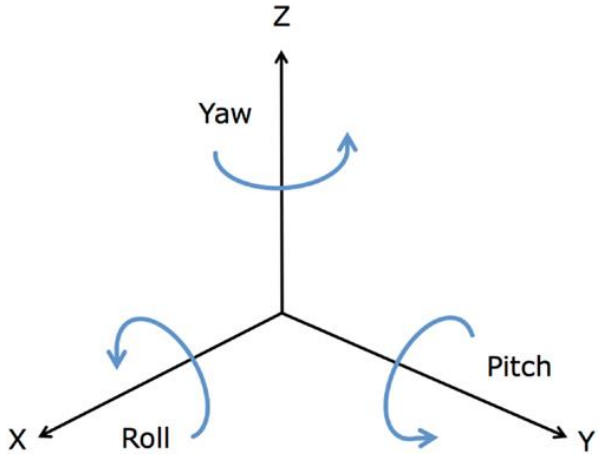

Figure 22 – Euler angles and polarity of rotations. From [127].

One can solve this problem by using the data of both accelerometer and gyroscope, either in a Kalman filter or in a complementary filter. While the first is more robust, it is also harder to implement without magnetic field data [128] – which is not present at the MPU-6050. For those reasons, we opted for the latter.

The complementary filter looks as follows, for the i-th Euler angles:

$$\begin{cases} roll_i = A \cdot (roll_{i-1} + \omega_x \cdot \Delta t) + (1 - A) \cdot \tan^{-1}(\frac{a_y}{a_z}) \cdot \frac{180}{\pi} \\ pitch_i = A \cdot \left(pitch_{i-1} + \omega_y \cdot \Delta t\right) + (1 - A) \cdot \tan^{-1}(\frac{-a_x}{\sqrt{a_y^2 + a_z^2}}) \cdot \frac{180}{\pi} \\ yaw_i = yaw_{i-1} + \omega_z \cdot \Delta t \end{cases} \quad (5)$$

, with $A = 0.968 \wedge \Delta t = \frac{1}{F_S}$.

Although this filter generates a good approximation of the real orientation, it suffers from two problems. The first is known as the “gimbal lock problem” and happens when the pitch is ±90°: due to the way the rotation matrices are calculated, the object loses one degree of freedom and generates “false” rotations on the 2D plane [129]. The second problem involves the drift in yaw. Since this value cannot be calculated from the acceleration measurements (or there would not be a referential axis), it inherits the disadvantage of using only the gyroscope data.

Another goal of the application was to display in real-time the dominant frequency and the relative power of the band where the PD characteristic tremor occurs – 4 to 12 Hz. Thus, for every 10 samples, the dominant frequency is extracted by:

1) Obtaining the power-spectral density estimate vector, using the periodogram function expressed in Eq. 6.
2) Getting the frequency correspondent to the maximum value of the power-spectral density estimate vector.

$$\hat{P}(f) = \frac{\Delta t}{N} \cdot \left| \sum_{n=0}^{N-1} h_n x_n e^{-j2\pi f \Delta t n} \right|^2 , \quad -1/2\Delta t < f \leq 1/2\Delta t \tag{6}$$

, where Δt is the sampling interval and h_n is a window function. In this case, the window function used is the Hamming – a function that minimises the ripple that results from the time-frequency conversion of a finite signal, giving a more accurate idea of the original signal's frequency spectrum. Mathematically, it can be expressed by [130]:

$$h(n) = \alpha + (1 - \alpha) \cos\left[\left(\frac{2\pi}{N}\right) n\right] , \quad \alpha = 0.54 \tag{7}$$

Finally, the relative power metric is obtained with:

$$P_{rel} = \frac{P_{tremor}}{P_{total}} \tag{8}$$

, where P_{total} is the average total power of the signal (3-50 Hz) and P_{tremor} the average power of the Parkinsonian tremor characteristic frequency band (4-12 Hz). The power is obtained by integrating the periodogram function in the wanted band. It is worth noting that P_{total} discards the 0-3 Hz range to remove the gravity's effect and potential aperiodic or low-frequency (often volitional) movements.

3.3.2.3. Recording GUI

When developing an application, usability is of the utmost importance, especially when its main users are not required to know but a few results. With that in mind, a GUI was designed (see Figure 23).

The recording window has four plots, a pair for each sensor. Each pair is comprised by an orientation plot and a total acceleration plot. The first allows the user to visually assess if there are any problems with the corresponding sensor. A mismatch

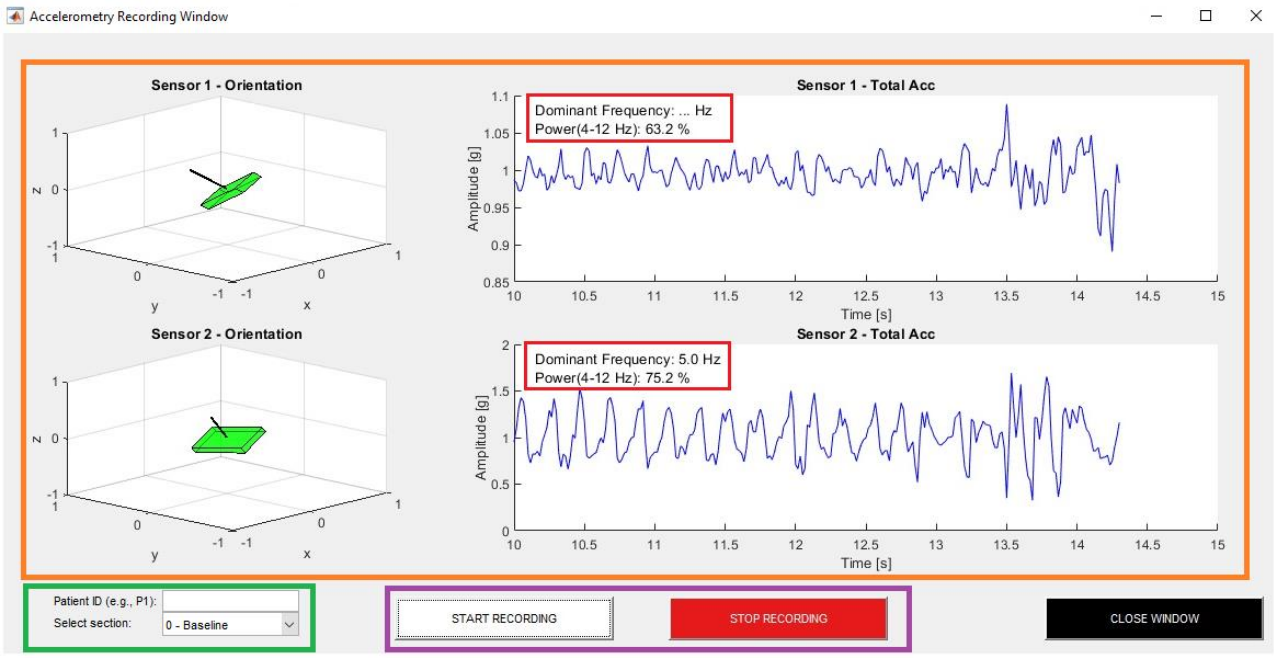

Figure 23 – Graphical user interface of the developed application for real-time data acquisition. The orange box highlights the graphs that display the orientation and some relevant information about the incoming data. Within these, the red boxes highlight the power of the displayed signal in the Parkinsonian tremor frequency range, and the dominant frequency within this range, if there is one. In the green box, the user can write the patient's ID and select the session's section of the current recording. The information is stored along the data. The user can start and stop a recording, using the buttons in the purple box. When the stop button is pressed, a dialog box asks whether the recording should be saved or discarded. The black button closes the window.

between the orientation of the physical sensor and its plotted counterpart is an indication that something is wrong. In this case, the recording should be aborted, and the sensors reset or replaced. The latter plot displays the total acceleration, calculated with Eq. (3), the dominant frequency and the power in the frequency band associated with Parkinsonian tremor. These values are continuously updated, and the total acceleration line is shown in blocks of 5 seconds. This allows the clinician to see some of the previous total acceleration values without constant distortion of the x-axis.

The application also allows the user to write the patient's ID, which later is automatically integrated in the filename of the data saved during the session. Additionally, the user can specify the current section of the protocol. This information is stored along with the recordings. Whenever the user stops a recording, a dialog box appears asking whether he wants to save it or not. Regardless of his choice, the plots are refreshed, and a new recording can be started, if he pleases.

3.4 Post-Recording Analysis

The wearable glove system saves the recorded signals in .mat files. This allows the data to be aligned with concurrent recordings (namely, LFPs) and further analysed. Tremor and rigidity are two Parkinsonian cardinal symptoms that can be inferred from these signals. The following sections describe the methods devised to extract the tremor and rigidity intensities from the data. It is worth noting that the characteristics of the applied filters were chosen to match the ones used in a toolbox that is being developed by the NCN lab.

3.4.1 Tremor Analysis

A 5th-order band-pass Butterworth filter in the band of 3–13 Hz is applied to the total acceleration signal, to exclude frequencies outside the Parkinsonian tremor frequency band. The tremor intensity is calculated in blocks of 5.12 seconds, i.e., 512 points of data collected as the sampling rate is set at 100 Hz. Each block is further divided in 8 sub-windows, each containing 64 data points.

Two adjacent sub-windows make up a set, so each block of 5.12 seconds contains 7 overlapping sets. To determine the tremor intensity in each block, the average of the dominant frequency's magnitude of the 7 sets within the block is calculated:

$$\mathrm{Trem} = \frac{1}{7}\sum_{n=1}^{N=7} \tau_n \tag{9}$$

, where τ_n denotes the dominant's frequency magnitude for set *n*. Alternatively, the median of the dominant frequency's magnitudes is also calculated.

The final step is the normalization of the tremor intensity to a well-defined scale, determined during clinical validation. This scale is attained by comparing the analytical tremor with the clinician's subjective classification.

3.4.2 Rigidity Analysis

The rationale behind the rigidity metric is the assumption that the cogwheeling effect has a specific impact on the angular velocity signal: whilst a high-amplitude repetitive motion in a non-rigid subject resembles a sinusoidal wave, in a rigid subject the signal contains more oscillations of smaller amplitudes over the sinusoidal wave, due to the ratcheting nature of the motion.

A 5th-order band-pass Butterworth filter, with cut-off frequencies of 0.25 Hz and 6 Hz is applied to the total angular velocity signal to eliminate the baseline velocity offsets and high frequency noise. This high cut-off frequency was determined in an iterative process, that aimed to maximise the relative difference of a used parameter (number of peaks) between rigid samples and non-rigid samples.

Subsequently, the signal is divided in blocks of 5.12 seconds, just like in the tremor analysis. For each block, the function starts by calculating the dominant frequency (D_{freq}) of the basal movement, using the periodogram function (see Eq. 6). Then, the number of peaks (N_p) is obtained via search of local maxima in the filtered signal (MATLAB's function "findpeaks"). Finally, the rigidity is calculated in the following manner:

$$\mathrm{Rig} = \frac{N_p}{D_{freq}} \tag{10}$$

Ideally, for a non-rigid subject, the number of peaks should match the duration of the block multiplied by the movement's dominant frequency and constitute the 0th-percentile. Nevertheless, like in the tremor's case, the rigidity intensity is ultimately normalised to a scale, which is obtained by matching the clinician's evaluation with the function's output.

3.5 Results

3.5.1 Validation Protocol

The developed glove system was intended to be validated in a clinical environment. For that reason, a simple but complete protocol was designed. This protocol is divided in 4 sections, which are further described in Table 7.

Table 7 – Protocol for wearable glove system validation.

Section	Duration	Description
1 – Rest	3 min	Patient maintains his upper limb relaxed on a solid surface.
2 – Movement of the wrist	1 min	Patient flexes the wrist in the y-z plane. Aided, if necessary.
3 – Finger tapping	1 min	Patient taps the thumb with its index finger. Aided, if necessary.
4 - Rigidity	3 min	Supination and flexion of the upper limb. Aided, if necessary.

As is common practice, the validation would establish a comparison between the system's objective metrics and the ones it aims to replace – the clinician's subjective scale. However, due to some constraints, namely the short span for the completion of this work and the logistics involved in scheduling a patient's consultation, the validation process could not take place in the clinic. In alternative, we tried to emulate the relevant symptoms, while also providing control measurements to establish comparisons.

A typical tremor recording consisted in an initial 10 seconds where an artefact was created (either by tapping on the chest or on the table), followed by a step increase

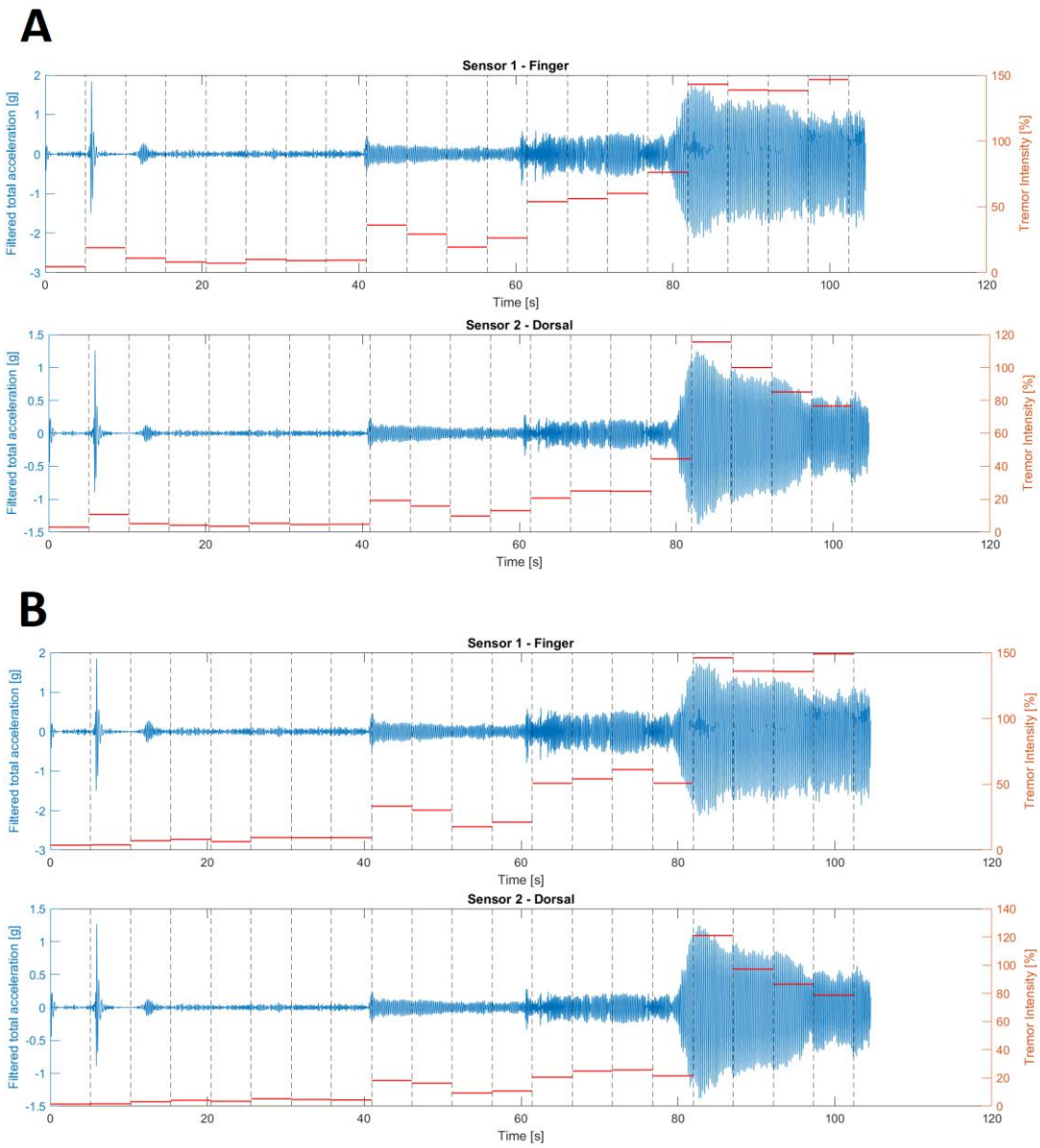

Figure 24 – Examples of analytical results for emulated tremor. The plots contain the filtered total accelerations of both sensors (finger and dorsal) and the tremor intensities, calculated with **(A)** the average and **(B)** the median of the dominant frequency's magnitudes.

of the total acceleration's amplitude in blocks of 20 seconds. This process was aided by the GUI's total acceleration plots in order to maintain the amplitude constant and the frequency within the Parkinsonian characteristic range. The generated artefact served to main purposes: seeing its effects on the analytical metrics and testing the function that enables the alignment of the neurostimulator and wearables recorded signals. Conversely, a typical rigidity recording was comprised by a period of 30 seconds of unrestrained supination and flexion of the upper limb followed by another 30 seconds of the same movement but with a counterforce (to create the rigidity effect).

3.5.2 Validation

As previously stated, the tremor intensity was calculated in two different ways: one used the average of the dominant frequency's magnitudes of a given block, while the other employed the median. The application of both methods is illustrated in Figure 24.

Regardless of the method, the evolution of the tremor intensity was consistent with the increase in total acceleration amplitude. One of the main differences between average and median usage was the fact that the artefact (~6 seconds) resulted in an increase of the calculated tremor intensity in the first, but not in the latter. In fact, one can see a similar phenomenon in the blocks containing an amplitude step transition – e.g., the 80 seconds block shows a tremor intensity that is between the intensities of the

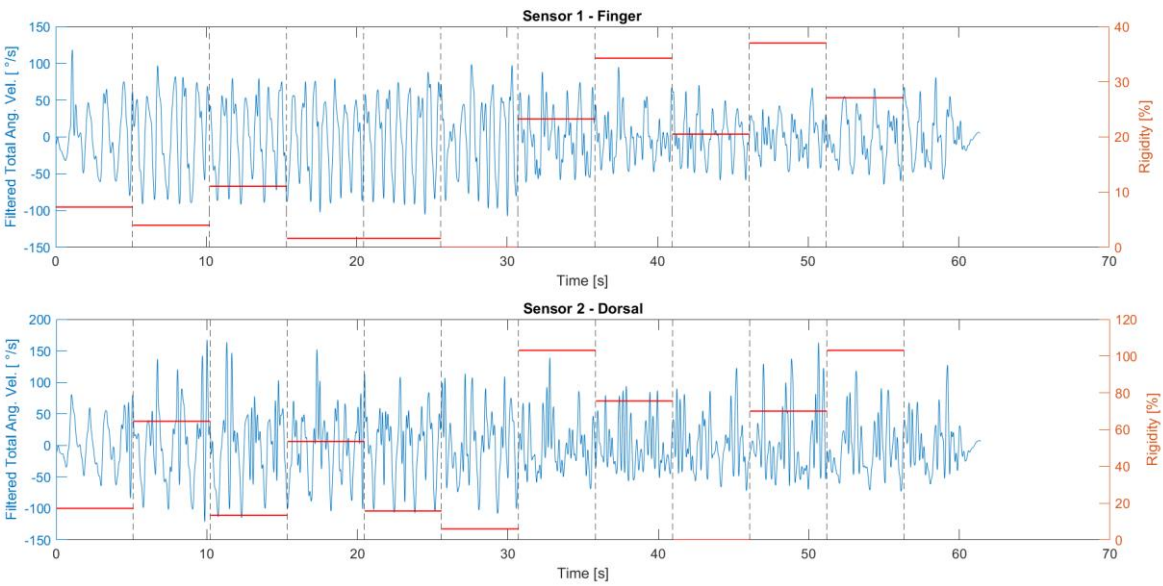

Figure 25 – Example of analytical results for emulated rigidity. The plots contain the filtered total angular velocities of both sensors (finger and dorsal) and the respective rigidity intensities. The first 30 seconds correspond to the motion without opposition and the last 30 seconds result from its introduction.

previous block and of the following one for the average, but not for the median. Regarding the tremor intensity scale, it is worth noting that the 100th-percentile was manually chosen for illustrative purposes. Only the clinical validation step will allow its adequate determination.

The application of the rigidity quantification method is illustrated in Figure 25. The transition between the first (without opposition) and second (with opposition) periods can be discerned around the 30-second mark. Overall, the first periods had lower rigidity intensities than the second. However, some exceptions are reported – e.g., the ones pertaining to the dorsal sensor's signal in Figure 25, where two blocks of the first period revealed high rigidity values and one block of the second period had low rigidity. In this respect, it is worth noting that in this recording the dorsal sensor's signal is not as smooth as the finger one. Similarly to the tremor's case, the 0th and 100th percentile of the intensity scale were manually chosen for illustrative purposes.

3.6 Discussion

The developed wearable system is portable, versatile, and user-friendly. It provides an intuitive GUI that tracks the orientation of the sensors in real-time, while displaying relevant information about the incoming data. The way in which the orientation is updated constitutes a minor limitation. Although it provides a reliable approximation of the real sensor orientation changes, it suffers from two problems: the gimbal lock problem and drift in the yaw. Fortunately, these problems are not inevitable, and the use of quaternions is being considered in future versions of the GUI.

Regarding the analytical functions, while the one used for tremor quantification relies on well-studied parameters (for tremor is the most successfully characterised PD symptom in the literature; see Table 5), the one used for the rigidity is innovative, as far as we can tell. Studies that propose new methods for rigidity quantification often resort to velocity parameters, obscuring the distinction between rigidity and bradykinesia. In this respect, the developed method aims to be velocity invariant (and does not take velocity into account), by removing possible offsets of the total angular velocity signal with a filter and normalising the number of counted peaks based on the frequency of the movement.

A major limitation of the presented work is the lack of clinical validation at the time of submission. Due to the limited time window for its conclusion, the functions were

tested with subjects that tried to emulate the symptoms. While one should acknowledge that the emulated symptoms may not be totally representative of the real symptoms, tremor seemed the one emulated with greater success. In this regard, the method that employed the median seemed the most robust, being insensitive to non-periodic artefacts. As for the rigidity quantification, the results show some potential, albeit the lessened confidence on its emulation.

All in all, the developed system tool shows good potential for clinical support and data analysis. Moreover, it provides a framework that can easily be enhanced with further functionalities. Among these, machine-learning models offer an interesting prospect of real-time symptom predictability, allowing the transition to systems that are adaptive in the true sense of the term.

3.7 Conclusions

The need to complement the brain signals and the lack of objective methods to quantify Parkinsonian symptoms in the clinic encouraged the development of a wearable system with these capabilities. The developed system has two main features: the real-time display and storage of motor signals, and the post-processing analysis. The first was materialized in an intuitive GUI, that can track the sensors orientation and give relevant information about the incoming data. The second consisted in a set of functions capable of reading and analysing the stored data. More concretely, these functions focused on the quantification of tremor and rigidity – the last of which was quantified in a novel way.

Overall, despite lacking clinical validation at the time of writing, the analytical functions showed good quantifying potential, especially in the tremor's case. Lastly, the developed system set up a framework that can be enriched by new functionalities, solving problems or needs that may emerge from clinical use.

Chapter 4

Chronic Data Analysis

The central goal of this thesis was to create visual and analytical tools for chronic DBS electrophysiology data. As already explained in section 2.2.3 and 2.5., Medtronic has a neurostimulator device, named Percept, capable of sensing and storing the patient's LFPs, with a system coined BrainSense™ Technology. The data storage feature is a recent improvement that enables the research of out-clinical (chronic) data, even though its resolution is vastly inferior to the one obtained during the clinical sessions.

In most facilities, the sessions still employ the conventional DBS approach: the patient is sent home with a set a of stimulation parameters that were manually chosen by the clinicians. The fact that these parameters persist until a new session, allied with the storage capability of the Percept, poses an excellent opportunity to test the therapy effects on real-world environments. In addition, while at home, the patients have the option to instruct the storage of LFPs during states or events predefined by the clinicians. Since these states can include symptoms or scheduled activities (such as medication), the analysis of the stored data has also the potential to bring forward chronic biomarkers. Hence, besides the creation of the mentioned tools, this thesis also set itself up to tackle some research questions.

As with the wearable system, MATLAB was the chosen programming language for this chapter. The main reason for this was the fact that some of the developed functions would be (and have been) integrated on an extensive analytical toolbox – specifically designed for the Percept + BrainSense™ system – that is being made in that language by the NCN lab.

4.1 BrainSense™ Dataset

The present work relied on a dataset directly provided by clinicians who are following patients implanted with the BrainSense™ system. The data was anonymised and provided under an established protocol that was approved by the ethics committee of Centro Hospitalar Universitário de São João (CHUSJ). Although this dataset contains features for clinical purposes, this work focused on the ones used in outside the clinic environments. Data from outside the clinic, or chronic data, can be of two types: event-

related or continuous. The next sections describe each of these. A fully detailed characterization of the dataset is in section 4.1.3.

4.1.1 Event

The BrainSense™ Event feature enables the neurostimulator to take LFP snapshots, whenever a clinician-defined event occurs, in the following manner:

1) Still in the clinic, the clinician activates this feature and creates up to 4 types of events (e.g., taking of medication, feeling good, feeling stuck, dyskinesia), indicating which events should trigger the snapshot.
2) Outside the clinic, whenever the patient reports an event that should be snapshotted (by selecting it on the mobile application), the neurostimulator records 30 seconds of LFP data at 250 Hz, converting it to the frequency domain and storing the average frequency domain content (Fast Fourier Transform, FFT). Each snapshot comprises 100 pairs of values, covering a range from 0 to 96.68 Hz.

The neurostimulator can only store up to 900 events (i.e., 450 per hemisphere, if bilateral) and 400 LFP snapshots (i.e., 200 per hemisphere), overwriting older data if the limit is exceeded.

4.1.2 Continuous

The BrainSense™ Timeline feature allows the neurostimulator to continuously record LFP activity, the moment a patient leaves the clinic until his return. This is how it works:

1) Still in the clinic, the clinician activates this feature and specifies a band approximately 5 Hz wide, which he deems to be of interest – generally containing frequency peaks.
2) Outside the clinic, LFP raw signals are measured at 250 Hz, converted to the frequency domain and the power of the specified band is calculated.
3) Every 10 minutes, the average value of the LFP power and the stimulation amplitude are stored in the neurostimulator memory.

Since there is a 60-day limit in the storage capacity of the neurostimulator, at the 61st day the 1st day's data starts to be overwritten, and so on.

4.1.3 Dataset Characteristics

A summary of the most relevant dataset features can be found in Table 8. All 6 patients have continuous data from out-clinical periods. The ranges in which the LFP power is

recorded are approximately 5 Hz wide and contain the frequency peaks of the patient. These frequency peaks can vary from period to period. Although all patients reported

Table 8 – Relevant characteristics of the dataset.

Patient	Number of out-clinical periods with continuous recording	Peak frequency (Hz)	Date range	Number of event snapshots [(1)]
1	6	–[(2)]	27/01/2020-21/02/2020	–
2	4	–[(2)]	30/07/2020-12/02/2021	–
4	4	**L:** 19.53/18.55 **R:** 21.48/18.55[(3)]	06/04/2021-12/05/2021	M: 56 D: 2
5	2	–[(2)]	13/04/2021-14/05/2021	–
6	2	**L:** 14.65/16.60 **R:** 12.70/15.63	28/05/2021-09/07/2021	M: 85 FS/R: 40 FW: 30 D: 17
7	1	**L:** 9.77 **R:** 9.77[(3)]	04/06/2021-09/07/2021	M: 39 FS/R: 1 FW: 119 D: 3

[(1)] **M** – Medication; **FS/R** – Feeling stuck/rigid; **FW** – Feeling well; **D** – Dyskinesias
[(2)] Not used
[(3)] Artefact present

events, only patients 4,6 and 7 have the associated LFP snapshots.

On a final note, it should be mentioned that most of the analyses were centred on patient 6, for two reasons. First, artefacts were detected on the right hemispheres of patients 4 and 7. Second, within the patients with available event snapshots, patient 6 is the only one that does not have an extremely unbalanced event type distribution.

4.2 Main Research Questions

As was mentioned in section 2.3.2.4, every hemisphere is anatomically and functionally unique. Considering the goal of aDBS – i.e., the personalisation of the DBS therapy to the patient's physiology –, one could, then, intuitively deduce that the therapy should be confined to the hemispherical level. The first research question arose from this intuition: *(1) Do the event profiles of a given hemisphere share an identifying baseline?*

As section 4.4.1.2 suggests, this question may be answered positively. With the intuition confirmed, the existence of a hemispherical baseline begged for further questioning. A potential line of inquiry resided in the evolution of this baseline, especially knowing that the Parkinsonian symptomatology changes over time. Following this logic, section 4.4.1.3 addressed the questions: *(2) Does the baseline change over time? And, if so, how, and why?*

Having the hemispherical baseline's dynamics described, one could not help but wonder if the differentiation of events could be done within these baselines. Or, in the form of a question: *(3) Can the events be differentiated through the hemispherical baseline?* Section 4.4.1.4 explored this scenario.

Finally, making full use of the chronic data, one aspired to see how the continuously acquired LFP power was related to the sporadic event snapshots, and if the first corroborated with some of the results obtained from previous questions. '*(4) Can event-related data be inferred by the LFP power signal?*' was, thus, the last main research question of the thesis.

4.3 Methods

To answer some of these questions, mathematical and statistical methods were used. The next subsections contain a brief description of the most relevant methods.

4.3.1 Dimensionality Reduction

Principal-Component Analysis (PCA) is a statistical procedure commonly used for dimensionality reduction in exploratory data analysis [131]. Conceptually, it minimises the effects of correlated/redundant variables, while promoting the formation of an independent set. PCA projects each data sample to a new coordinate system, such that the first principal component (where the first coordinate lies) corresponds to the direction that maximises the variance of the projected data. The i-th principal component is the direction orthogonal to the previous $i-1$ principal components that maximises the data variance.

- Consider a data matrix with size *N x P*, where *P* is the number of variables within a data sample and *N* the number of data samples. The PCA transformation can be thought as the multiplication of the data matrix by a *P x L*, where *L* is the number of new dimensions (principal components) and *P* the number of weights (one for each variable within a data sample).

4.3.2 Machine-Learning Classifiers

Machine-learning methods were extensively used throughout the work. More precisely, Support Vector Machine (SVM), Decision Tree (DT), and K-Nearest Neighbours (KNN) classifiers were compared.

- SVM is one of the most popular ML algorithms used by data scientists. In a nutshell, SVM searches for the best decision boundaries that separate any two classes with the highest generalization ability [132]. These boundaries are called hyperplanes. For a set of *p*-dimensional data points, the algorithm seeks $(p-1)$-dimensional hyperplanes. If the search is successful, the data is said to be linearly separable. For datasets that are not linearly separable, SVM offers some powerful transformation techniques, such as kernels. Kernels project the data to

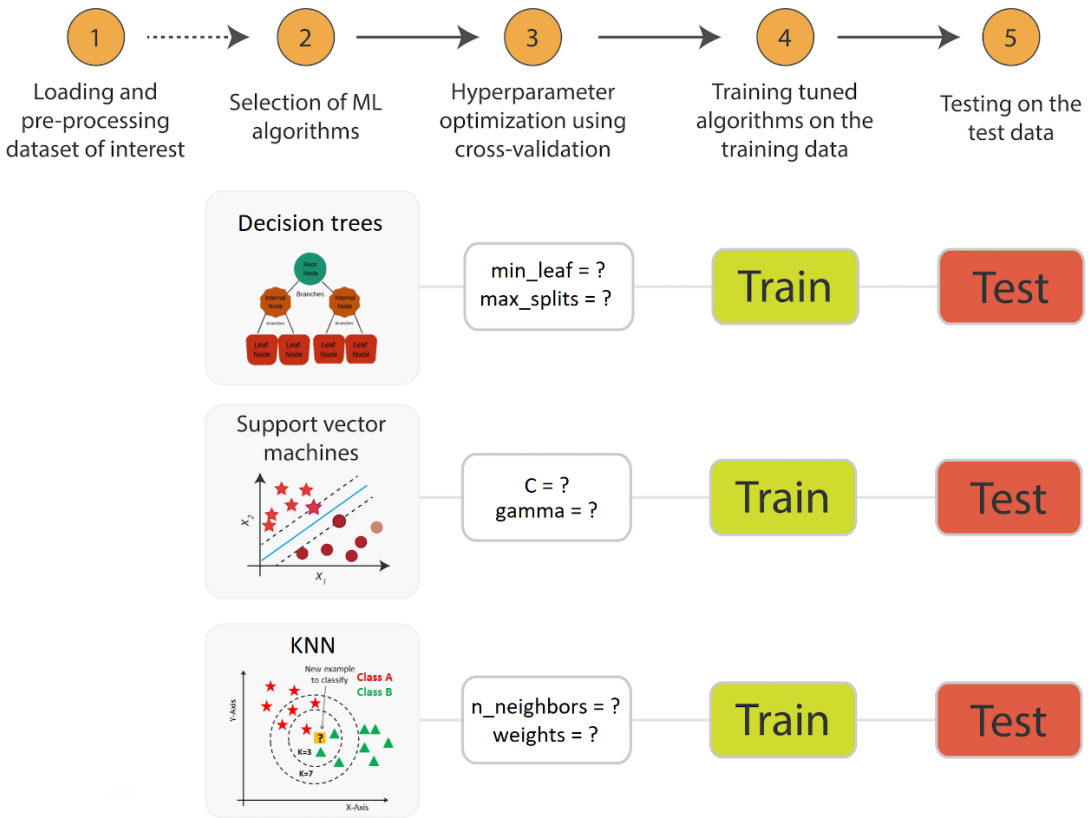

Figure 26 – Scheme of the steps involved in the creation of ML-based predictive models. The scheme has five main steps: pre-processing, algorithm selection, hyperparameter optimization, training, and testing. Pre-processing can include dimensionality reduction methods. The hyperparameters of SVM, DT and KNN are optimised with Bayesian and cross-validation algorithms. The tuned algorithms are trained and tested on several data partitions. Adapted from [133].

new dimensions, allowing the algorithm to find linear hyperplanes in a higher-dimensional space.

- DT is a powerful and popular ML tool for classification problems. It can be thought of as a tree-like structure, where each node denotes a test on an attribute of the data, each branch represents an outcome of a test, and each leaf node contains a class label [132]. The algorithm tries to identify the optimal split points within the tree, in a recursive manner. The algorithm is generally tweaked to find smaller trees preferable over larger trees, for the latter are more susceptible to overfitting.
- KNN is one of the simplest and easier to understand ML algorithms. One can think of it as an analogy-maker. Mostly used for classification purposes, KNN classifies a new data point based on the similarity with previously stored data points [132]. For a set of *p*-dimensional data points, the algorithm calculates the *p*-dimensional distances between the new unlabelled point and all labelled points. The K closest points are used to label the new point. A disadvantage of this algorithm is that it does not truly "learn" any features from the data and just stores a training dataset for further comparisons. This results in increased inefficiency, as the dataset grows.

The use of any of these learners required an optimization process, as illustrated in Figure 26. During optimization, a Bayesian optimization algorithm was applied to each learner, in conjunction with a 5-fold cross-validation method, to decide the optimal hyperparameters. Then, the tuned algorithms were trained with a training set, applied to a holdout set (test set) and evaluated. This last step was repeated for multiple data partitions. It is important to note that a change in the pre-processing methods (first step) entailed the repetition of all the subsequent steps.

4.3.2 Classifier Performance Evaluation

The F1-score is an evaluating metric, used in binary classification problems, that combines precision and recall.

$$F1\ score = 2 \cdot \frac{precision \cdot recall}{precision + recall} \tag{11}$$

, with:

$$precision = \frac{TP}{TP + FP} \tag{12}$$

$$recall = \frac{TP}{TP + FN} \tag{13}$$

, where TP denotes the number of points correctly labelled with the positive class, FP the number of points wrongly labelled with the positive class, and FN the number of points incorrectly labelled with the negative class.

In multi-class classification problems where all the classes are equally important, macro averaging is recommended [134]. The macro-averaged F1-score is calculated by taking the arithmetic mean of all the per-class F1-scores:

$$Macro\ F1\ score = \frac{1}{N} \cdot \sum_{n=1}^{N} F1\ score_n \tag{14}$$

, where N denotes the total number of classes.

4.4 Results and Discussion

4.4.1 Event Analysis

4.4.1.1 Exploration

Since there is still a literature gap concerning chronic data, especially event-related data, this work kicked off with an exploratory mindset. In other words, several ideas were tested besides the ones instantiated in the main research questions. Many of these ideas gave rise to visuo-analytical tools, some of which are illustrated in Figure 27.

The analysis of a patient's circadian data (represented by Figure 27A and Figure 27B) may be useful to detect temporal patterns in the frequency and valence of the reported events. Moreover, it might also provide information on the patient's routine and compliance with his treatment. For example, several >24h intervals between consecutive medications are suggestive that the patient frequently forgets to report (given that medication is usually taken 3-5 times a day). Additionally, one can also analyse the frequency of event co-registrations (episodes where the patient reports multiple events in a short span of time).

As for the FFT profiles, one can study the power of the events in different frequency bands, either with relation to the stimulation amplitude (see Figure 27C) or throughout time. The fact that the events are recorded in both hemispheres, in bilaterally implanted patients, can also give rise to a hemispherical comparative study of the captured FFTs, as in Figure 27D. Furthermore, one can also explore the differences

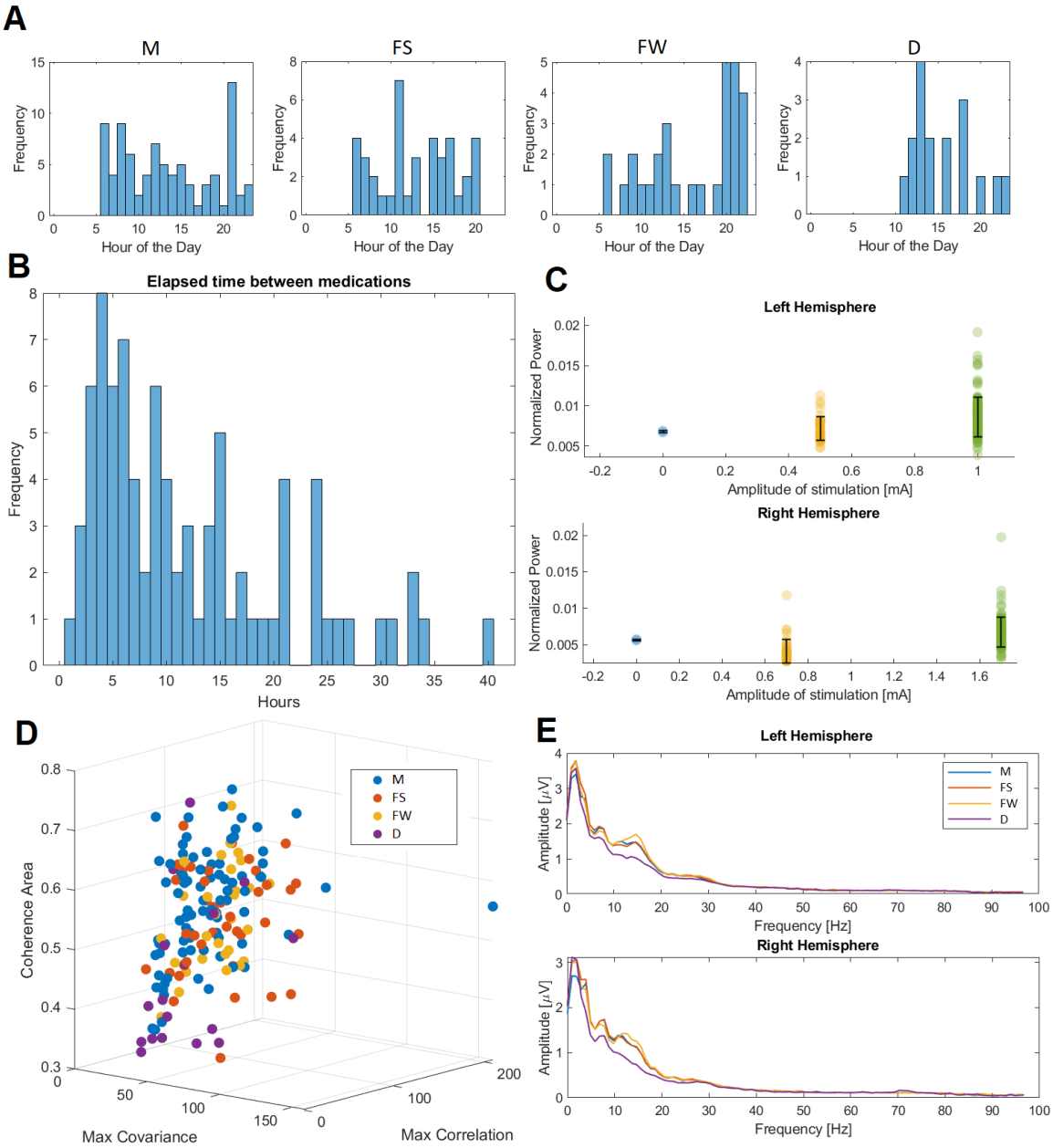

Figure 27 – Some examples of the developed functions for event-related data analysis. All the examples are from the same patient. **(A)** Histograms that represent the distribution of each event type, throughout the day. **(B)** Histogram that gives the elapsed time between reported medications. **(C)** Total power of the events based on the stimulation amplitude at the moment of capture. **(D)** A 3D representation of the event-FFTs containing the correlation, covariance, and coherence between hemispheres. **(E)** Mean FFT profile for each event type. ***M*** *– Medication;* ***FS*** *– Feeling stuck;* ***FW*** *– Feeling well;* ***D*** *– Dyskinesias.*

between FFT profiles of different event types. This can be done in several ways, some of which: average FFT plotting (Figure 27E), frequency band power comparison, correlation analysis, etc.

Most importantly, all these analyses may be combined in the generation of clinical profiles, that could in the future allow the mapping of the clinical responses (i.e., adapting a patient's the therapy using combinations of previous profiles from other patients).

4.4.1.2 Hemispherical Baseline

(1) Do the event profiles of a given hemisphere share an identifying baseline?

To answer the first research question, we analysed all the available LFP snapshots. The idea was to find if FFT profiles from the same hemisphere would share a particular baseline. Initially, we decided to use visual representations of the data. Given that each data sample has 100 dimensions (100 frequency-magnitude pairs) and that we were

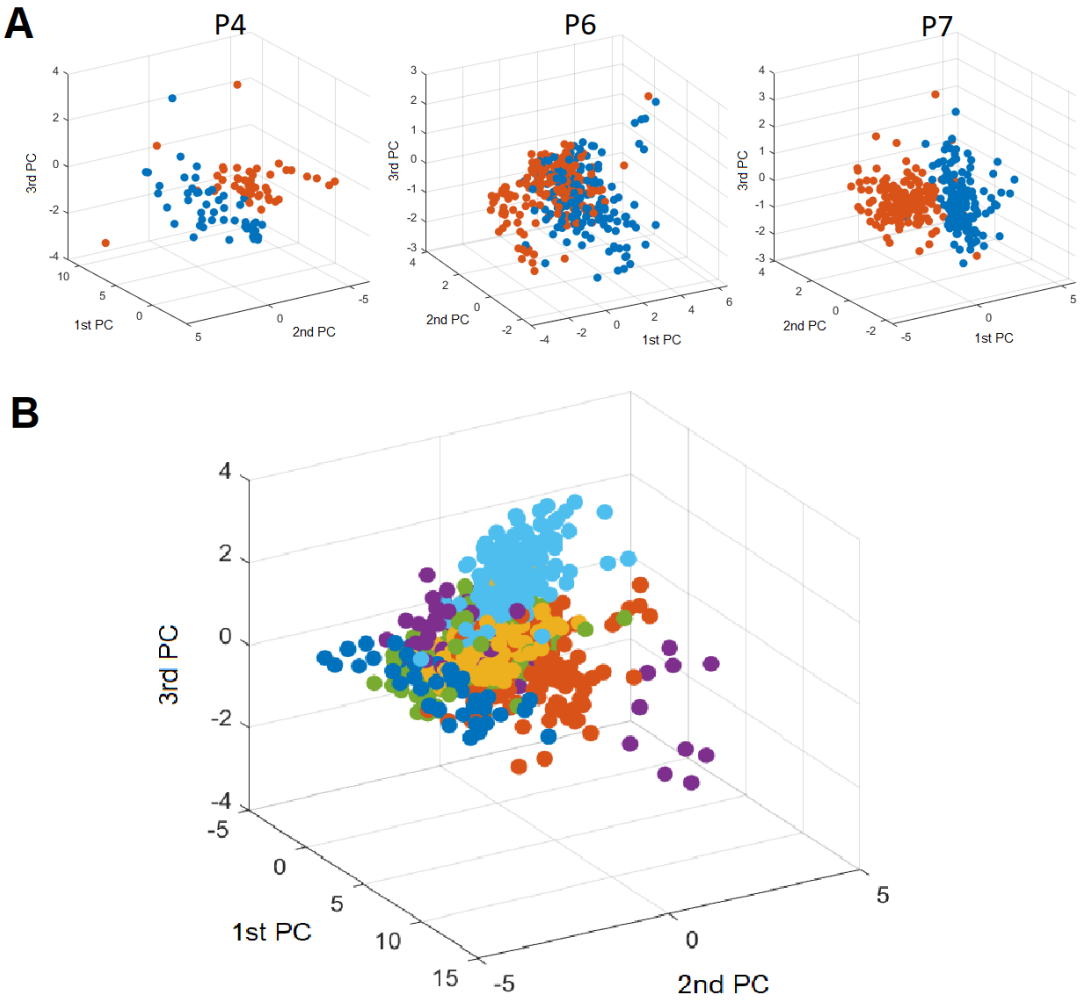

Figure 28 – 3D representations of hemispherical events after PCA. (A) Each 3D graph contains the PCA-projected FFT data from an individual. Blue points represent events from the left hemisphere, and orange points from the right hemisphere. **(B)** Graph that contains all the events in (A). Each colour represents a single hemisphere (N=6).

unsure of whether some frequency bands could be ignored, we decided to feed a PCA algorithm with the entire profile.

Thereupon, 3-dimensional representations of the first three principal components of the FFTs were made for each patient. For every graph of Figure 28A, events (points) from the same hemisphere tended to group in the 3-dimensional space. The fact that the clustering is more pronounced in patients 4 and 7, is probably due to stimulation artefacts that were detected on the right hemispheres of both patients. While these groupings corroborated the existence of hemispherical "baselines", we also wanted to see if these baselines maintained their uniqueness between patients. For that, we applied the same dimensionality reduction and visualisation methods to the whole dataset. The obtained representation (see Figure 28B) suggested, as well, a clustering between events of the same patient's hemisphere.

These visual cues prompted a second step in the analysis: the creation of predictive models. For that, SVM, Decision Tree, and KNN classifiers were chosen as learners for the same profiles (the input included the 100 frequency-magnitude pairs). As previously mentioned, these classifiers were first optimized with all the available data, in order to obtain the most fitting hyperparameters. Only then were the learner's performances evaluated in multiple iterations. Each iteration started by splitting the data in training and testing sets, in a 70:30 ratio. Given that the number of events per patient (and, consequently, per hemisphere) varied significantly, the split forced the aforementioned ratio for all classes (hemispheres) and all the learning algorithms took the class frequencies as the prior probabilities. The overall weighted F1-scores are summarised in Table 9.

Table 9 – Performance metrics of ML algorithms for hemisphere classification. The results are for the hemispheres of patients 4, 6, and 7. The values are under the form of mean ± std (N=1000).

ML Algorithm	Macro F1-score
Support Vector Machine	0.95 ± 0.02
Decision Tree	0.96 ± 0.02
K-Nearest Neighbours	0.99 ± 0.01

All three classifiers achieved very high performances. KNN was the leading learner, with an overall macro F1-score of 0.99. These results show that event FFT profiles from the same hemisphere share some traits that can be easily identified – therefore, supporting the existence of hemispherical baselines.

4.4.1.3 Baseline Temporal Evolution

(2) Does the baseline change over time? And, if so, how, and why?

The second research question was tackled with a different approach. First, we created 3D representations of all the events of each hemisphere, throughout time. The goal was to see if one could visually spot any changes in the event FFT profiles over time. Knowing that the stimulation amplitude can affect the LFP signals, we also plotted the stimulation amplitude evolution (see Figure 29).

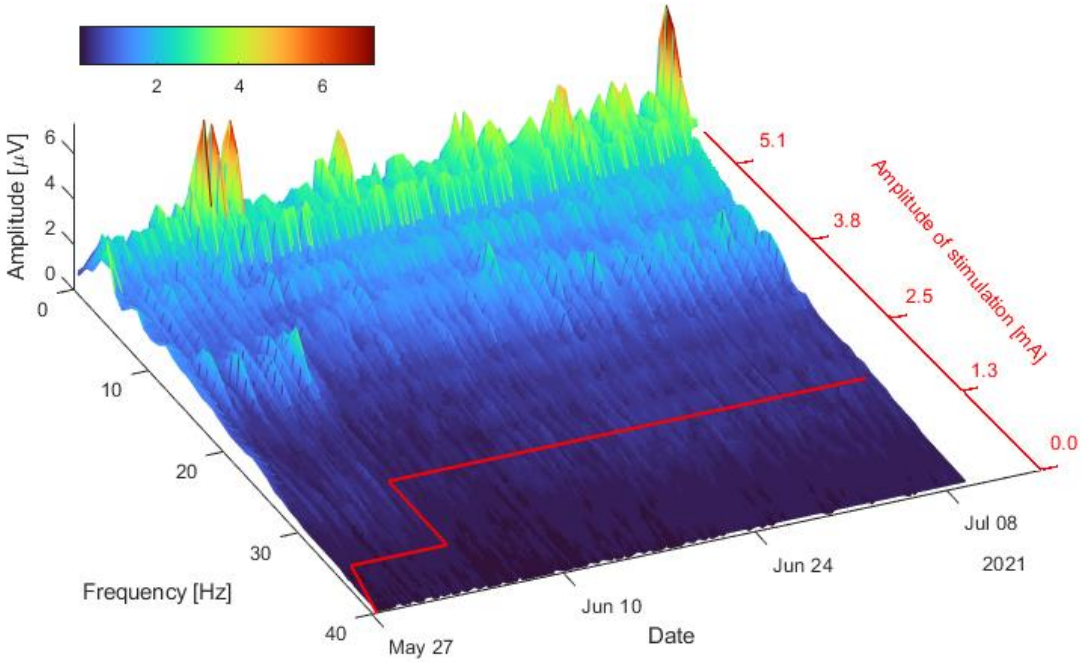

Figure 29 – 3D representation of the FFT profile temporal evolution. The stimulation amplitude is layered as a red line on the time-frequency plot. The data is from the right hemisphere of P6. FFT profiles are shown in the 4-40 Hz range.

A careful examination of the plots revealed that a significant change in the FFT profiles was coincident with the readjustment of the stimulation amplitude. In Figure 29, this change was most patent in the peak frequency shift on the 10-15 Hz range. In fact, the shift was more pronounced where the change in stimulation amplitude was higher (for this patient, the shift is not as clear in the left hemisphere, where the stimulation amplitude change was from 0.5 to 1 mA).

To verify the effect of the stimulation amplitude on the hemisphere's baseline, we employed the same methodology used in the first research question. For each hemisphere, we created a 3D representation of the three principal components of the respective events, labelling each according to the concurrent stimulation amplitude (see

Figure 30). Given that the discerned change was at the 10-15 Hz range, we also tested feeding the PCA algorithm with a narrower frequency band (4-40 Hz).

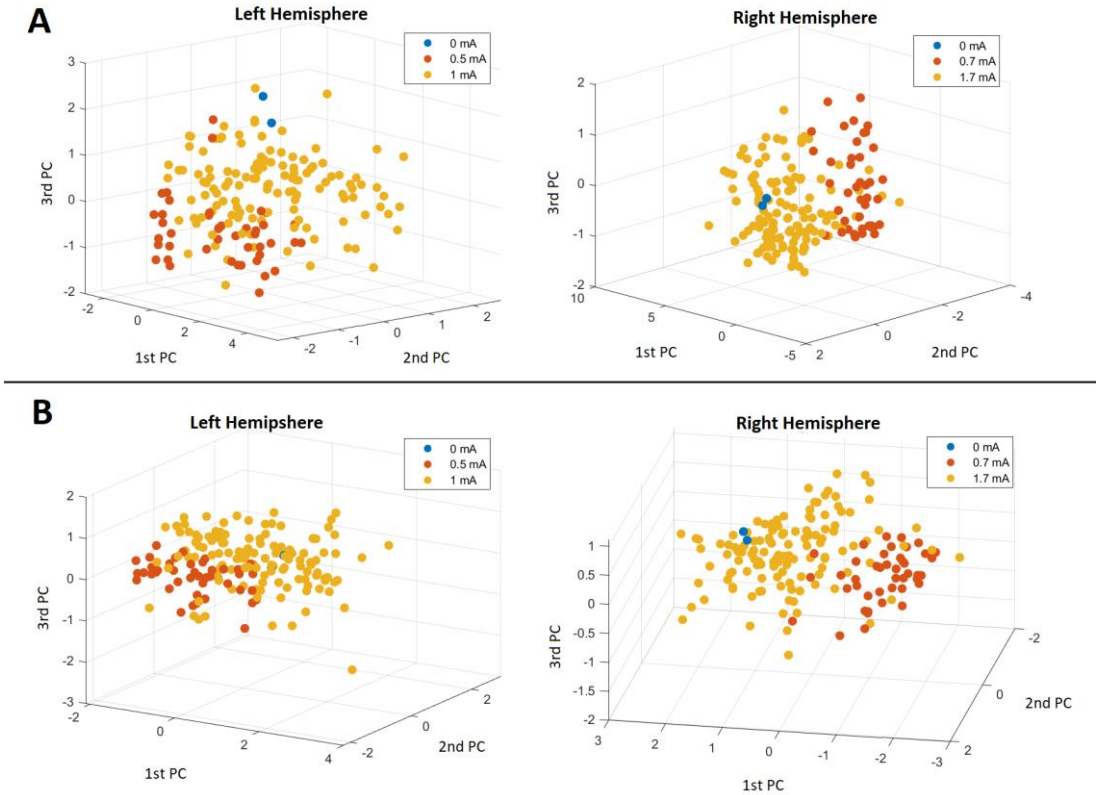

Figure 30 – 3D representations of events labelled according to stimulation amplitude, after PCA. All graphs contain data from patient 6. Each 3D graph contains the PCA-projected FFT data from a hemisphere. Different colours represent different stimulation amplitudes. The PCA algorithm was fed with the event-FFT profiles in the **(A)** 0-96 Hz and **(B)** 4-40 Hz ranges.

Noticing the clustering tendency, we proceeded with the creation of predictive models. Classes (stimulation amplitudes) with less than 5 values were ignored, because their quantity was deemed insufficient. The same types of classifiers and optimization

Table 10 – Performance metrics of ML algorithms for stimulation amplitude classification. The results are from patient 6. The values are under the form of mean $\pm$ std (N=1000).

Hemisphere	ML Algorithm	F1-score		
		0-96 Hz	4-40 Hz	PCA (0-96 Hz)
Right	SVM	0.97 ± 0.02	0.97 ± 0.03	0.97 ± 0.03
	DT	0.93 ± 0.05	0.89 ± 0.06	0.88 ± 0.05
	KNN	0.97 ± 0.03	0.96 ± 0.03	0.96 ± 0.03
Left	SVM	0.93 ± 0.04	0.89 ± 0.04	0.90 ± 0.05
	DT	0.84 ± 0.08	0.86 ± 0.06	0.77 ± 0.09
	KNN	0.88 ± 0.05	0.89 ± 0.04	0.88 ± 0.05

methods were used. The 4-40 Hz range and the principal components that explained at least 95% of the variance in the whole FFT range (0-96 Hz) were also used to feed the classifiers, in addition to the whole FFT profiles. The obtained results are summarised and compared in Table 10.

Although all three classifiers had high performance metrics, SVM turned out to be the most reliable across hemispheres. The results show that feeding the algorithm with the entire FFT profiles was not significantly different from feeding it with only the 4-40 Hz range, or with the new dimensions obtained with PCA. This suggests that the stimulation amplitude has a concrete effect on the hemispherical baseline and that it mainly occurs within the 4-40 Hz frequency range.

4.4.1.4 Event Type Differentiation

(3) Can the events be differentiated through the hemispherical baseline?

A visual analysis of the FFT profiles prompted the response to the third question. Figure 31 shows the mean and standard deviation values of the FFT profiles for each event type in patient 6. As previously stated, this patient had two periods of out-clinical recordings. Given that the stimulation amplitudes of both hemispheres varied from one period to another – changing the hemispherical baseline as suggested by section 4.4.1.3 –, we individually analysed each of the periods. A meticulous examination of the Figure 31 showed that the event-generic FFT profiles were very similar throughout the whole range (shared baseline), except in the alpha/low-beta range – where the mean ampltiude of the dyskinesias is lower than the others. However, when plotted with the standard deviations (31B), the generic profiles overlapped. Hence, a different analysis was made to further verify this differences.

We calculated the power in several frequency bands for each event. Then, the obtained results were plotted according to the event type, as illustrated by Figure 32. From these, two main observations were extracted. First, medication had generally the highest variance – which was not suprising, given that it is the only event that is scheduled and does not directly depend on the patient symptoms (although this is not always the case, as one explains in section 4.5). Second, beta was the only band where the dyskinesias power was consistently lower ($p < 0.05$) throughout the hemispheres (though the beta subrange differs between periods A and B) – which is in accordance with the literature that states that beta activity is inversely correlated with the presence of dyskinesias [42].

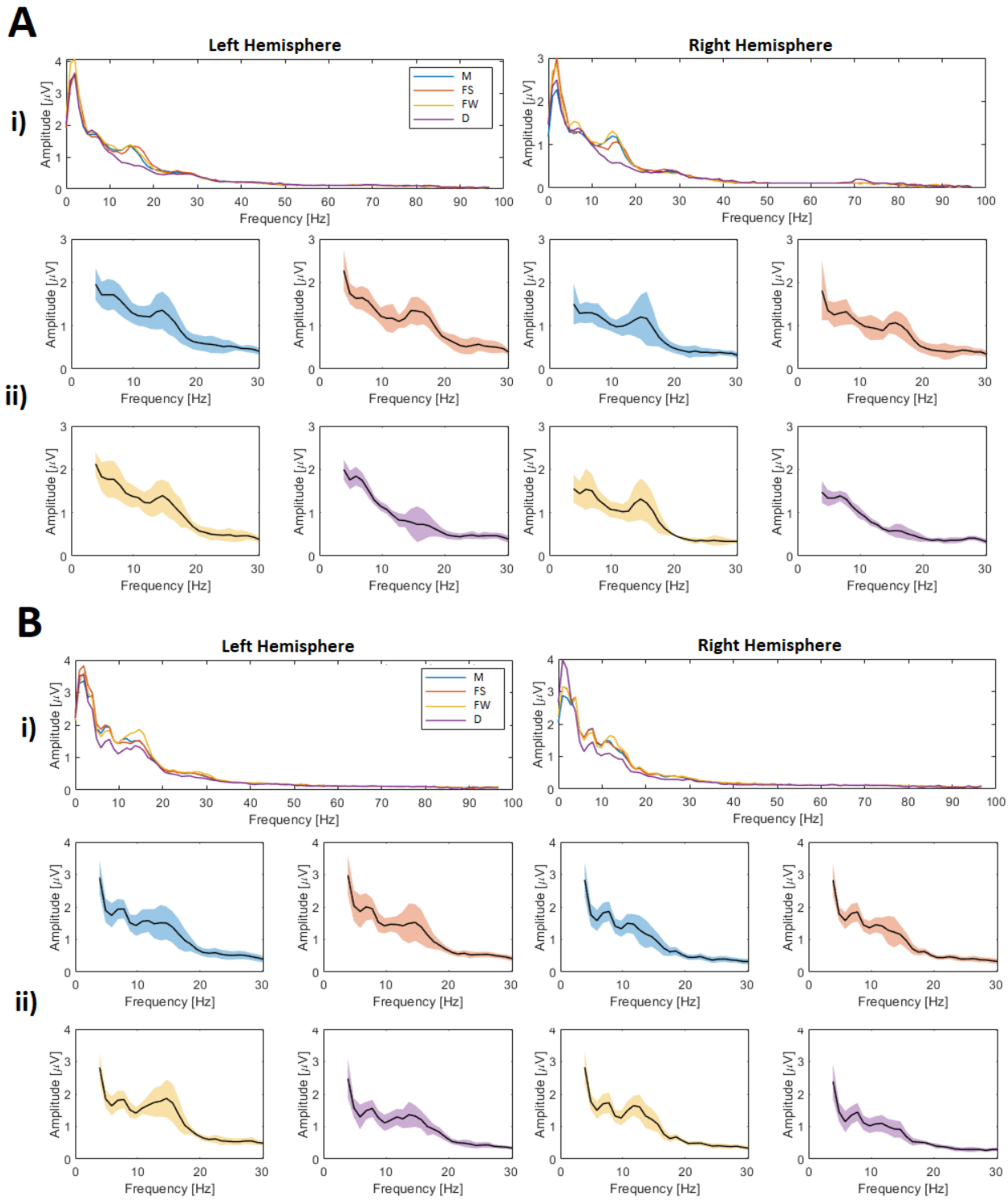

Figure 31 – FFT profiles of the four event types. All graphs contain data from patient 6, where **(A)** corresponds to the first out-clinical period and **(B)** the second. The plots in **(i)** contain the means of the four event types in each hemisphere. The plots in **(ii)** illustrate the mean and standard deviation values of medication (blue), feeling stuck (red), feeling well (yellow), and dyskinesias (purple) events in the 4-30 Hz frequency range of each hemisphere.

With these observations in mind, we decided to see if predictive models were capable of distinguishing dyskinesias from the rest of the events, with and without medication. The tested algorithms, SVM and DT, were fed with the power in five frequency bands: theta (θ, 4-7 Hz), alpha (α, 8-12 Hz), low-beta (low-β, 13-20 Hz), high-beta (high-β, 21-35 Hz), and gamma (γ, 31-96 Hz). The results are summarised in Table 11.

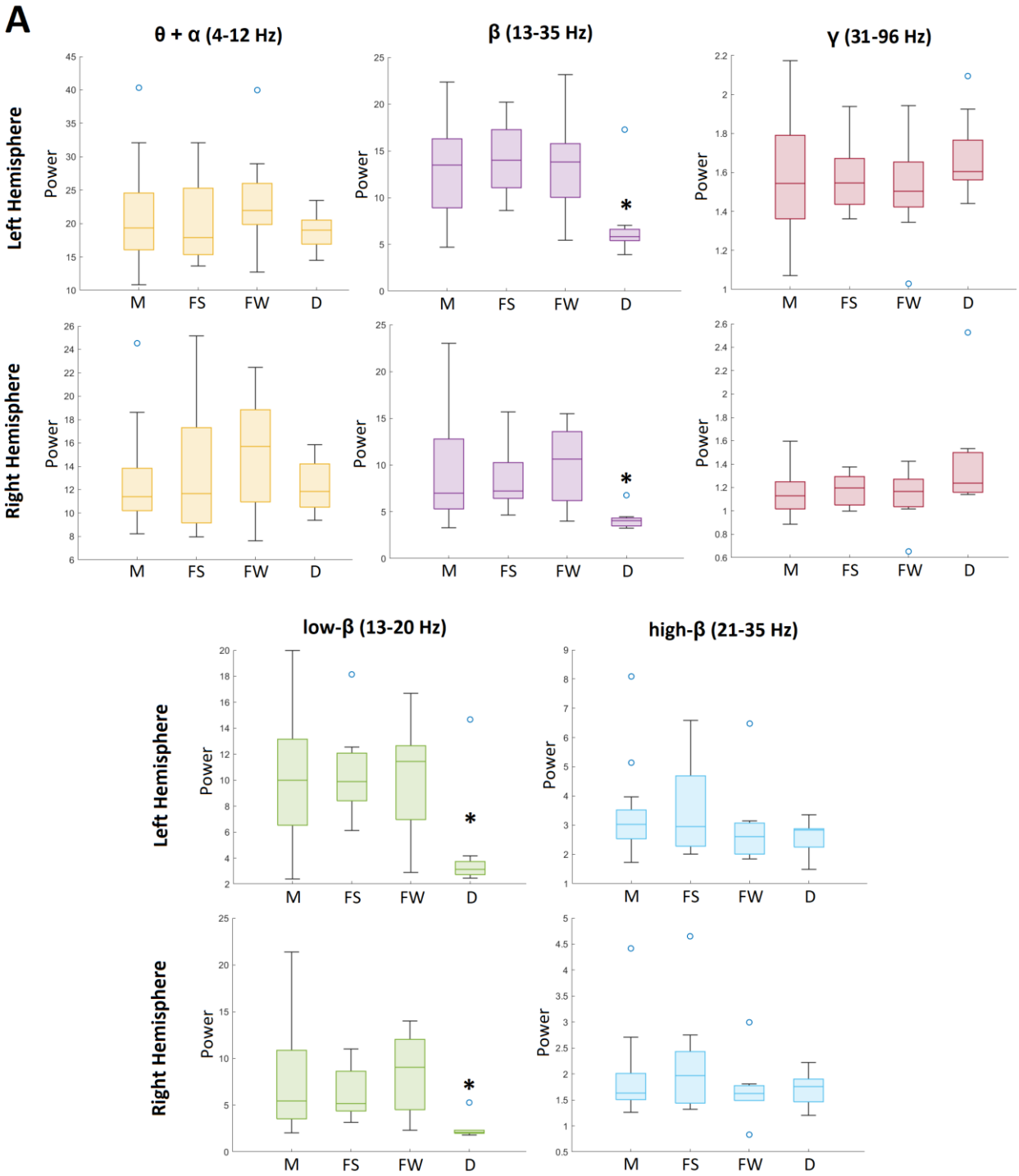

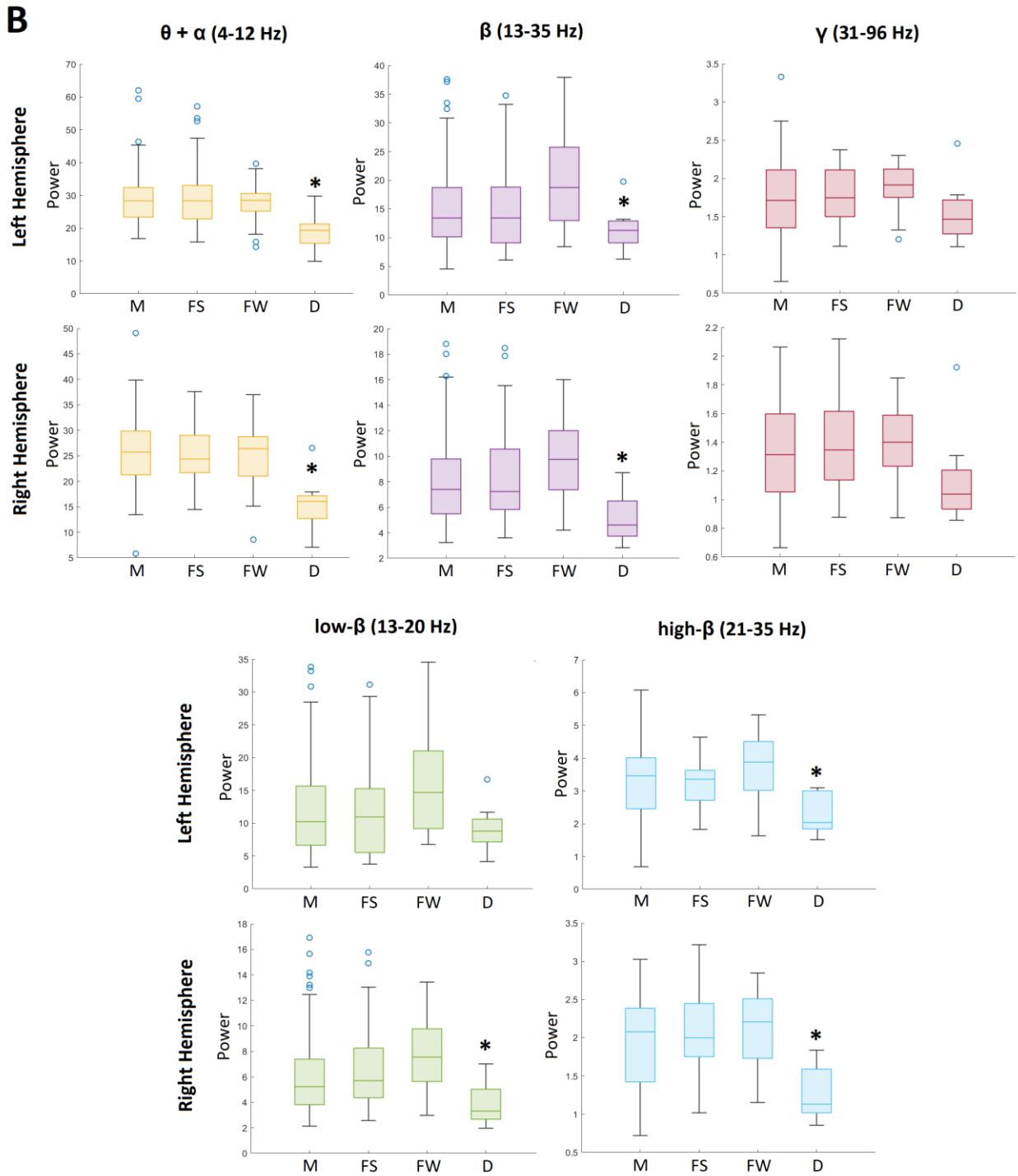

Figure 32 – Power in various frequency bands for four different hemisphere baselines. All graphs contain data from patient 6, where **(A)** corresponds to the first out-clinical period and **(B)** the second. Each graph has the minimum, 25th percentile, median, 75th, and maximum values for the four types of events: M – Medication; FS – Feeling stuck; FW – Feeling well; D – Dyskinesias. The frequency ranges are, respectively: θ+α (yellow), β(purple), low-β(green), high-β(blue), and γ(red). The asterisk marks the instances where dyskinesias are statistically different from at least one other event type ($p<0.05$).

Table 11 – Performance metrics of ML algorithms for dyskinesias binary classification. The results are from patient 6. The values are under the form of mean $\pm$ std (N=1000).

Period	Hemisphere	ML Algorithm	F1-score	
			Power bands (with medication)	Power bands (without medication)
(A) 28/05/2021-03/06/2021	Right	SVM	0.80 ± 0.09	0.84 ± 0.12
		DT	0.84 ± 0.10	0.84 ± 0.14
	Left	SVM	0.73 ± 0.11	0.90 ± 0.09
		DT	0.78 ± 0.10	0.90 ± 0.10
(B) 03/06/2021-09/07/2021	Right	SVM	0.63 ± 0.03	0.70 ± 0.07
		DT	$-$*	0.60 ± 0.07
	Left	SVM	$-$*	0.71 ± 0.08
		DT	$-$*	0.67 ± 0.11

*Less than 0.5

Overall, SVM learners were more robust than the DT learners, for the latter did not perform as well in period B. The fact that the performance increased when medication events were discarded corroborates the stochastic nature of medication – i.e., it introduces randomness to the dataset. It is also worth mentioning that the standard deviations are significantly high. This happens because the number dyskinesias (positive class) cases is very small, and the misclassification of one of these strongly affects the F1-score metric.

4.4.2 Event & Continuous Analysis

4.4.2.1 Exploration

Similarly to the analysis of event-related data, an exploratory phase complemented the answering of the main research question of this section. Some of the developed functions are illustrated in Figure 33.

The use of continuous data enables the creation of temporal representations, such as the one in Figure 33A. Here, one can observe the circadian evolution of the LFP power in the form of peaks and valleys: in both hemispheres the power drops significantly during the nights and increases throughout the days. Interestingly, the power tends to reach its daily maximum just before the drop at night. This drop most likely reflects the

time at which the patient falls asleep, for the brain's activity is known to drop significantly in frequency bands other than delta during sleep. In this respect, the LFP power may

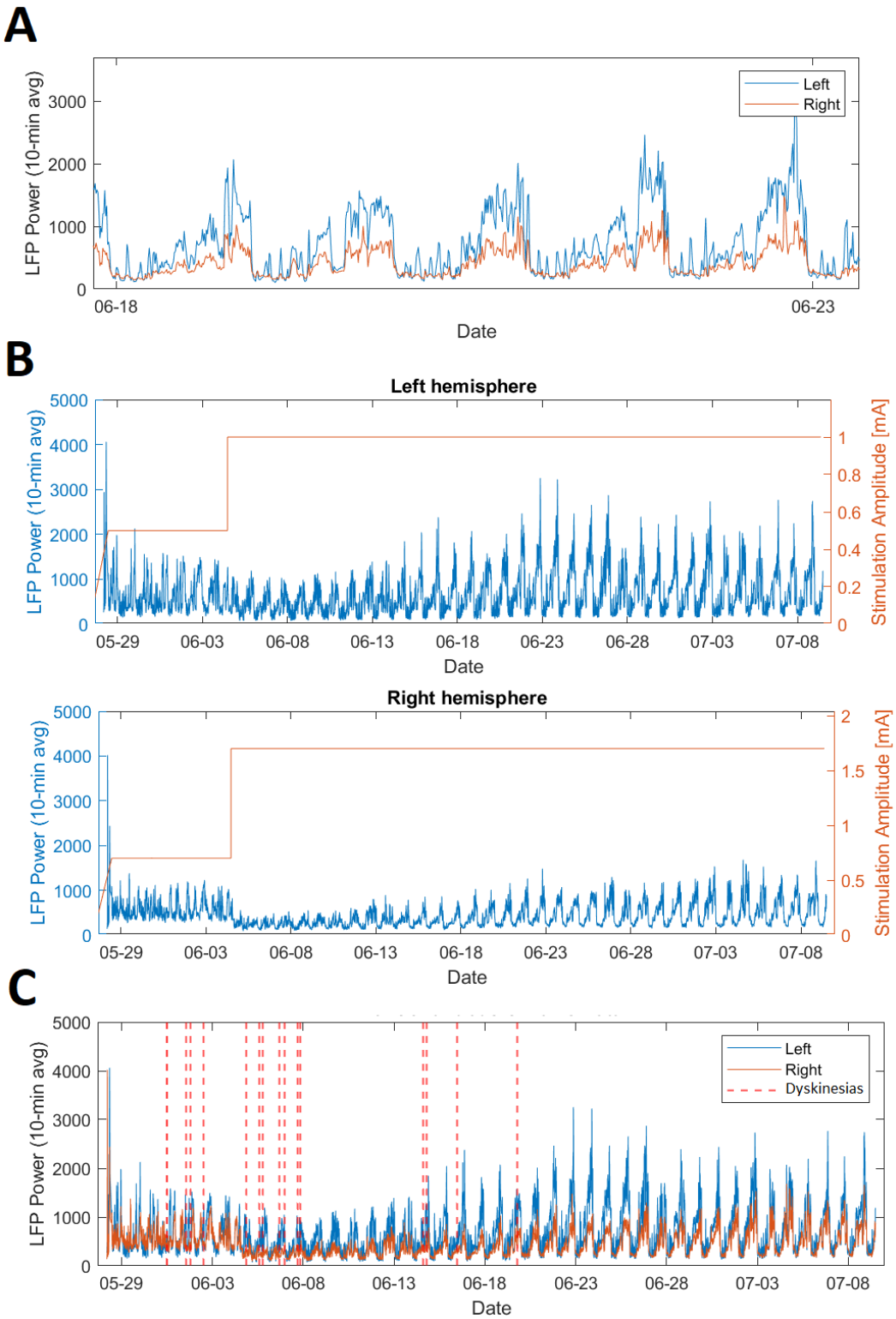

Figure 33 – Representations of LFP Power temporal evolution. All graphs contain data from patient 6. **(A)** Plot that contains the LFP power of both hemispheres in a 5-day period. **(B)** Pair of plots that contain the LFP power and stimulation amplitude of both hemispheres. **(C)** Dyskinesias occurrences alongside the LFP power of both hemispheres.

reflect potential disruptions on the patient's circadian rhythm. Besides the circadian analysis, the figure (33B) illustrates how a change in the baseline amplitude of the LFP power signal is coincident with the variation of the stimulation amplitudes – a phenomenon also patent in the event snapshots (see section 4.4.1.3). Lastly, in Figure 33C, one can see when the reported events occurred alongside the continuously acquired power.

4.4.2.2 Correlation between Event Power and Continuous LFP Power

(4) Can event-related data be inferred by the LFP power signal?

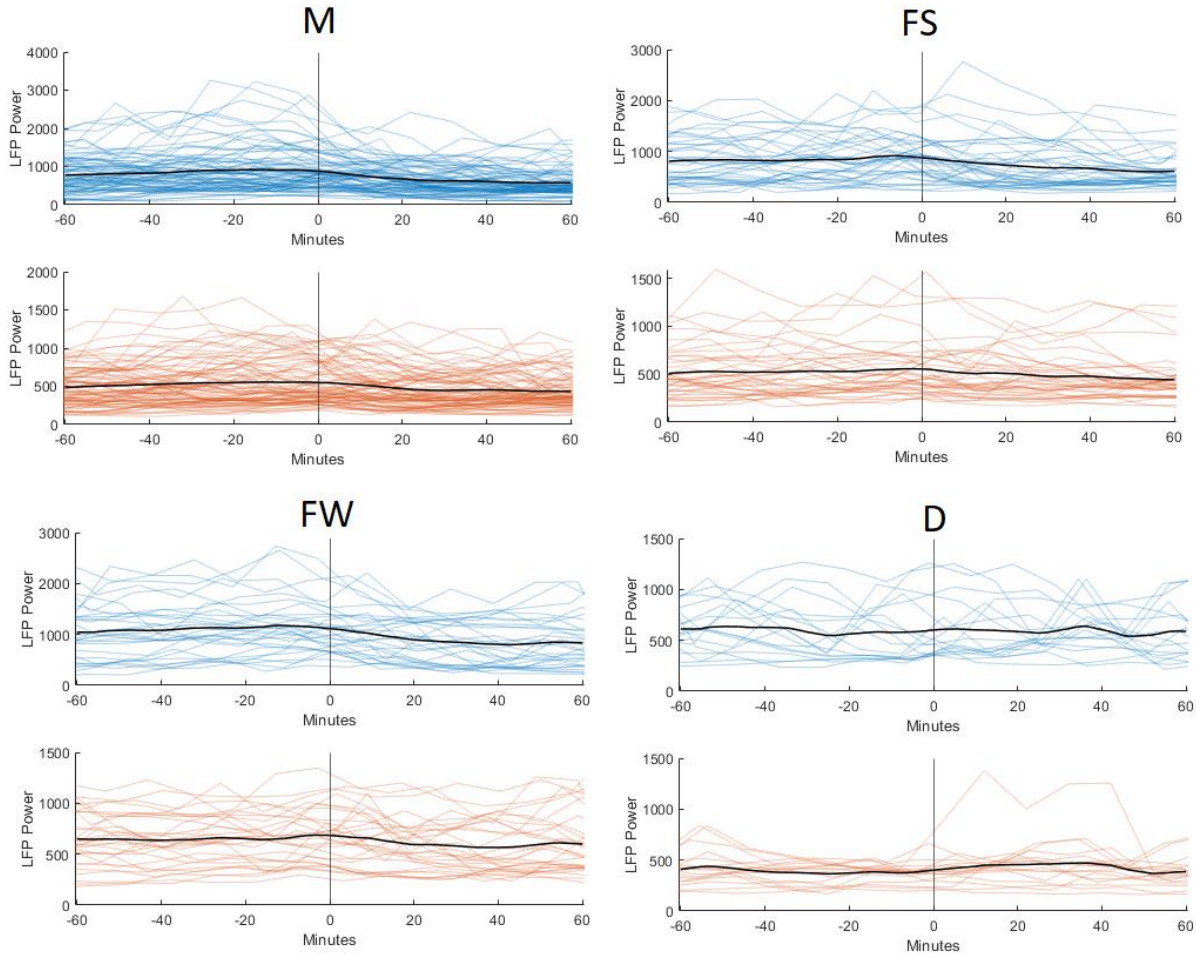

Figure 34 – LFP Power evolution with triggered events. All graphs contain data from patient 6. The left hemisphere is represented by the blue lines and the right hemisphere by the orange lines. Each graph fixes the events at the 0-minute mark and displays the LFP power within the ± 1 hour vicinity. The four event types are: **M** – Medication; **FS** – Feeling stuck; **FW** – Feeling well; **D** – Dyskinesias. The black lines represent the interpolated LFP power means of the respective events.

An event-triggered analysis was the starting point to the answer to the last main research question. By grouping the events according to their type and outlining the respective LFP power in the events' vicinities, one obtained the graphs in Figure 34. Two key observations can be made about these. First, the LFP power in the left hemisphere is appreciably higher than in the right hemisphere. The second observation has to do with the fact that the LFP power around the dyskinesias is lower than around other types of

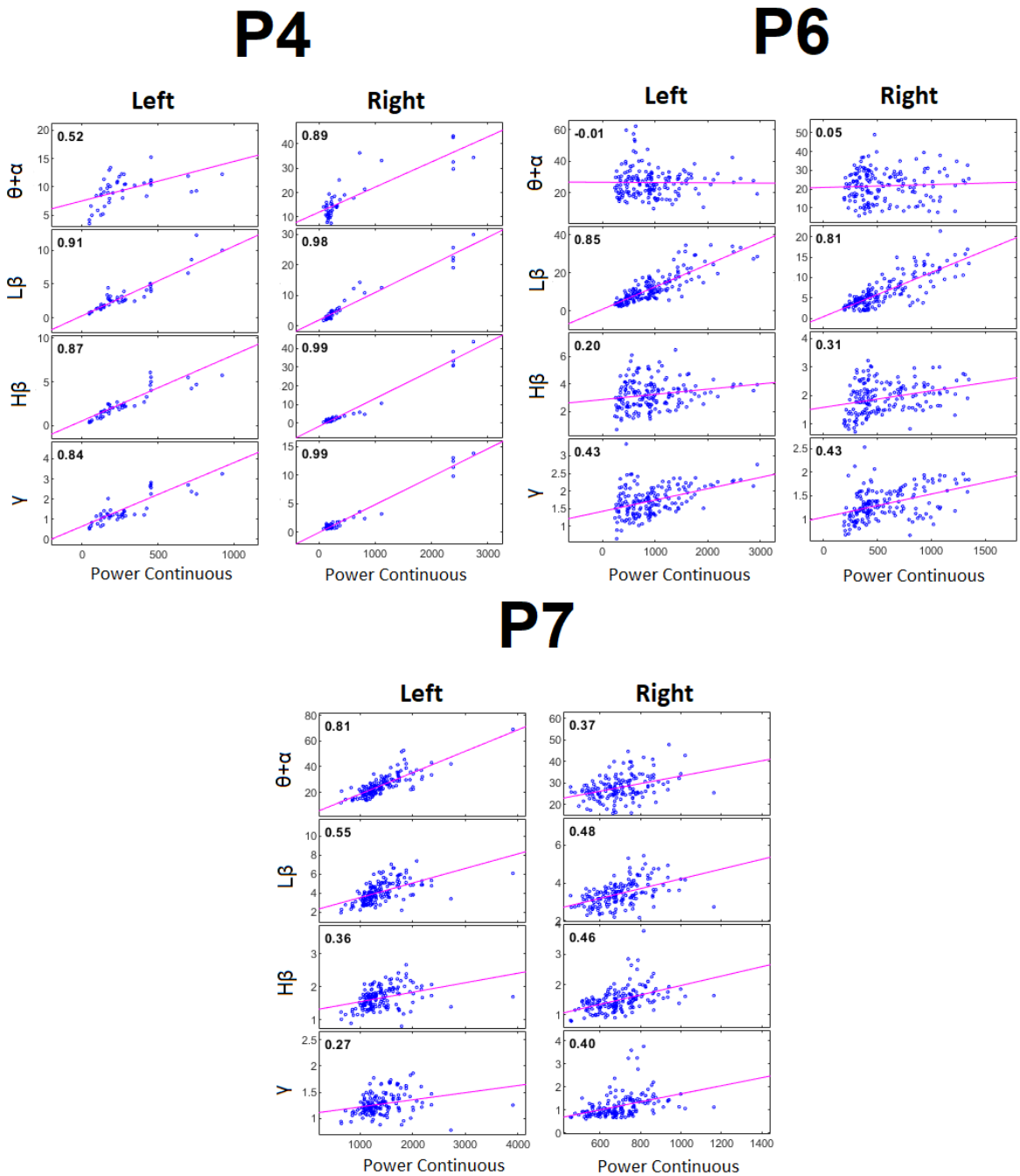

Figure 35 – Correlation between continuous LFP power and the power of multiple frequency bands. The plots contain data from patients 4,6, and 7. The frequency bands are from the top to the bottom: theta and alpha (4-12 Hz), low-beta (13-20 Hz), high-beta (21-35 Hz), and gamma (31-96 Hz).

events, especially in the left hemisphere. This is compatible with the results of section 4.4.1.4, where the same patient's dyskinesias had lower power in the beta band.

Having a qualitative match between the power of some events and the near LFP power elicited the possibility of a quantitative match. To test this through, we decided to plot the correlation between the last LFP power value before the event and the power of several frequency bands of the event, in multiple patients. The obtained results are illustrated in Figure 35.

Except for the right hemisphere of patient 7, the power of the bands that contained the frequency peaks (around which the continuous LFP power was recorded, see Table 8) were strongly correlated ($r > 0.75$) to the LFP power: in this case, the low- and high-beta bands for P4; the low-beta band for P6; and the alpha and theta bands for P7. Interestingly, the right hemisphere of patient 4 shows strong correlations for all the frequency bands. The probable cause of both anomalies is the presence of artefacts on these hemispheres. In any case, these results are indicative that even an LFP signal with very low-resolution may contain relevant information about the state of a patient.

4.5 Limitations & Future Work

This work has some limitations, such as the reduced amount of data, which can be regarded as the major one. This is especially true for section 4.4.1.4 where only one patient (6) had enough event variety for a detailed analysis. Fortunately, the NCN lab expects a new batch of data to arrive soon. This increase in data will not only allow the validation of the obtained results, but also make a wider array of analyses available. For example, it would be interesting to compare data from periods where the stimulation amplitudes are the same in one or both hemispheres – i.e., studying the effect of contralateral stimulation or of the disease progression on the FFT profiles. Furthermore, one could compare periods with and without stimulation. This may provide a clear view on the optimal stimulation timing for maximising or minimising the frequency and intensity of any given event – allowing the creation of simple, but efficient, ON/OFF adaptive systems.

Concerning the patients, the inclusion of the type of PD (akinetic-rigid vs. tremor dominant) may be an important factor to consider, as suggested by [135]. As for the events, a distinction between scheduled medication and SOS medication could be useful because the latter is associated with deleterious states (such as, feeling stuck or dyskinesias) and could provide a new framework for the study of medication events.

Given the constraint on the number of events, one should also reflect on the adequacy of the chosen events. Perhaps, events where symptoms are manifest should be prioritised over subjective states. In this respect, different research centres could promote a convergence on event selection and the cross-validation of results, by engaging with each other.

On a different note, the comparison between intra-operative and chronic recordings may also be an interesting line of research. The reason for that is the fact that the implanted lead can suffer minor displacements throughout time, which, in turn, can provoke changes in the FFT profiles. Thus, the intra-operative recordings could provide a mapping of these profiles for several locations and orientations.

4.6 Conclusions

The need of visuo-analytical tools for the chronic data obtained with the recent Medtronic's Percept™ + BrainSense™ Technology system fuelled the present thesis. Furthermore, the opportunity of exploring uncharted territory – for the literature is still scarce in this domain – encouraged the use of some the developed tools in a research-oriented manner. In fact, four research questions were formulated and tackled throughout this work. Each question produced relevant findings, which are summarised in the following answers:

1) *Do the event profiles of a given hemisphere share an identifying baseline?*

   The results supported the existence of hemispherical baselines and strengthened the idea that aDBS should operate at the hemispherical level.

2) *Does the baseline change over time? And, if so, how, and why?*

   The results showed that different stimulation amplitudes generate different hemispherical baselines, with higher variations resulting in more notorious changes of the FFT profiles. However, the reasons for these changes or degree to which these are due to stimulation artefacts could not be inferred.

3) *Can the events be differentiated through the hemispherical baseline?*

   The results suggest that event differentiation may be possible. Dyskinesias were successfully differentiated from other types of events, with the main differences residing in the beta activity. Notwithstanding, a generalization of this phenomenon could not be made, for the analysis was limited to just one patient.

4) *Can event-related data be inferred by the LFP power signal?*

The results showed that the continuous LFP power is highly correlated with the event power in the frequency band in which it is continuously acquired.

The work had some limitations, most of which derived from the size of the dataset. Overall, both the developed tools and the findings foster the analysis of new data and the opening of new lines of research, that otherwise would have to wait until adequate tools were created.

Chapter 5

Conclusion

Despite the recent technological advancements on the hardware and software fronts, the DBS field is yet to create robust adaptive systems that work both in- and outside the clinical settings. A major step towards these systems lies on the choice of reliable biomarkers. Current knowledge posits the existence of potential biomarkers in both LFPs and the patient's motricity. In fact, the latter is commonly used to evaluate the efficacy of the DBS stimulation protocol during clinical sessions. However, this process still relies on subjective metrics. Thus, it becomes necessary to develop systems for the acquisition and objective analysis of these motor signals.

To fulfil this need, a wearable system was developed from scratch. This system has two main features: a GUI that allows the user to record and see information about the patient's motor data in real-time, and a bundle of functions for posterior analysis of the recorded data. These functions mainly focus on the quantification of tremor and rigidity, two of the Parkinsonian cardinal symptoms. While the quantification of tremor uses known parameters, a novel way for rigidity quantification is proposed. Overall, the functions showed great potential for the forthcoming clinical validation step.

Besides the development of a wearable system, this work focused on a more challenging need. Devices with data storage capacity recently enabled the research of chronic data. Yet, current analytical toolboxes do not make use of all the available data, nor are they suited for non-data-scientists use. To fill this gap, several visuo-analytical tools were developed and integrated in an extensive toolbox. The lack of research concerning event-related data further encouraged the application of these tools in a research-oriented manner. Therefore, four research questions were formulated.

All the questions were successfully addressed. While some of the findings are in accordance with previous studies – namely that aDBS should actuate not at the patient, but at the hemispherical level, or that the beta band may be a good biomarker for dyskinesias – the other findings are not well-portrayed in the literature. In this regard, the collection of further data plays a vital role not only in their validation, but also in the establishment of new lines of research.

All in all, this work seized the opportunity to fill multiple needs with one deed, by building tools that can easily be integrated in future aDBS systems, whilst laying the groundwork for the further study of chronic DBS data.

Future work

As fruitful as this work might have been, there are some aspects that await further improvement. Concerning the developed wearable system, different methods for updating the orientation of the sensors – namely the use of quaternions – should be considered for future versions of the application. Also, at the time of writing, the NCN lab is waiting for the scheduling of clinical sessions, so that the system can be validated with patients manifesting Parkinsonian symptoms. New functionalities are also on the table, such as quantification methods for additional symptoms, or the use of machine-learning models in real-time symptom prediction.

As for the study of chronic data, information regarding the patient – such as the subtype of PD or the longevity of the medication therapy – may be valuable in future studies. Moreover, an extensive analysis on the event landscape should be performed, so that the most adequate can be selected. But, more importantly, larger datasets should be used. On this score, new data is being provided soon to the NCN lab. This will enable the improvement of the developed tools and the creation of new ones, along with the opening of new lines of research, such as the study of “on-off” states, contralateral stimulation, and disease progression.

Finally, one cannot help but to envision the joining of the two pieces of this thesis: the creation of aDBS systems that incorporate the developed wearable and the captured chronic data, in real-world environments. For instance, the wearable could trigger the snapshot feature of the neurostimulator, overruling the patient’s need to self-report. But, for this to become a reality, a lot of hard work lies ahead.

References

[1] Dorsey, E. R., Elbaz, A., Nichols, E., Abbasi, N., Abd-Allah, F., Abdelalim, A., Adsuar, J. C., Ansha, M. G., Brayne, C., Choi, J.-Y. J., Collado-Mateo, D., Dahodwala, N., Do, H. P., Edessa, D., Endres, M., Fereshtehnejad, S.-M., Foreman, K. J., Gankpe, F. G., Gupta, R., … Murray, C. J. L. (2018). Global, regional, and national burden of Parkinson's disease, 1990–2016: A systematic analysis for the Global Burden of Disease Study 2016. *The Lancet Neurology*, *17*(11), 939–953. https://doi.org/10.1016/S1474-4422(18)30295-3

[2] Estimation of the 2020 Global Population of Parkinson's Disease (PD). (n.d.). *MDS Abstracts*. Retrieved 13 June 2022, from https://www.mdsabstracts.org/abstract/estimation-of-the-2020-global-population-of-parkinsons-disease-pd/

[3] Zhang, X.-X., Tian, Y., Wang, Z.-T., Ma, Y.-H., Tan, L., & Yu, J.-T. (2021). The Epidemiology of Alzheimer's Disease Modifiable Risk Factors and Prevention. *The Journal of Prevention of Alzheimer's Disease*, *8*(3), 313–321. https://doi.org/10.14283/jpad.2021.15

[4] Dorsey, E. R., Sherer, T., Okun, M. S., & Bloem, B. R. (2018). The Emerging Evidence of the Parkinson Pandemic. *Journal of Parkinson's Disease*, *8*(s1), S3–S8. https://doi.org/10.3233/JPD-181474

[5] Kouli, A., Torsney, K. M., & Kuan, W.-L. (2018). Parkinson's Disease: Etiology, Neuropathology, and Pathogenesis. In T. B. Stoker & J. C. Greenland (Eds.), Parkinson's Disease: Pathogenesis and Clinical Aspects. Codon Publications. http://www.ncbi.nlm.nih.gov/books/NBK536722/

[6] Elbaz, A., Clavel, J., Rathouz, P. J., Moisan, F., Galanaud, J.-P., Delemotte, B., Alpérovitch, A., & Tzourio, C. (2009). Professional exposure to pesticides and Parkinson disease. Annals of Neurology, 66(4), 494–504. https://doi.org/10.1002/ana.21717

[7] Hernán, M. A., Takkouche, B., Caamaño-Isorna, F., & Gestal-Otero, J. J. (2002). A meta-analysis of coffee drinking, cigarette smoking, and the risk of Parkinson's disease. Annals of Neurology, 52(3), 276–284. https://doi.org/10.1002/ana.10277

[8] Dopaminergic system. (n.d.). Brain for Ai Wiki. Retrieved 13 June 2022, from https://brain-for-ai.fandom.com/wiki/Dopaminergic_system

[9] Cernera, S., Eisinger, R. S., Wong, J. K., Ho, K. W. D., Lopes, J. L., To, K., Carbunaru, S., Ramirez-Zamora, A., Almeida, L., Foote, K. D., Okun, M. S., & Gunduz, A. (2020). Long-term Parkinson's disease quality of life after staged DBS: STN vs GPi and first vs second lead. Npj Parkinson's Disease, 6(1), 1–10. https://doi.org/10.1038/s41531-020-0115-3

[10] Aarsland, D., Creese, B., Politis, M., Chaudhuri, K. R., ffytche, D. H., Weintraub, D., & Ballard, C. (2017). Cognitive decline in Parkinson disease. Nature Reviews. Neurology, 13(4), 217–231. https://doi.org/10.1038/nrneurol.2017.27

[11] Chapter 186: Parkinson's Disease | Harrison's Manual of Medicine. (n.d.). Retrieved 13 June 2022, from https://harrisons.unboundmedicine.com/harrisons/view/Harrisons-Manual-of-Medicine/623107/all/Chapter_186:_Parkinson's_Disease?refer=true

[12] Vasta, R., Nicoletti, A., Mostile, G., Dibilio, V., Sciacca, G., Contrafatto, D., Cicero, C. E., Raciti, L., Luca, A., & Zappia, M. (2017). Side effects induced by the acute levodopa challenge in Parkinson's Disease and atypical parkinsonisms. PLOS ONE, 12(2), e0172145. https://doi.org/10.1371/journal.pone.0172145

[13] Koschel, J., Ray Chaudhuri, K., Tönges, L., Thiel, M., Raeder, V., & Jost, W. H. (2021). Implications of dopaminergic medication withdrawal in Parkinson's disease. Journal of Neural Transmission. https://doi.org/10.1007/s00702-021-02389-x
[14] Marsden, C. D. (1994). Problems with long-term levodopa therapy for Parkinson's disease. Clinical Neuropharmacology, 17 Suppl 2, S32-44.
[15] Pandey, S., & Srivanitchapoom, P. (2017). Levodopa-induced Dyskinesia: Clinical Features, Pathophysiology, and Medical Management. Annals of Indian Academy of Neurology, 20(3), 190–198. https://doi.org/10.4103/aian.AIAN_239_17
[16] Okun, M. S. (2012). Deep-Brain Stimulation for Parkinson's Disease. New England Journal of Medicine, 367(16), 1529–1538. https://doi.org/10.1056/NEJMct1208070
[17] Rizzone, M. G., Fasano, A., Daniele, A., Zibetti, M., Merola, A., Rizzi, L., Piano, C., Piccininni, C., Romito, L. M., Lopiano, L., & Albanese, A. (2014). Long-term outcome of subthalamic nucleus DBS in Parkinson's disease: From the advanced phase towards the late stage of the disease? Parkinsonism & Related Disorders, 20(4), 376–381. https://doi.org/10.1016/j.parkreldis.2014.01.012
[18] Schuepbach, W. m. m., Rau, J., Knudsen, K., Volkmann, J., Krack, P., Timmermann, L., Hälbig, T. d., Hesekamp, H., Navarro, S. m., Meier, N., Falk, D., Mehdorn, M., Paschen, S., Maarouf, M., Barbe, M. t., Fink, G. r., Kupsch, A., Gruber, D., Schneider, G.-H., … Deuschl, G. (2013). Neurostimulation for Parkinson's Disease with Early Motor Complications. New England Journal of Medicine, 368(7), 610–622. https://doi.org/10.1056/NEJMoa1205158
[19] Louis, E. D. (2016). Treatment of Medically Refractory Essential Tremor. New England Journal of Medicine, 375(8), 792–793. https://doi.org/10.1056/NEJMe1606517
[20] Meoni, S., Fraix, V., Castrioto, A., Benabid, A. L., Seigneuret, E., Vercueil, L., Pollak, P., Krack, P., Chevrier, E., Chabardes, S., & Moro, E. (2017). Pallidal deep brain stimulation for dystonia: A long term study. Journal of Neurology, Neurosurgery, and Psychiatry, 88(11), 960–967. https://doi.org/10.1136/jnnp-2016-315504
[21] Chiken, S., & Nambu, A. (2016). Mechanism of Deep Brain Stimulation: Inhibition, Excitation, or Disruption? The Neuroscientist: A Review Journal Bringing Neurobiology, Neurology and Psychiatry, 22(3), 313–322. https://doi.org/10.1177/1073858415581986
[22] McIntyre, C. C., & Hahn, P. J. (2010). Network perspectives on the mechanisms of deep brain stimulation. Neurobiology of Disease, 38(3), 329–337. https://doi.org/10.1016/j.nbd.2009.09.022
[23] Kang, G., & Lowery, M. (2014). Effects of antidromic and orthodromic activation of STN afferent axons during DBS in Parkinson's disease: A simulation study. Frontiers in Computational Neuroscience, 8. https://www.frontiersin.org/article/10.3389/fncom.2014.00032
[24] Tawfik, V. L., Chang, S.-Y., Hitti, F. L., Roberts, D. W., Leiter, J. C., Jovanovic, S., & Lee, K. H. (2010). Deep Brain Stimulation Results in Local Glutamate and Adenosine Release: Investigation into the Role of Astrocytes. Neurosurgery, 67(2), 367–375. https://doi.org/10.1227/01.NEU.0000371988.73620.4C
[25] McGregor, M. M., & Nelson, A. B. (2019). Circuit Mechanisms of Parkinson's Disease. Neuron, 101(6), 1042–1056. https://doi.org/10.1016/j.neuron.2019.03.004
[26] Deep Brain Stimulation in Parkinson's Disease Market Global Trends, Market Share, Industry Size, Growth, Opportunities and Market Forecast—2022 to 2028. (2022, March 10). Orion Market Reports. https://orionmarketreports.com/deep-brain-stimulation-in-parkinsons-disease-market/89638/
[27] Gardner, J. (2013). A history of deep brain stimulation: Technological innovation and the role of clinical assessment tools. Social Studies of Science, 43(5), 707–728. https://doi.org/10.1177/0306312713483678
[28] Unified Parkinson Disease Rating Scale (UPDRS). (n.d.). Theracycle Physical Therapy Exercise Bike and Rehabilitation Equipment. Retrieved 13 June 2022, from https://www.theracycle.com/resources/links-and-additional-resources/updrs-scale/

[29] Krauss, J. K., Lipsman, N., Aziz, T., Boutet, A., Brown, P., Chang, J. W., Davidson, B., Grill, W. M., Hariz, M. I., Horn, A., Schulder, M., Mammis, A., Tass, P. A., Volkmann, J., & Lozano, A. M. (2021). Technology of deep brain stimulation: Current status and future directions. Nature Reviews. Neurology, 17(2), 75–87. https://doi.org/10.1038/s41582-020-00426-z

[30] Neumann, W.-J., Turner, R. S., Blankertz, B., Mitchell, T., Kühn, A. A., & Richardson, R. M. (2019). Toward Electrophysiology-Based Intelligent Adaptive Deep Brain Stimulation for Movement Disorders. Neurotherapeutics, 16(1), 105–118. https://doi.org/10.1007/s13311-018-00705-0

[31] Steigerwald, F., Matthies, C., & Volkmann, J. (2019). Directional Deep Brain Stimulation. Neurotherapeutics, 16(1), 100–104. https://doi.org/10.1007/s13311-018-0667-7

[32] Medtronic. (n.d.). Deep Brain Stimulation Systems—Percept Platform. Retrieved 13 June 2022, from https://www.medtronic.com/us-en/healthcare-professionals/products/neurological/deep-brain-stimulation-systems/percept-pc.html

[33] Fasano, A., & Helmich, R. C. (2019). Tremor habituation to deep brain stimulation: Underlying mechanisms and solutions. Movement Disorders, 34(12), 1761–1773. https://doi.org/10.1002/mds.27821

[34] Cernera, S., Alcantara, J. D., Opri, E., Cagle, J. N., Eisinger, R. S., Boogaart, Z., Pramanik, L., Kelberman, M., Patel, B., Foote, K. D., Okun, M. S., & Gunduz, A. (2021). Wearable sensor-driven responsive deep brain stimulation for essential tremor. Brain Stimulation, 14(6), 1434–1443. https://doi.org/10.1016/j.brs.2021.09.002

[35] Carron, R., Chaillet, A., Filipchuk, A., Pasillas-Lépine, W., & Hammond, C. (2013). Closing the loop of deep brain stimulation. Frontiers in Systems Neuroscience, 7, 112. https://doi.org/10.3389/fnsys.2013.00112

[36] Habets, J. G. V., Heijmans, M., Kuijf, M. L., Janssen, M. L. F., Temel, Y., & Kubben, P. L. (2018). An update on adaptive deep brain stimulation in Parkinson's disease. Movement Disorders: Official Journal of the Movement Disorder Society, 33(12), 1834–1843. https://doi.org/10.1002/mds.115

[37] Little, S., & Brown, P. (2012). What brain signals are suitable for feedback control of deep brain stimulation in Parkinson's disease? Annals of the New York Academy of Sciences, 1265, 9–24. https://doi.org/10.1111/j.1749-6632.2012.06650.x

[38] Neumann, W.-J., Staub-Bartelt, F., Horn, A., Schanda, J., Schneider, G.-H., Brown, P., & Kühn, A. A. (2017). Long term correlation of subthalamic beta band activity with motor impairment in patients with Parkinson's disease. Clinical Neurophysiology, 128(11), 2286–2291. https://doi.org/10.1016/j.clinph.2017.08.028

[39] Brown, P. (2007). Abnormal oscillatory synchronisation in the motor system leads to impaired movement. Current Opinion in Neurobiology, 17(6), 656–664. https://doi.org/10.1016/j.conb.2007.12.001

[40] Hammond, C., Bergman, H., & Brown, P. (2007). Pathological synchronization in Parkinson's disease: Networks, models and treatments. Trends in Neurosciences, 30(7), 357–364. https://doi.org/10.1016/j.tins.2007.05.004

[41] Lmf, D., Aa, K., M, H., A, K., G-H, S., & P, B. (2005). Levodopa-induced modulation of subthalamic beta oscillations during self-paced movements in patients with Parkinson's disease. Eur J Neurosci, 21, 1403–1412.

[42] Alonso-Frech, F., Zamarbide, I., Alegre, M., Rodríguez-Oroz, M. C., Guridi, J., Manrique, M., Valencia, M., Artieda, J., & Obeso, J. A. (2006). Slow oscillatory activity and levodopa-induced dyskinesias in Parkinson's disease. Brain, 129(7), 1748–1757. https://doi.org/10.1093/brain/awl103

[43] Meidahl, A., Tinkhauser, G., Herz, D., Cagnan, H., Debarros, J., & Brown, P. (2017). Adaptive Deep Brain Stimulation for Movement Disorders: The Long Road to Clinical Therapy. Movement Disorders : Official Journal of the Movement Disorder Society. https://doi.org/10.1002/mds.27022

[44] Hirschmann, J., Butz, M., Hartmann, C. J., Hoogenboom, N., Özkurt, T. E., Vesper, J., Wojtecki, L., & Schnitzler, A. (2016). Parkinsonian Rest Tremor Is Associated With Modulations of Subthalamic High-Frequency Oscillations. Movement Disorders, 31(10), 1551–1559. https://doi.org/10.1002/mds.26663

[45] Swann, N. C., de Hemptinne, C., Miocinovic, S., Qasim, S., Wang, S. S., Ziman, N., Ostrem, J. L., San Luciano, M., Galifianakis, N. B., & Starr, P. A. (2016). Gamma Oscillations in the Hyperkinetic State Detected with Chronic Human Brain Recordings in Parkinson's Disease. The Journal of Neuroscience, 36(24), 6445–6458. https://doi.org/10.1523/JNEUROSCI.1128-16.2016

[46] Storzer, L., Butz, M., Hirschmann, J., Abbasi, O., Gratkowski, M., Saupe, D., Vesper, J., Dalal, S. S., & Schnitzler, A. (2017). Bicycling suppresses abnormal beta synchrony in the Parkinsonian basal ganglia. Annals of Neurology, 82(4), 592–601. https://doi.org/10.1002/ana.25047

[47] Ramirez-Zamora, A., Giordano, J., Gunduz, A., Brown, P., Sanchez, J., Foote, K., Almeida, L., Starr, P., Brontë-Stewart, H., Hu, W., Mcintyre, C., Goodman, W., Kumsa, D., Grill, W., Walker, H., Johnson, M., Vitek, J., Greene, D., Rizzuto, D., & Okun, M. (2018). Evolving Applications, Technological Challenges and Future Opportunities in Neuromodulation: Proceedings of the Fifth Annual Deep Brain Stimulation Think Tank. Frontiers in Neuroscience, 11, 734. https://doi.org/10.3389/fnins.2017.00734

[48] Basu, I., Graupe, D., Tuninetti, D., Shukla, P., Slavin, K. V., Metman, L. V., & Corcos, D. M. (2013). Pathological tremor prediction using surface electromyogram and acceleration: Potential use in `ON–OFF' demand driven deep brain stimulator design. Journal of Neural Engineering, 10(3), 036019. https://doi.org/10.1088/1741-2560/10/3/036019

[49] Alam, M. N., Johnson, B., Gendreau, J., Tavakolian, K., Combs, C., & Fazel-Rezai, R. (2016). Tremor quantification of Parkinson's disease—A pilot study. 2016 IEEE International Conference on Electro Information Technology (EIT), 0755–0759. https://doi.org/10.1109/EIT.2016.7535334

[50] Ferreira-Sánchez, M. del R., Moreno-Verdú, M., & Cano-de-la-Cuerda, R. (2020). Quantitative Measurement of Rigidity in Parkinson's Disease: A Systematic Review. Sensors, 20(3), 880. https://doi.org/10.3390/s20030880

[51] Association, E. P. D. (n.d.). Rigidity. Retrieved 29 June 2022, from https://www.epda.eu.com/about-parkinsons/symptoms/motor-symptoms/rigidity/

[52] Arlotti, M., Rosa, M., Marceglia, S., Barbieri, S., & Priori, A. (2016). The adaptive deep brain stimulation challenge. Parkinsonism & Related Disorders, 28, 12–17. https://doi.org/10.1016/j.parkreldis.2016.03.020

[53] Massano, J., & Bhatia, K. P. (2012). Clinical Approach to Parkinson's Disease: Features, Diagnosis, and Principles of Management. Cold Spring Harbor Perspectives in Medicine, 2(6), a008870. https://doi.org/10.1101/cshperspect.a008870

[54] Vaillancourt, D. E., & Newell, K. M. (2000). The dynamics of resting and postural tremor in Parkinson's disease. Clinical Neurophysiology, 111(11), 2046–2056. https://doi.org/10.1016/S1388-2457(00)00467-3

[55] Heida, T., Wentink, E. C., & Marani, E. (2013). Power spectral density analysis of physiological, rest and action tremor in Parkinson's disease patients treated with deep brain stimulation. Journal of NeuroEngineering and Rehabilitation, 10, 70. https://doi.org/10.1186/1743-0003-10-70

[56] Baumann, C. R. (2012). Epidemiology, diagnosis and differential diagnosis in Parkinson's disease tremor. Parkinsonism & Related Disorders, 18, S90–S92. https://doi.org/10.1016/S1353-8020(11)70029-3

[57] Ferrigno, L., Miele, G., Milano, F., Rodio, A., Santoni, F., De Angelis, A., Moschitta, A., Carbone, P., & Cerro, G. (2020). A real-time tracking system for tremor and trajectory estimation in Parkinson's disease affected patients. 2020 IEEE International Symposium on Medical Measurements and Applications (MeMeA), 1–6. https://doi.org/10.1109/MeMeA49120.2020.9137210

[58] Buijink, A., Contarino, M. F., Koelman, J., Speelman, J., & Rootselaar, A.-F. (2012). How to Tackle Tremor – Systematic Review of the Literature and Diagnostic Work-Up. Frontiers in Neurology, 3, 146. https://doi.org/10.3389/fneur.2012.00146
[59] The Neurological Examination - Fundamentals of Neurology: An Illustrated Guide. (n.d.). Retrieved 29 June 2022, from https://doctorlib.info/neurology/fundamentals-neurology/3.html
[60] Sun, F. T., & Morrell, M. J. (2014). The RNS System: Responsive cortical stimulation for the treatment of refractory partial epilepsy. Expert Review of Medical Devices, 11(6), 563–572. https://doi.org/10.1586/17434440.2014.947274
[61] Miocinovic, S., Hemptinne, C. de, Qasim, S. E., Ostrem, J., & Starr, P. (2015). Patterns of Cortical Synchronization in Isolated Dystonia Compared With Parkinson Disease. JAMA Neurology. https://doi.org/10.1001/jamaneurol.2015.2561
[62] de Hemptinne, C., Ryapolova-Webb, E. S., Air, E. L., Garcia, P. A., Miller, K. J., Ojemann, J. G., Ostrem, J. L., Galifianakis, N. B., & Starr, P. A. (2013). Exaggerated phase–amplitude coupling in the primary motor cortex in Parkinson disease. Proceedings of the National Academy of Sciences of the United States of America, 110(12), 4780–4785. https://doi.org/10.1073/pnas.1214546110
[63] Grahn, P. J., Mallory, G. W., Khurram, O. U., Berry, B. M., Hachmann, J. T., Bieber, A. J., Bennet, K. E., Min, H.-K., Chang, S.-Y., Lee, K. H., & Lujan, J. L. (2014). A neurochemical closed-loop controller for deep brain stimulation: Toward individualized smart neuromodulation therapies. Frontiers in Neuroscience, 8. https://www.frontiersin.org/article/10.3389/fnins.2014.00169
[64] Satzer, D., Lanctin, D., Eberly, L. E., & Abosch, A. (2014). Variation in Deep Brain Stimulation Electrode Impedance over Years Following Electrode Implantation. Stereotactic and Functional Neurosurgery, 92(2), 94–102. https://doi.org/10.1159/000358014
[65] Marquez-Chin, C., & Popovic, M. R. (2020). Functional electrical stimulation therapy for restoration of motor function after spinal cord injury and stroke: A review. BioMedical Engineering OnLine, 19, 34. https://doi.org/10.1186/s12938-020-00773-4
[66] Almeida, L., Rawal, P. V., Ditty, B., Smelser, B. L., Huang, H., Okun, M. S., Guthrie, B. L., & Walker, H. C. (2016). Deep Brain Stimulation Battery Longevity: Comparison of Monopolar Versus Bipolar Stimulation Modes. Movement Disorders Clinical Practice, 3(4), 359–366. https://doi.org/10.1002/mdc3.12285
[67] Xie, T., Padmanaban, M., Bloom, L., MacCracken, E., Bertacchi, B., Dachman, A., & Warnke, P. (2017). Effect of low versus high frequency stimulation on freezing of gait and other axial symptoms in Parkinson patients with bilateral STN DBS: A mini-review. Translational Neurodegeneration, 6, 13. https://doi.org/10.1186/s40035-017-0083-7
[68] Baizabal-Carvallo, J. F., & Alonso-Juarez, M. (2016). Low-frequency deep brain stimulation for movement disorders. Parkinsonism & Related Disorders, 31, 14–22. https://doi.org/10.1016/j.parkreldis.2016.07.018
[69] Dayal, V., Limousin, P., & Foltynie, T. (2017). Subthalamic Nucleus Deep Brain Stimulation in Parkinson's Disease: The Effect of Varying Stimulation Parameters. Journal of Parkinson's Disease, 7(2), 235–245. https://doi.org/10.3233/JPD-171077
[70] Akbar, U., Raike, R. S., Hack, N., Hess, C. W., Skinner, J., Martinez-Ramirez, D., DeJesus, S., & Okun, M. S. (2016). Randomized, Blinded Pilot Testing of Nonconventional Stimulation Patterns and Shapes in Parkinson's Disease and Essential Tremor: Evidence for Further Evaluating Narrow and Biphasic Pulses. Neuromodulation: Technology at the Neural Interface, 19(4), 343–356. https://doi.org/10.1111/ner.12397
[71] Steigerwald, F., Timmermann, L., Kühn, A., Schnitzler, A., Reich, M. M., Kirsch, A. D., Barbe, M. T., Visser-Vandewalle, V., Hübl, J., van Riesen, C., Groiss, S. J., Moldovan, A., Lin, S., Carcieri, S., Manola, L., & Volkmann, J. (2018). Pulse duration settings in subthalamic stimulation for Parkinson's disease. Movement Disorders, 33(1), 165–169. https://doi.org/10.1002/mds.27238

[72] Miocinovic, S., Khemani, P., Whiddon, R., Zeilman, P., Martinez-Ramirez, D., Okun, M. S., & Chitnis, S. (2014). Outcomes, management, and potential mechanisms of interleaving deep brain stimulation settings. Parkinsonism & Related Disorders, 20(12), 1434–1437. https://doi.org/10.1016/j.parkreldis.2014.10.011
[73] Ocklenburg, S., & Güntürkün, O. (2012). Hemispheric Asymmetries: The Comparative View. Frontiers in Psychology, 3, 5. https://doi.org/10.3389/fpsyg.2012.00005
[74] Little, S., Beudel, M., Zrinzo, L., Foltynie, T., Limousin, P., Hariz, M., Neal, S., Cheeran, B., Cagnan, H., Gratwicke, J., Aziz, T. Z., Pogosyan, A., & Brown, P. (2016). Bilateral adaptive deep brain stimulation is effective in Parkinson's disease. Journal of Neurology, Neurosurgery & Psychiatry, 87(7), 717–721. https://doi.org/10.1136/jnnp-2015-310972
[75] Merk, T., Peterson, V., Köhler, R., Haufe, S., Richardson, R. M., & Neumann, W.-J. (2022). Machine learning based brain signal decoding for intelligent adaptive deep brain stimulation. Experimental Neurology, 351, 113993. https://doi.org/10.1016/j.expneurol.2022.113993
[76] Fleming, J. E., Dunn, E., & Lowery, M. M. (2020). Simulation of Closed-Loop Deep Brain Stimulation Control Schemes for Suppression of Pathological Beta Oscillations in Parkinson's Disease. Frontiers in Neuroscience, 14. https://www.frontiersin.org/article/10.3389/fnins.2020.00166
[77] Tinkhauser, G., Pogosyan, A., Little, S., Beudel, M., Herz, D. M., Tan, H., & Brown, P. (2017). The modulatory effect of adaptive deep brain stimulation on beta bursts in Parkinson's disease. Brain: A Journal of Neurology, 140(4), 1053–1067. https://doi.org/10.1093/brain/awx010
[78] Azodi-Avval, R., & Gharabaghi, A. (2015). Phase-dependent modulation as a novel approach for therapeutic brain stimulation. Frontiers in Computational Neuroscience, 9. https://www.frontiersin.org/article/10.3389/fncom.2015.00026
[79] Arlotti, M., Marceglia, S., Foffani, G., Volkmann, J., Lozano, A. M., Moro, E., Cogiamanian, F., Prenassi, M., Bocci, T., Cortese, F., Rampini, P., Barbieri, S., & Priori, A. (2018). Eight-hours adaptive deep brain stimulation in patients with Parkinson disease. Neurology, 90(11), e971–e976. https://doi.org/10.1212/WNL.0000000000005121
[80] Kuhner, A., Schubert, T., Cenciarini, M., Wiesmeier, I. K., Coenen, V. A., Burgard, W., Weiller, C., & Maurer, C. (2017). Correlations between Motor Symptoms across Different Motor Tasks, Quantified via Random Forest Feature Classification in Parkinson's Disease. Frontiers in Neurology, 8, 607. https://doi.org/10.3389/fneur.2017.00607
[81] Khobragade, N., Tuninetti, D., & Graupe, D. (2018). On the need for adaptive learning in on-demand Deep Brain Stimulation for Movement Disorders. Annual International Conference of the IEEE Engineering in Medicine and Biology Society. IEEE Engineering in Medicine and Biology Society. Annual International Conference, 2018, 2190–2193. https://doi.org/10.1109/EMBC.2018.8512664
[82] Shah, S. A., Tinkhauser, G., Chen, C. C., Little, S., & Brown, P. (2018). Parkinsonian Tremor Detection from Subthalamic Nucleus Local Field Potentials for Closed-Loop Deep Brain Stimulation. Conference Proceedings : ... Annual International Conference of the IEEE Engineering in Medicine and Biology Society. IEEE Engineering in Medicine and Biology Society. Annual Conference, 2018, 2320–2324. https://doi.org/10.1109/EMBC.2018.8512741
[83] LeMoyne, R., Mastroianni, T., Whiting, D., & Tomycz, N. (2020). Parametric evaluation of deep brain stimulation parameter configurations for Parkinson's disease using a conformal wearable and wireless inertial sensor system and machine learning. Annual International Conference of the IEEE Engineering in Medicine and Biology Society. IEEE Engineering in Medicine and Biology Society. Annual International Conference, 2020, 3606–3611. https://doi.org/10.1109/EMBC44109.2020.9175408
[84] Mohammed, A., Bayford, R., & Demosthenous, A. (2020). A Framework for Adapting Deep Brain Stimulation Using Parkinsonian State Estimates. Frontiers in Neuroscience, 14, 499. https://doi.org/10.3389/fnins.2020.00499

[85] Tahafchi, P., Molina, R., Roper, J. A., Sowalsky, K., Hass, C. J., Gunduz, A., Okun, M. S., & Judy, J. W. (2017). Freezing-of-Gait detection using temporal, spatial, and physiological features with a support-vector-machine classifier. Annual International Conference of the IEEE Engineering in Medicine and Biology Society. IEEE Engineering in Medicine and Biology Society. Annual International Conference, 2017, 2867–2870. https://doi.org/10.1109/EMBC.2017.8037455

[86] Golshan, H. M., Hebb, A. O., Hanrahan, S. J., Nedrud, J., & Mahoor, M. H. (2016). A Multiple Kernel Learning approach for human behavioral task classification using STN-LFP signal. Annual International Conference of the IEEE Engineering in Medicine and Biology Society. IEEE Engineering in Medicine and Biology Society. Annual International Conference, 2016, 1030–1033. https://doi.org/10.1109/EMBC.2016.7590878

[87] Golshan, H. M., Hebb, A. O., Hanrahan, S. J., Nedrud, J., & Mahoor, M. H. (2018). A hierarchical structure for human behavior classification using STN local field potentials. Journal of Neuroscience Methods, 293, 254–263. https://doi.org/10.1016/j.jneumeth.2017.10.001

[88] Golshan, H. M., Hebb, A. O., & Mahoor, M. H. (2020). LFP-Net: A deep learning framework to recognize human behavioral activities using brain STN-LFP signals. Journal of Neuroscience Methods, 335, 108621. https://doi.org/10.1016/j.jneumeth.2020.108621

[89] Zaker, N., Zhang, J. J., Hanrahan, S., Nedrud, J., & Hebb, A. O. (2015). A new approach for automated detection of behavioral task onset for patients with Parkinson's disease using subthalamic nucleus local field potentials. 2015 49th Asilomar Conference on Signals, Systems and Computers, 780–784. https://doi.org/10.1109/ACSSC.2015.7421240

[90] Habets, J. G. V., Janssen, M. L. F., Duits, A. A., Sijben, L. C. J., Mulders, A. E. P., Greef, B. D., Temel, Y., Kuijf, M. L., Kubben, P. L., & Herff, C. (2020). Machine learning prediction of motor response after deep brain stimulation in Parkinson's disease—Proof of principle in a retrospective cohort. PeerJ, 8, e10317. https://doi.org/10.7717/peerj.10317

[91] He, S., Baig, F., Mostofi, A., Pogosyan, A., Debarros, J., Green, A. L., Aziz, T. Z., Pereira, E., Brown, P., & Tan, H. (2021). Closed-Loop Deep Brain Stimulation for Essential Tremor Based on Thalamic Local Field Potentials. Movement Disorders, 36(4), 863–873. https://doi.org/10.1002/mds.28513

[92] Amoozegar, S., Pooyan, M., & Roughani, M. (2019). Toward a closed-loop deep brain stimulation in Parkinson's disease using local field potential in parkinsonian rat model. Medical Hypotheses. https://doi.org/10.1016/j.mehy.2019.109360

[93] Angeles, P., Tai, Y., Pavese, N., Wilson, S., & Vaidyanathan, R. (2017). Automated assessment of symptom severity changes during deep brain stimulation (DBS) therapy for Parkinson's disease. IEEE .. International Conference on Rehabilitation Robotics, 2017, 1512–1517. https://doi.org/10.1109/icorr.2017.8009462

[94] Khobragade, N., Graupe, D., & Tuninetti, D. (2015). Towards fully automated closed-loop Deep Brain Stimulation in Parkinson's disease patients: A LAMSTAR-based tremor predictor. 2015 37th Annual International Conference of the IEEE Engineering in Medicine and Biology Society (EMBC). https://doi.org/10.1109/EMBC.2015.7318928

[95] Watts, J., Khojandi, A., Shylo, O., & Ramdhani, R. A. (2020). Machine Learning's Application in Deep Brain Stimulation for Parkinson's Disease: A Review. Brain Sciences, 10(11), E809. https://doi.org/10.3390/brainsci10110809

[96] Shamir, R. R., Dolber, T., Noecker, A. M., Walter, B. L., & McIntyre, C. C. (2015). Machine Learning Approach to Optimizing Combined Stimulation and Medication Therapies for Parkinson's Disease. Brain Stimulation, 8(6), 1025–1032. https://doi.org/10.1016/j.brs.2015.06.003

[97] Khojandi, A., Shylo, O., Mannini, L., Kopell, B. H., & Ramdhani, R. A. (2017). Stratifying Parkinson's Patients With STN-DBS Into High-Frequency or 60 Hz-Frequency Modulation Using a Computational Model. Neuromodulation: Journal of the International Neuromodulation Society, 20(5), 450–455. https://doi.org/10.1111/ner.12607

[98] Adams, J. L., Dinesh, K., Snyder, C. W., Xiong, M., Tarolli, C. G., Sharma, S., Dorsey, E. R., & Sharma, G. (2021). A real-world study of wearable sensors in Parkinson's disease. Npj Parkinson's Disease, 7(1), 1–8. https://doi.org/10.1038/s41531-021-00248-w
[99] Channa, A., Popescu, N., & Ciobanu, V. (2020). Wearable Solutions for Patients with Parkinson's Disease and Neurocognitive Disorder: A Systematic Review. Sensors (Basel, Switzerland), 20(9), 2713. https://doi.org/10.3390/s20092713
[100] Düking, P., Achtzehn, S., Holmberg, H.-C., & Sperlich, B. (2018). Integrated Framework of Load Monitoring by a Combination of Smartphone Applications, Wearables and Point-of-Care Testing Provides Feedback that Allows Individual Responsive Adjustments to Activities of Daily Living. Sensors, 18(5), 1632. https://doi.org/10.3390/s18051632
[101] Kubota, K. J., Chen, J. A., & Little, M. A. (2016). Machine learning for large-scale wearable sensor data in Parkinson's disease: Concepts, promises, pitfalls, and futures. Movement Disorders: Official Journal of the Movement Disorder Society, 31(9), 1314–1326. https://doi.org/10.1002/mds.26693
[102] van den Noort, J. C., Verhagen, R., van Dijk, K. J., Veltink, P. H., Vos, M. C. P. M., de Bie, R. M. A., Bour, L. J., & Heida, C. T. (2017). Quantification of Hand Motor Symptoms in Parkinson's Disease: A Proof-of-Principle Study Using Inertial and Force Sensors. Annals of Biomedical Engineering, 45(10), 2423–2436. https://doi.org/10.1007/s10439-017-1881-x
[103] Daneault, J.-F., Carignan, B., Codère, C. É., Sadikot, A. F., & Duval, C. (2012). Using a smart phone as a standalone platform for detection and monitoring of pathological tremors. Frontiers in Human Neuroscience, 6, 357. https://doi.org/10.3389/fnhum.2012.00357
[104] Pulliam, C. L., Heldman, D. A., Orcutt, T. H., Mera, T. O., Giuffrida, J. P., & Vitek, J. L. (2015). Motion sensor strategies for automated optimization of deep brain stimulation in Parkinson's disease. Parkinsonism & Related Disorders, 21(4), 378–382. https://doi.org/10.1016/j.parkreldis.2015.01.018
[105] Scanlon, B. K., Levin, B. E., Nation, D. A., Katzen, H. L., Guevara-Salcedo, A., Singer, C., & Papapetropoulos, S. (2013). An accelerometry-based study of lower and upper limb tremor in Parkinson's disease. Journal of Clinical Neuroscience: Official Journal of the Neurosurgical Society of Australasia, 20(6), 827–830. https://doi.org/10.1016/j.jocn.2012.06.015
[106] Delrobaei, M., Memar, S., Pieterman, M., Stratton, T. W., McIsaac, K., & Jog, M. (2018). Towards remote monitoring of Parkinson's disease tremor using wearable motion capture systems. Journal of the Neurological Sciences, 384, 38–45. https://doi.org/10.1016/j.jns.2017.11.004
[107] Mo, J., & Priefer, R. (2021). Medical Devices for Tremor Suppression: Current Status and Future Directions. Biosensors, 11(4), 99. https://doi.org/10.3390/bios11040099
[108] di Biase, L., Summa, S., Tosi, J., Taffoni, F., Marano, M., Cascio Rizzo, A., Vecchio, F., Formica, D., Di Lazzaro, V., Di Pino, G., & Tombini, M. (2018). Quantitative Analysis of Bradykinesia and Rigidity in Parkinson's Disease. Frontiers in Neurology, 9, 121. https://doi.org/10.3389/fneur.2018.00121
[109] Powell, D., Threlkeld, A. J., Fang, X., Muthumani, A., & Xia, R. (2012). Amplitude- and velocity-dependency of rigidity measured at the wrist in Parkinson's disease. Clinical Neurophysiology: Official Journal of the International Federation of Clinical Neurophysiology, 123(4), 764–773. https://doi.org/10.1016/j.clinph.2011.08.004
[110] Costa, P., Rosas, M. J., Vaz, R., & Cunha, J. P. (2015). Wrist rigidity assessment during Deep Brain Stimulation surgery. 2015 37th Annual International Conference of the IEEE Engineering in Medicine and Biology Society (EMBC), 3423–3426. https://doi.org/10.1109/EMBC.2015.7319128
[111] Djurić-Jovičić, M., Jovičić, N. S., Roby-Brami, A., Popović, M. B., Kostić, V. S., & Djordjević, A. R. (2017). Quantification of Finger-Tapping Angle Based on Wearable Sensors. Sensors (Basel, Switzerland), 17(2), E203. https://doi.org/10.3390/s17020203
[112] Mentzel, T. Q., Lieverse, R., Levens, A., Mentzel, C. L., Tenback, D. E., Bakker, P. R., Daanen, H. A. M., & van Harten, P. N. (2016). Reliability and validity of an instrument for the

assessment of bradykinesia. Psychiatry Research, 238, 189–195. https://doi.org/10.1016/j.psychres.2016.02.011

[113] Smits, E. J., Tolonen, A. J., Cluitmans, L., van Gils, M., Conway, B. A., Zietsma, R. C., Leenders, K. L., & Maurits, N. M. (2014). Standardized handwriting to assess bradykinesia, micrographia and tremor in Parkinson's disease. PloS One, 9(5), e97614. https://doi.org/10.1371/journal.pone.0097614

[114] Shahar, R. T., & Agmon, M. (2021). Gait Analysis Using Accelerometry Data from a Single Smartphone: Agreement and Consistency between a Smartphone Application and Gold-Standard Gait Analysis System. Sensors (Basel, Switzerland), 21(22), 7497. https://doi.org/10.3390/s21227497

[115] Seel, T., Raisch, J., & Schauer, T. (2014). IMU-Based Joint Angle Measurement for Gait Analysis. Sensors (Basel, Switzerland), 14(4), 6891–6909. https://doi.org/10.3390/s140406891

[116] Mihradi, S., Ferryanto, Dirgantara, T., & Mahyuddin, A. I. (2011). Development of an optical motion-capture system for 3D gait analysis. 2011 2nd International Conference on Instrumentation, Communications, Information Technology, and Biomedical Engineering, 391–394. https://doi.org/10.1109/ICICI-BME.2011.6108633

[117] Gao, S., Chen, J.-L., Dai, Y.-N., Wang, R., Kang, S.-B., & Xu, L.-J. (2021). Piezoelectric-Based Insole Force Sensing for Gait Analysis in the Internet of Health Things. IEEE Consumer Electronics Magazine, 10(1), 39–44. https://doi.org/10.1109/MCE.2020.2986828

[118] Huo, W., Angeles, P., Tai, Y. F., Pavese, N., Wilson, S., Hu, M. T., & Vaidyanathan, R. (2020). A Heterogeneous Sensing Suite for Multisymptom Quantification of Parkinson's Disease. IEEE Transactions on Neural Systems and Rehabilitation Engineering: A Publication of the IEEE Engineering in Medicine and Biology Society, 28(6), 1397–1406. https://doi.org/10.1109/TNSRE.2020.2978197

[119] RC+S (For those interested in beta testing). (n.d.). Retrieved 13 June 2022, from https://braininitiative.nih.gov/sites/default/files/pdfs/rcs_device_information_508c.pdf

[120] Medtronic Launches First-of-Its-Kind Adaptive Deep Brain Stimulation (aDBS) Trial in Parkinson's Disease Patients. (n.d.). Medtronic News. Retrieved 13 June 2022, from https://news.medtronic.com/2021-01-14-Medtronic-Launches-First-of-Its-Kind-Adaptive-Deep-Brain-Stimulation-aDBS-Trial-in-Parkinsons-Disease-Patients

[121] Rheede, J. J. van, Feldmann, L. K., Busch, J. L., Fleming, J. E., Mathiopoulou, V., Denison, T., Sharott, A., & Kühn, A. A. (2022). Diurnal modulation of subthalamic beta oscillatory power in Parkinson's disease patients during deep brain stimulation (p. 2022.02.09.22270606). medRxiv. https://doi.org/10.1101/2022.02.09.22270606

[122] Thenaisie, Y., Palmisano, C., Canessa, A., Keulen, B. J., Capetian, P., Jiménez, M. C., Bally, J. F., Manferlotti, E., Beccaria, L., Zutt, R., Courtine, G., Bloch, J., Gaag, N. A. van der, Hoffmann, C. F., Moraud, E. M., Isaias, I. U., & Contarino, M. F. (2021). Towards adaptive deep brain stimulation: Clinical and technical notes on a novel commercial device for chronic brain sensing. Journal of Neural Engineering, 18(4), 042002. https://doi.org/10.1088/1741-2552/ac1d5b

[123] Dias, C., Castro, D., Aroso, M., Ventura, J., & Aguiar, P. (2021). A memristor-based neuromodulation device for real-time monitoring and adaptive control of in vitro neuronal populations. https://doi.org/10.1101/2021.05.20.444941

[124] Themes, U. F. O. (2016, June 19). Parkinson's disease. Neupsy Key. https://neupsykey.com/parkinsons-disease-2/

[125] MPU6050 by Electronic Cats. (2022). [C++]. ElectronicCats. https://github.com/ElectronicCats/mpu6050 (Original work published 2019)

[126] Arduino Timer Tutorial. (n.d.). Retrieved 13 June 2022, from https://circuitdigest.com/microcontroller-projects/arduino-timer-tutorial

[127] Ellis, K., Godbole, S., Marshall, S., Lanckriet, G., Staudenmayer, J., & Kerr, J. (2014). Identifying Active Travel Behaviors in Challenging Environments Using GPS, Accelerometers, and

Machine Learning Algorithms. Frontiers in Public Health, 2. https://www.frontiersin.org/article/10.3389/fpubh.2014.00036
[128] Sabatini, A. M. (2011). Kalman-filter-based orientation determination using inertial/magnetic sensors: Observability analysis and performance evaluation. Sensors (Basel, Switzerland), 11(10), 9182–9206. https://doi.org/10.3390/s111009182
[129] Gimbal lock. (2022). In Wikipedia. https://en.wikipedia.org/w/index.php?title=Gimbal_lock&oldid=1082887600
[130] Hamming Window—An overview | ScienceDirect Topics. (n.d.). Retrieved 13 June 2022, from https://www.sciencedirect.com/topics/engineering/hamming-window
[131] Jolliffe, I. T. (2002). Principal Component Analysis (1-6,78-108). Springer Science & Business Media.
[132] Machine Learning Foundations. (n.d.). Retrieved 13 June 2022, from https://link.springer.com/book/10.1007/978-3-030-65900-4
[133] RAVARANI. (2016, May 16). Expanding your machine learning toolkit: Randomized search, computational budgets, and new algorithms. Cambridge Coding Academy. https://cambridgecoding.wordpress.com/2016/05/16/expanding-your-machine-learning-toolkit-randomized-search-computational-budgets-and-new-algorithms-2/
[134] Leung, K. (2022, June 20). Micro, Macro & Weighted Averages of F1 Score, Clearly Explained. Medium. https://towardsdatascience.com/micro-macro-weighted-averages-of-f1-score-clearly-explained-b603420b292f
[135] Feldmann, L. K., Lofredi, R., Neumann, W.-J., Al-Fatly, B., Roediger, J., Bahners, B. H., Nikolov, P., Denison, T., Saryyeva, A., Krauss, J. K., Faust, K., Florin, E., Schnitzler, A., Schneider, G.-H., & Kühn, A. A. (2022). Toward therapeutic electrophysiology: Beta-band suppression as a biomarker in chronic local field potential recordings. Npj Parkinson's Disease, 8(1), 1–9. https://doi.org/10.1038/s41531-022-00301-2